A STUDY ON OPTIMUM LAYOUT DESIGN OF PIEZOMETERS IN EARTH-FILL DAMS

A THESIS SUBMITTED TO
THE GRADUATE SCHOOL OF NATURAL AND APPLIED SCIENCES
OF
MIDDLE EAST TECHNICAL UNIVERSITY

BY

SALİH GÖKMEN

IN PARTIAL FULFILLMENT OF THE REQUIREMENTS
FOR
THE DEGREE OF MASTER OF SCIENCE
IN
CIVIL ENGINEERING

JULY 2021

Approval of the thesis:

A STUDY ON OPTIMUM LAYOUT DESIGN OF PIEZOMETERS IN EARTH-FILL DAMS

submitted by **SALİH GÖKMEN** in partial fulfillment of the requirements for the degree of **Master of Science** i**n Civil Engineering Department, Middle East Technical University** by,

Prof. Dr. Halil Kalıpçılar
Dean, Graduate School of **Natural and Applied Sciences** _____

Prof. Dr. Ahmet Türer
Head of the Department, **Civil Engineering** _____

Prof. Dr. A. Melih Yanmaz
Supervisor, **Civil Engineering Department, METU** _____

Examining Committee Members:

Prof. Dr. Zuhal Akyürek
Civil Engineering, METU _____

Prof. Dr. A. Melih Yanmaz
Civil Engineering, METU _____

Prof. Dr. Elçin Kentel
Civil Engineering, METU _____

Prof. Dr. İsmail Yücel
Civil Engineering, METU _____

Prof. Dr. Can Elmar Balas
Civil Engineering, Gazi University _____

Date: 16.07.2021

I hereby declare that all information in this document has been obtained and presented in accordance with academic rules and ethical conduct. I also declare that, as required by these rules and conduct, I have fully cited and referenced all material and results that are not original to this work.

Name, Last name : Salih GÖKMEN

Signature :

ABSTRACT

A STUDY ON OPTIMUM LAYOUT DESIGN OF PIEZOMETERS IN EARTH-FILL DAMS

Gökmen, Salih
Master of Science, Civil Engineering
Supervisor : Prof. Dr. A. Melih Yanmaz

July 2021, 92 pages

Excessive pore water pressure is one of the causes of failure in earth-fill dams. Therefore, distribution of pore water pressure within the dam body must be observed throughout the lifetime of the structure. The observation can be performed by means of an instrumentation system installed within the embankment. The system consists of sensors placed at specific loations. There are no standard guidelines to assign required number of the sensors and their proper locations within the body. Currently, instrumentation systems are always designed by only experiences, arbitrary desires or overrated approaches to be on the safe side. These procedures may cause unnecessarily high costs and questionable information about the structural behaviour. In this study, behaviour of the pore water pressure distribution under steady state, rapid fill, and rapid drawdown conditions is examined by analyzing various earth-fill dam cross-sections with different parameters. According to the results, best locations and number of the piezometers are determined to establish an ideal piezometer layout within the dam body. This layout is proposed to be the most economical and realistic design of monitoring system which provides appropriate information about number and locations of the sensors.

Keywords: Earth-fill dams, seepage analysis, pore water pressure, piezometer, optimum placement

ÖZ

TOPRAK DOLGU BARAJLARDA PİYEZOMETRELERİN OPTİMUM YERLEŞTİRİLMESİ ÜZERİNE BİR ÇALIŞMA

Gökmen, Salih
Yüksek Lisans, İnşaat Mühendisliği
Tez Yöneticisi: Prof. Dr. A. Melih Yanmaz

Temmuz 2021, 92 sayfa

Toprak dolgu barajların yıkılma sebeplerinden biri boşluk suyu basıncının istenmeyen seviyelere ulaşmasıdır. Bu sebeple boşluk suyu basıncının baraj gövdesi içerisindeki dağılımının, barajın hizmet ömrü boyunca kapsamlı şekilde gözlemlenmesi gerekmektedir. Gözlem, baraj gövdesi içerisine yerleştirilen bir ölçüm sistemi ile yapılmaktadır. Bu sistem piyezometre adı verilen sensörlerden oluşmaktadır. Ancak piyezometrelerin sayısını ve yerleştirilmesi gereken konumları belirten herhangi bir kılavuz bulunmamaktadır. Günümüzde ölçüm sistemleri geçmişteki tecrübelere, isteğe bağlı seçimlere veya güvenli tarafta kalmak amacıyla abartılan yaklaşımlara bağlı kalınarak tasarlanmaktadır. Bu durum gereksiz derecede yüksek maliyetlerle birlikte, yapının durumu hakkında doğruluğundan emin olunamayan bilgiler elde edilmesine sebep olmaktadır. Bu çalışmada, çeşitli toprak dolgu baraj kesitleri değişken parametrelerle analiz edilerek boşluk suyu basıncının zamandan bağımsız akım, haznenin ani dolma ve ani çekilme durumları altındaki davranışı incelenmiştir. Piyezometrelerin baraj gövdesi içerisindeki konumu ve sayısına bağlı en ideal cihaz yerleşimi elde edilmiştir. Piyezometreler uygun konumlara yeterli sayıda yerleştirilerek, ölçüm sisteminin ekonomik ve gerçeğe en yakın sonuçlar verecek şekilde tasarlanması sağlanmıştır.

Anahtar Kelimeler: Toprak dolgu barajlar, sızma analizi, boşluk suyu basıncı, piyezometre, optimum yerleşim

to my Family…

ACKNOWLEDGMENTS

I would like to thank my supervisor Prof. Dr. A. Melih Yanmaz for his encouragement and support. This study would not be completed without his contribution, guidance, and spectacular attention.

I appreciate careful editing and constructive criticism of Professor Elçin Kentel. Special thanks are extended to Dr. Onur Arı for his useful suggestions.

TABLE OF CONTENTS

LIST OF TABLES

TABLES

LIST OF FIGURES

FIGURES

LIST OF SYMBOLS

A	Area of an element
a	Column vector of deformations
A'	Area throughout the boundary
B	Gradient matrix
b	Intensity of body force
B	Gradient matrix
B'	Strain-displacement matrix
B_c	Crest width, [m]
c	Cohesion, [kPa]
C	Hydraulic conductivity matrix
C'	Constitutive matrix
D	Point load
d	Perpendicular distance from point load
E	Modulus of elasticity, [kPa]
e	Vertical distance from slice
F_f	Force equilibrium factor of safety
F_m	Moment equilibrium factor of safety
F_n	Incremental force
F_w	Resultant external water force
G	Edge of an element

g	Gravitational acceleration, [m/s²]
H	Dam height, [m]
H_n	Nodal head
H_t	Total head, [m]
i	Hydraulic gradient
k	Hydraulic conductivity, [m/day]
kW	Seismic load on the slice
k_x	Hydraulic conductivity in horizontal direction, [m/day]
k_y	Hydraulic conductivity in vertical direction, [m/day]
L	Depth of water level measured from the reservoir surface, [m]
m	Upstream face slope of shell section
m_v	Coefficient of volume compressibility, [1/kPa]
n	Upstream face slope of clay core
N_i	Interpolating function
N_n	Normal force
Ø	Angle of friction
p	Downstream face slope of shell section
p_s	Incremental surface pressure
Q	Flux, [m³/day]
q	Unit discharge, [m³/s/m]
R	Moment arm
t	Time

u	Pore water pressure
v	Element volume
W	Weight of slice
X	Horizontal distance of the piezometer from the origin point
Y	Vertical distance of the piezometer from the origin point
z	Downstream face slope of shell section
α	Perpendicular distance from resultant
γ	Unit weight, [kN/m³]
θ	Volumetric water content
θ_r	Residual water content, [m³/m³]
θ_s	Saturated water content, [m³/m³]
λ	Storage term
μ	Poisson's ratio
ρ	Mass density, [g/cm³]
ω	Angle of the point load from the horizontal axis
τ	Element thickness

CHAPTER 1

INTRODUCTION

1.1 General

Embankment dams exist in various types and each type brings its individual failure conditions and design criteria beside the common ones that are valid for every type. These criteria depend on properties of the material used and state of the structure which must be correctly processed while designing it. For this reason the design step requires qualification by comprehensive knowledge and experience to be able to provide the required stability and prevent failures that result great disasters.

Water stored in the reservoir tends to seep from upstream face to downstream within the dam body. Along the phreatic line, pore water pressure of the filling material equals to atmospheric pressure and increases with depth. Excess pore water pressure may reduce the shear strength of the material and even cause failure at upstream slope of the dam (Beenanga et al., 2016).

Pore water pressure is formed by water stored in reservoir and level of water affects the distribution of pore water pressure in various ways. Uncontrolled changes in the water level and its duration may cause pore pressure to reach unfavorable extent and this situation can end up with a disaster. In order to prevent this, distribution of the pore water pressure within the embankment must be observed consistently during its lifetime and conditions affecting the pore water pressure must be controlled appropriately.

The value of pore water pressure is measured by piezometers placed into embankments. The observation of pore water pressure can be achieved by regularly collecting the survey data from the piezometers to be aware of current condition of the embankment and take precautions, if necessary.

1.2 The Aim and Scope of the Study

To the best of the author's knowledge, no study has been conducted for optimum piezometer placement of earth-fill dams. For this reason piezometer instrumentation of the dams could be insufficient or superfluous according to designers' choice. So, the data collected from the instruments can be misleading or cost of equipment can be high or low, depending on using more or less than the required number of piezometers. In order to obtain correct placing, several conditions affecting pore water pressure, which are steady state, rapid fill, and rapid drawdown (ASCE 1989), should be analyzed on many cross-sections with various parameters and their effects on the stability of upstream face must be assessed. Since these conditions are related with upstream side and effects of upstream conditions on pore water pressures of downstream slope is negligible (Kılıç 2017), this study relatively focuses on upstream side of clay cored earth-fill dams. Analyses are executed by Geo Studio software and its packages SEEP/W, SIGMA/W and SLOPE/W to examine the upstream slope stability under steady state, rapid fill, and rapid drawdown conditions. After this first step, an algorithm is developed and presented at the final stage.

In Chapter 2, information about monitoring system of earth-fill dams is briefly explained. Elements to be monitored and instruments used are summarized. Chapter 3 comprises summary of the software and methods used in analyses. Chapter 4 gives information about criteria affecting the safety of embankment and its behaviour under different pore water pressure conditions. In Chapter 5, the algorithm for selecting best piezometer placement is developed and discussed. Finally the conclusions and recommendations are presented in Chapter 6.

CHAPTER 2

MONITORING SYSTEMS OF CLAY CORED EARTH-FILL DAMS

2.1 General

Failure of earth-fill dams induced by various sources has always been a main problem about the safety. Therefore, dam behavior should be assessed continuously to take necessary remedial actions on time using the information gathered from an integrated instrumentation system. The undesired incidents or failures can be prevented by applying the correct type of instrumentation.

Some failure modes can be considered as crest movement, slope deformation, excessive pore water pressures or seepage, outflow from the dam body, and tilting of spillway (Yanmaz, 2018). These incidents can be inspected by some types of instrumentation for clay cored earth-fill dams. The types of instrumentation used for evaluation of common problems are summarized in Table 2.1.

Table 2.1. Typical problems and related instruments used in monitoring system (FERC, 1991)

Problem/Concern	**Typical instrumentation**
Seepage or leakage	Visual observation, and some instruments, such as weirs and piezometers
Boils or piping	Visual observation, piezometers, and weirs
Uplift pressure, pore water pressure, or phreatic surface	Visual observation, wells, and piezometers
Drain function or adequacy	Visual observation, piezometers, and some measurements
Erosion, scour, or sedimentation	Visual observation, sounding, and underwater inspection, survey
Dissolution of foundation strata	Test of water quality
Total or surface movement (translation, rotation)	Visual observation, exact position, and level surveys, tiltmeters, and some measurements

Table 2.1. (continued)

Internal movement and deformation in embankments	Settlement plates, cross-arm devices, fluid leveling devices, some settlement sensors, and sounding devices
Internal movement and deformation of concrete structures of dams	Tiltmeters, inclinometers, and extensometers
Movement of foundation or abutment	Visual observation, piezometers, inclinometers, and extensometers
Quality of foundation	Visual observation, pressure, and flow measurements
Slope stability	Visual observation, inclinometers, extensometers, shear strips, and piezometers
Joint or crack movement	Crack meters and reference points
Stresses or strains	Pressure cells, stress meters, and strain meters
Seismic loading	Accelerographs
Condition of tension anchors	Jacking tests, load cells, and extensometers
Condition of concrete	Visual observation and some analyses
Concrete expansion	Visual observation, and measurements by some sensors like tiltmeters, plumblines, inclinometers, and extensometers
Steel deterioration	Visual observation, sonic thickness measurements, test coupons

The most common cause of failure encountered on embankments are overtopping and seepage (Johnson and Illes, 1976).

Settlements at the base and earthquakes generally cause movements which may generate critical deformations. On the other hand, structural settlement may form because of saturation within the embankment and potential of overtopping may increase due to decreasing freeboard during the passage of extreme flood discharge.

Seepage is caused by the difference between the water levels at upstream and downstream. The amount of seepage must be related with these levels in terms of seepage rate and pore water pressure.

Excessive amount of seepage may lead to washing of impervious zone or foundation material. Hence the stability decreases and potential risk gains significance. However, all dams generate some seepage which may be uncritical unless having high rates (INDNR, 2003). Therefore, rate of the seepage must be known during the lifetime of dams and this can only be possible by configuring a monitoring system comprising various types of instruments.

Monitoring the seepage is achieved by flowmeters to measure the amount of flow within the embankment. Also the difference in pore water pressure becomes an indicator as explained above and piezometers are used for measuring the pore water pressure.

The pore water pressure within the embankment increases as the water depth gets higher and may reach to excessive levels especially in impervious zones and foundation layer (FERC, 1991). Therefore, core zone is desired to be installed with piezometers while the foundation is assumed to be impervious.

Water level variations caused by seasonal effects or operative demands may necessitate rapid drawdown or rapid fill of the reservoir. Since these are essential hydraulic loading conditions for upstream slope stability, the upstream shell zone is desired to be installed with piezometers as well as the core zone.

As already discussed, value of the pore water pressure must be known to decide if it is exigently critical or in permissible limits. This is the reason why this study motivates to develop a deterministic instrumentation layout for optimal pore water pressure monitoring system. The types of instrumentation to monitor pore water pressure within the embankment are listed in Table 2.2.

Table 2.2. Assessment of the instruments used for pore water pressure (FERC, 1991)

Type	**Advantages**	**Limitations**
Staff Gage	Simple device, cheap, and reliable.	Impossible to be automated.
Float-Type Water Level Gage	Simple device, cheap, reliable. Can easily be automated.	Must be placed in water and used with readout device. Requires ice protection
Ultrasonic Water Level Sensor	Simple, cheap, and reliable. No need to touch water. Can easily be automated.	Must be used with readout device. Correction is needed for air temperature. Factors, such as debris and ice can cause false readings.
Bubbler	Simple device, inexpensive, reliable. Easily automated.	Must be used with readout device. Sensor must be placed in water.
Observation Well	Simple device, cheap, reliable. Can easily be automated.	Can only be used in uniform materials, not preferred for stratified soils. Impervious soils may cause long lag time.
Open Standpipe Piezometer	Simple device, cheap, reliable. Can easily be automated. Easy to monitor and maintain. Measurements can be conducted under changing water levels.	Depending on the permeability of the soil, lagging time may increase. Freezing risk at vicinity of water surface. Flow conditions may clog the porous tips. Not applicable for artesian conditions. Deficiencies may occur due to compaction during construction. Consolidation of soil around standpipe may cause damage.
Closed Standpipe Piezometer		Same as that of open standpipe piezometer stated above and applicable for artesian conditions.

Table 2.2. (continued)

Type	Advantages	Limitations
Twin-tube Hydraulic Piezometer	Simple, cheap, and reliable. Lag time is short and not affected by construction conditions.	Impossible to be installed through a borehole. Not applicable for retrofitting. Readout must be at a location where is protected from freezing. Monitoring and maintenance are complicated. Periodically requires de-airing. System must be placed at a certain elevation under the phreatic line. Moderately hard to be automated.
Pneumatic Piezometer	Moderately simple, cheap, and reliable. Lag time is very short. Can be placed on any elevation. Cannot be affected by freezing.	Monitoring and maintenance may be complex. Must be used with a readout devices in dry air. Automation is possible for short distances only. Can be affected by barometric pressure. Readout is moderately expensive.
Vibrating Wire Piezometer	Moderately complex and expensive. Easy to monitor. Lag time is very short. Can be placed on any elevation. Not affected by freezing. Can be used for long distances. Can easily be automated.	Requires protection for lightning. Transducer and readout are expensive. Can be affected by temperature and barometric pressure changes. Requires calibration check.
Bonded Resistance Strain Gage (Electronic) Piezometer	Moderately complex and expensive. Easy monitoring. Lag time is very short. Can be placed on any elevation. Not affected by freezing. Can be used for long distances. Can easily be automated.	Requires protection for lightning. Not preferred for long-term usage. Expensive system. May be affected by length of the cable and moisture.

History of pore water pressure monitoring and the most used types of piezometers which are available in market are explained comprehensively since this study focuses only on piezometers.

2.2 Literature Review

The first safety assessment method for embankments is visual inspection (Bartholomew and Murray, 1987). Instrumentation and monitoring technology were invented later (Mancebo et al., 2012). In 19th century open pipe piezometers were first used for dams servicing for irrigation or located on alluvial soil to survey the leakage beneath them in USA, Europe, Asia, and India (Seyed-Kolbadi et al., 2020).

In dam engineering, instrumentation and monitoring of the structures and reservoir area are crucial concerns (Mizuna and Hirose, 2009). Installing the appropriate instrumentation and their monitoring are extremely helpful for investigating the safety of dams. In the Britain, water level fluctuations in an earth dam was monitored by instrumentation in 1907. In the USA, the first water level and pore water pressure measurements by installing hydrostatic instruments in earth dams were done by the rehabilitation office (Dunnicliff, 1993). Installation of the hydrostatic pressure instruments for Cobol Dam in 1938-1939 is one of the early instrumentation examples for dams (Majoros and Sneed, 1981). An instrument which can measure the pressure in earth dams by using a sensor with a stretched wire was designed by Roy Karlson (ASCE, 2000). Also, the researches on using instruments for evaluation of construction performance and construction methods have begun in 1930s and design of two piped hydraulic piezometers was achieved by this attempt (Jansen, 2012). In the following decade usage of vibrating wire sensors for monitoring the dam behaviour became popular.

With the advancement in technology, the instrumentation has evolved to higher level. Data collecting and processing became easier by microcomputer technology and electronics which provides more accurate results. Present-day vibrating wire sensors are demonstrated to be convenient for many environmental conditions (Zhu et al., 2011) and they have high level of stability, reliability, and life span. The vibrating wire sensors become the most applicable type of instrumentation nowadays (Masoumi et. al., 2018). For this reason this type of piezometer is considered in the development of best piezometer configuration in this study.

Monitoring of the performance of dams using proper instrumentation is of great importance since current and apparent potential damage indicators are assessed with reference to the data collected from these instruments. Old dams may be retrofitted by a set of instruments to follow the performance of the dam concerned according to the remaining life time (Yanmaz and Arı, 2008), (Arı and Yanmaz, 2009), (Yanmaz and Arı, 2011). The effectiveness of the instrumentation system of the first hard-fill dam in Turkey (Cindere Dam) has been evaluated by Yanmaz and Sezgin (2009) as a pioneering study in Turkey. In a different study, a methodology has been developed by Arı and Yanmaz (2018) for optimum layout design of pressure cells for concrete faced rockfill dams.

2.3 Piezometers

Piezometers measure pressure and are generally used to obtain the value of pore water pressure or ground water level. The most popular piezometers are hydraulic, pneumatic, casagrande, strain gauge, and vibrating wire.

2.3.1 Hydraulic Piezometers

Hydraulic piezometers comprise a porous filter enclosing a reservoir of water, which is separated from a pressure gauge by flexible, water-filled tubes (Figure 2.1). The tubes are used to circulate water through the system, removing air and ensuring that the reservoir remains full of water. Tubes enable to observe change in pressure. This change is read by using manometers, pressure gauges, and pressure transducers.

The fluid in the tubings must not contain air, because air bubbles may increase the response time. Therefore, de-airing is required to prevent this kind of errors.

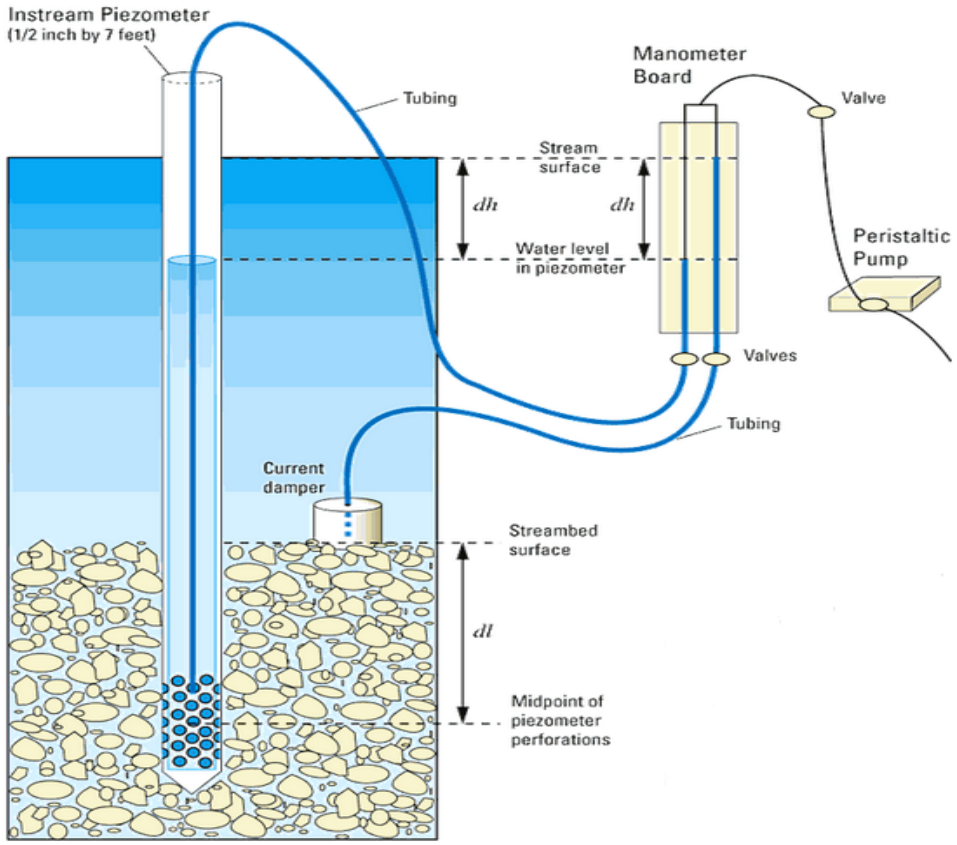

Figure 2.1. Illustration of hydraulic piezometer (USGS 2005)

Advantages of hydraulic piezometers;

- Very simple and reliable mechanism
- Piezometer tip can be flushed
- Inaccessible components do not have any moving parts
- Can measure permeability
- Can read negative pressure.

Limitations;

- Vulnerable against freezing
- Requires periodic de-airing by special devices
- Used for very limited piezometric heads.

2.3.2 Pneumatic Piezometers

The pneumatic piezometer consists of a porous tip sealed at the measuring end (Figure 2.2). Twin armoured plastic tubes inside connect the tip to the remote reading point. Twin tubes connect the transducer within the piezometer tip to either a pneumatic terminal panel or a readout unit. When pore water pressure is exerted on the diaphragm, reverse pressure is applied until pressure equilibrium is reached, then the readout unit displays the reading.

Figure 2.2. Pneumatic piezometer (Soil instruments, 2013)

Advantages of pneumatic piezometers;

- Short lag time,
- Durable to freezing
- Easy to calibrate.

Limitations;

- Readings are time consuming
- Difficult to automate
- Nitrogen or carbon dioxide supply is needed.

2.3.3 Casagrande (Standpipe) Piezometers

Casagrande piezometers are used to measure the pore water pressure in medium-low permeable soils. They are composed of a filter unit connected to the surface with single or twin tube (Figure 2.3). Standpipe piezometers are used to monitor the groundwater table level in high-permeability soils. The standpipe filter unit consists of a Casagrande filter not sealed in the borehole with bentonite, or a slotted tube covered by geotechnical fabric in order to filter the water entrainment.

Figure 2.3. Casagrande piezometer (Soil instruments, 2021)

2.3.4 Strain Gauge Piezometers

This type of piezometers (Figure 2.4) comprise internal strain gauges that transforms the mechanical motion into electronic signal. The strain experienced by stainless steel diaphragm due to the pressure causes resistance on strain gauge. This resistance creates a signal which is proportional to the applied pressure. The signal is detected and processed by data logger, then transformed into pressure unit.

Figure 2.4. Strain gauge piezometer (Geosense, 2021)

Advantages of strain gauge piezometers;

- Can be automated
- Fast response
- High accuracy
- Easy to read.

Limitations;

- Long cables cannot be used during installation and use of different cable lengths causes calibration offsets
- Moisture and electrical connections may cause errors
- Must be protected against lightning.

2.3.5 Vibrating Wire Piezometers

This piezometer consists of a tensioned steel wire and a flexible sensitive diaphragm as shown in Figure 2.5. One end of the wire is anchored to the diaphragm while the other end is attached into stainless steel inner body. Opposing coils are placed within the inner body. When voltage or swept frequency excitation is applied to the coils, a magnetic field is formed and the wire starts to oscillate. Oscillation of the wire generates an alternating current. Frequency of this current is sensed and processed by readout unit or data logger into form of pressure unit. When exerted to hydraulic pressure, the sensitive diaphragm deflects and causes change in tension of the wire.

This change affects the oscillation frequency with respect to the level of the hydraulic pressure.

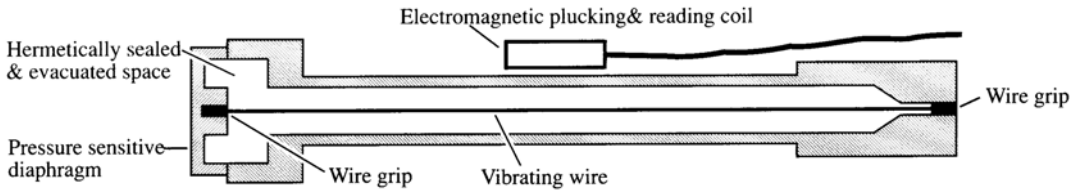

Figure 2.5. Illustration of vibrating wire type piezometer (Geosense, 2021)

Advantages of vibrating wire piezometers;

- Can be automated
- Can read negative pore water pressures
- Short lag time
- Easy to read
- Long cables (even more than 2000 m) can be used during installation.

Limitations;

- Must be protected against lightning.

Besides being available as a single piece during installation, multiple sensors can be connected by one common cable which has multiple cores inside so that they can be installed in single borehole as well. Single and multiple vibrating wire piezometers are shown in Figure 2.6.

Figure 2.6. Single and multiple vibrating wire piezometers (Geosense, 2021)

Vibrating wire piezometers are inexpensive and they can operate to measure pore water pressures in the range 70 to 6895 kPa (Geosense, 2021). Also, they can measure negative pressures which is a very significant feature especially for the data collection of the embankments under drawdown conditions. When the advantages and limitations of all type of piezometers are considered, vibrating wire becomes the most reasonable type. Therefore, this type of piezometer is considered while determining the piezometer layout in earth-fill dams in this thesis.

CHAPTER 3

THE METHODOLOGY

3.1 Seepage Modeling

Steady state, rapid drawdown, and rapid fill conditions are directly related with pore water pressure which has significant effect on the slope stability. Therefore, stability of embankments can be checked by determining pore water pressure first.

A finite element software, comprising many analysis packages, Geo Studio is utilized for all analyses throughout the study. The package SEEP/W (Geo-Slope Int. Ltd. 2012a) is used for determining the pore water pressures and seepage rates.

SEEP/W analysis can provide results about conductivity, total head, pore water pressure, seepage rate, and flow velocity by using characteristic properties of materials, such as hydraulic and strength parameters defined in Chapter 4. These parameters are used in volumetric water content and hydraulic conductivity functions by adhering to Darcy's Law, which is:

$$q = -k.i \tag{3.1}$$

where q is the volumetric flow rate per unit area, and i is the hydraulic gradient.

Conservation of mass in 2-D case can be stated as follows:

$$\frac{\partial}{\partial x}\left(k_x \frac{\partial H}{\partial x}\right) + \frac{\partial}{\partial y}\left(k_y \frac{\partial H}{\partial y}\right) + Q = \frac{\partial \theta}{\partial t} \tag{3.2}$$

where H is total head, k_x and k_y are hydraulic conductivities along x and y directions, respectively, t is time, θ is the volumetric water content, and Q is flux. The difference between incoming and outgoing fluxes at a point is the same as difference in volumetric water content. According to the Equation 3.2, horizontal and vertical flow

rates and fluxes applied externally are equal to the storage which changes by time (Geo-Slope Int Ltd. 2014a; Wang and Anderson, 1982).

Finite element method is used to solve Equation 3.2. So the software is able to obtain the most critical failure arc of the slope with respect to sliding and can visualize deformation and stress distribution.

2-D seepage equation is obtained by using Galerkin method as:

$$\tau\int_A([B^T][C][B])dA\{H_n\} + \tau\int_A(\lambda < N_i >^T < N_i >)dA\{H_n\}, t = q\tau\int_G(< N_i >^T)dG \qquad (3.3)$$

where B is gradient matrix, C is matrix of hydraulic conductivity, H_n is the nodal head vector, N_i is interpolating function vector, q is unit discharge, τ is element thickness, t is elapsed time, λ is storage term, A is designation for summation over the area of an element, and G is designation for summation over the edge of an element.

3.2 Slope Stability Modeling

3.2.1 Finite Element Method

Slope stability calculations are conducted by using SIGMA/W (Geo-Slope Int. Ltd. 2013) and SLOPE/W (Geo-Slope Int. Ltd. 2012b) packages of the software. SIGMA/W deals with stress distribution in forms of tangential pressure, horizontal and vertical stress and pore water pressure, and their consecutive deformation analyses while SLOPE/W executes the analysis of slope stability by using the resulting data from SEEP/W and SIGMA/W in form of stress loadings.

The finite element equation used by SIGMA/W is:

$$\int_v[B'^T][C'][B']dv\{a\} = b\int_v < N_i >^T dv + p_s\int_{A'} < N_i >^T dA' + \{F_n\} \qquad (3.4)$$

where B' is matrix of strain-displacement, C' is constitutive matrix, $\{a\}$ is column vector of horizontal and vertical deformations, $<N_i>$ is row vector of interpolating

functions, A' is area throughout the boundary, v is element volume, b is intensity of body force, p_s is incremental surface pressure and $\{F_n\}$ is incremental force.

Vertical body force is calculated with the integral below:

$$\gamma_s \int_v (< N_i >^T) dv \tag{3.5}$$

Similarly, horizontal forces are calculated by using force intensity, b_s in the same integral as shown below:

$$b_s \int_v (< N_i >^T) dv \tag{3.6}$$

3.2.2 Limit Equilibrium Method

This method is used by SLOPE/W while conducting analyses for safety factor of upstream slope of the embankments. This analysis contains two types of safety factors which are mentioned as moment equilibrium and force equilibrium based on calculating by either forces or moments exerting to the critical slip surface.

Safety factor by moment equilibrium is expressed as ratio of total resisting moments to total driving moments for an assumed failure arc and calculated by the formulation given below:

$$F_m = \frac{\sum (c'\beta R + (N_n - u\beta)\ R\ \tan \emptyset')}{\sum Wx - \sum N_n f + \sum kWe \pm \sum Dd \pm \sum F_w a} \tag{3.7}$$

Safety factor by force equilibrium is expressed as ratio of total resisting forces to total driving forces acting on an assumed failure arc and calculated as the formulation given below:

$$F_f = \frac{\sum (c'\beta\ \cos\alpha + (N - u\beta)\ \tan \emptyset' \cos\alpha)}{\sum N \sin\alpha + \sum kW - \sum D \cos\omega \pm \sum F_w} \tag{3.8}$$

where c' is cohesion, $\emptyset'$ is internal friction angle, u is pore water pressure, W is weight of slice, N_n is normal force on the slice, D is point load, kW is seismic load on the

slice, R is moment arm, x is the horizontal distance from slice, e is the vertical distance from slice, d is perpendicular distance from point load, α is perpendicular distance from resultant, ω is angle of the point load from the horizontal, and F_w is the resultant external water forces.

Prior studies state that both methods are widely used for slope stability analyses and they provide reliable results for theoretical studies and actual designs (Kılıç, 2017). Besides, finite element method is asserted to be superior for actual designs while limit equilibrium method is suggested mostly for engineering practice (Geo-Slope Int. Ltd. 2012b). Therefore, limit equilibrium method is used in the analyses conducted in this study.

CHAPTER 4

PRELIMINARY ANALYSES

4.1 General

For earth-fill dams, upstream slope failure is one of the common types of failure that must be considered in design stage. According to the results from statistical investigations, majority of dams are in earth-fill type and they have higher percentage of destruction when compared to concrete dams (ICOLD 1983; Shi et al., 2015). This situation necessitates the awareness of potential risks, hence behaviour analysis of earth dams becomes significant (Rashidi and Haeri 2017).

Therefore, causes of upstream slope failure are going to be investigated and regarding criteria will be examined to comprehend this issue. Results of these investigations and examinations may help to establish a relationship between the structure and the parameters like dam height, water level, and so on. By doing this, the necessity of piezometers can be figured out in more apparent way. Consequently, a conservative approach can be achieved to take precautions and to obtain best instrumentation layout.

The parameters, governing the upstream slope stability under steady state, rapid drawdown, and rapid fill conditions are considered in two groups as external and internal parameters. External parameters are upstream face slope, dam height, rapid fill and drawdown rates, whereas internal parameters comprise characteristics of the filling materials. The software that has been used in this study processes the corresponding characteristics in two groups as hydraulic parameters and strength parameters. Hydraulic parameters, such as hydraulic conductivity (K_s), saturated water content (θ_s), and residual water content (θ_r) are used in seepage analyses for volumetric water content function and hydraulic conductivity function calculations while the strength parameters, Modulus of elasticity (E), unit weight (γ), Poisson's

ratio (μ), friction angle ($\emptyset$), and cohesion (c) are used in slope stability analyses. Effects of these parameters on the dam bahaviour have been observed specifically. Friction angle has been given multiple values and analyses are conducted again to particularly see whether its effect on the behaviour is favorable or not. This process is only applied on upstream shell, which comprises compacted sandy gravel with some clay.

A model dam section that is used in analyses is chosen as simply zoned which comprises a clay core and shells from compacted sandy gravel with some clay as shown in Figure 4.1. Filter zone is neglected because preliminary analyses conducted by the author show that its existence does not significantly affect the behaviour of upstream slope in conditions of steady state, rapid fill, and rapid drawdown.

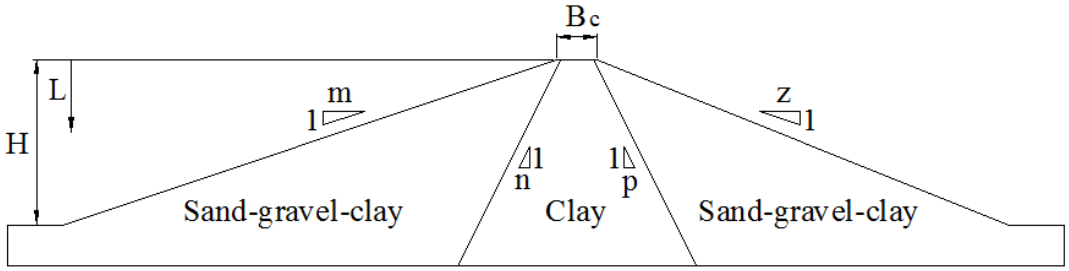

Figure 4.1. Definition sketch of the model dam cross-section that is used in analyses

H : Height of dam

L : Depth of water level measured from the reservoir surface

m : Upstream face slope of shell section

n : Upstream face slope of clay core

p : Downstream face slope of clay core

z : Downstream face slope shell section

B_c : Crest width

Downstream slope is chosen constant as 1V:3H because there is no need to observe different downstream conditions since the downstream sides of the earth-fill dams

are affected negligibly by the changes in upstream conditions (Çalamak et al., 2015) and downstream slope is not critical than the upstream slope under rapid fill, rapid drawdown and steady state conditions considered in this study.

Side slopes are governed by the strength parameters which are decisive elements of safety factor of the slope stability. Therefore, side slopes must satisfy the minimum allowable safety factors which vary with different loading conditions.

The maximum rapid fill rate is chosen as 2 m/day which is conformed to the previous studies for similar dam cross-sections (Kılıç, 2017; Çalamak et al., 2020).

The drawdown rates are chosen regardless of any regulations or rule of thumbs because there cannot be any certain permissible drawdown rate which is valid for all embankment dams. The maximum allowable drawdown rate changes from dam to dam since it depends on the permeability of the material and the length of drainage path (Beenenga et al., 2016). Therefore, drawdown rates are determined to satisfy allowable safety factors for upstream slope against sliding. The relevant safety factors are specified by some standards for different conditions.

Tables 4.1 and 4.2 summarize proper safety factor values against sliding according to different standards (Kılıç, 2017).

Table 4.1. Recommended minimum values of safety factor for rapid drawdown condition

Required Minimum Safety Factors for Rapid Drawdown Condition	
United States Army Corps of Engineers (USACE 2003)	1.3
Federal Energy Regulatory Commission (FERC 1991)	1.1
United States Bureau of Reclamation (USBR 1987)	1.3
California Department of Water Resources (Persson 1997)	1.25
United States Department of Agriculture (NRCS 2005)	1.2
American Society of Civil Engineers (ASCE 1989)	1.3

Table 4.2. Recommended minimum values of safety factor for steady-state seepage condition

Required Minimum Safety Factors for Steady-State Seepage Condition	
United States Army Corps of Engineers (USACE 2003)	1.5
Federal Energy Regulatory Commission (FERC 1991)	1.5
United States Bureau of Reclamation (USBR 1987)	1.5
California Department of Water Resources (Persson 1997)	1.5
United States Department of Agriculture (NRCS 2005)	1.5
American Society of Civil Engineers (ASCE 1989)	1.5

At the beginning of the analyses, 1V:3H slope value is chosen for both upstream and downstream slopes which is desirable for simply zoned dams with clay core and shells from compacted sandy gravel some clay (USBR, 1987), and various alternatives for upstream face are used in accordance with the factors given in Table 4.1 and Table 4.2.

Upstream and downstream slopes of clay core are taken as 1V:0.5H (Bilgi, 1990).

Use of various strength parameters are considered to be realistic to observe their effects on the safety. For this reason, several friction angle values are used in the analyses, additionally.

Hydraulic parameters are kept constant since the effect of drawdown is tackled in this study. Therefore, constant hydraulic properties are used with various drawdown rates.

The full reservoir level is considered to be 3 meters lower than the crest level for all embankment heights.

The model dam height is desired to vary from 40 m to 200 m with 20 m increments to see the behaviour at different heights, similar to the study conducted by Arı and Yanmaz (2018).

The values of dam height, side slope, rapid fill and drawdown rate chosen by the relevant sources are collected in the Table 4.3, material properties used in analyses are shown in Tables 4.3 and 4.4.

Table 4.3. External parameters used in analyses

Dam Height (m)	40, 60, 80, 100, 120, 140, 160, 180, 200
Upstream Slope of Shell (V:H)	1:3, 1:3.5, 1:4
Downstream Slope of Shell (V:H)	1:3
Slope of Core (V:H)	1:0.5
Drawdown Rate (m/day)	0.5, 0.75, 1.0, 1.5, 2.0
Fill Rate (m/day)	2.0

Values of hydraulic parameters, such as hydraulic conductivity (K_s), saturated water content (θ_s) and residual water content (θ_r) were taken from Carsel and Parrish (1988). The value of volume compressibility coefficient (m_v) was taken from Carter and Bentley (1991).

Table 4.4. Hydraulic Parameters

Material Type	**Volumetric Water Content Function**		**Hydraulic Conductivity Function**	
	θ_s (m^3/m^3)	**m_v (1/kPa)**	**θ_r (m^3/m^3)**	**K_s (m/day)**
Clay	0.38	$5x10^{-5}$	0.068	0.048
Sand-Gravel	0.5	$5x10^{-7}$	0.02	86
Sand	0.43	$5x10^{-6}$	0.045	7

Strength parameters, such as modulus of elasticity (E) and Poisson's ratio (μ) were taken from Bowles (1996) while unit weight (γ), cohesion (c), and angle of friction ($\varnothing$) were taken from Bilgi (1990).

Table 4.5. Strength Parameters

Material Type	**E (kPa)**	**γ (kN/m³)**	**μ**	**c (kPa)**	**Angle of Friction (°)**
Clay	50000	19	0.4	59	20
Sand-Gravel	100000	21	0.3	40	26
Sand	75000	20	0.35	0	23

At the beginning of modeling, the full reservoir water level, dam geometry, material zones, hydraulic properties, and soil characteristics of the filling material have been defined for steady state condition in SEEP W to obtain initial pore water pressures. SIGMA W is used for obtaining the stress distributions of steady state condition and transient conditions, such as rapid fill and drawdown. Analysis type of "insitu" is used for steady state and "coupled stress/pwp" is used for transient conditions. Lastly, SLOPE W is used to obtain safety factors of upstream slopes.

When all the inputs are defined, firstly SEEP W obtains the initial pore water pressures in the embankment. Then, "Insitu" type of SIGMA W analysis calculates the stresses under the initial condition. These initial pore water pressure and stress values are used by "coupled stress/pwp" type of SIGMA W analysis to calculate their distribution with respect to time. Finally, safety factors against sliding are calculated throughout the specified time interval by SLOPE W.

Analysis steps for rapid drawdown and rapid fill conditions are shown in Figure 4.2.

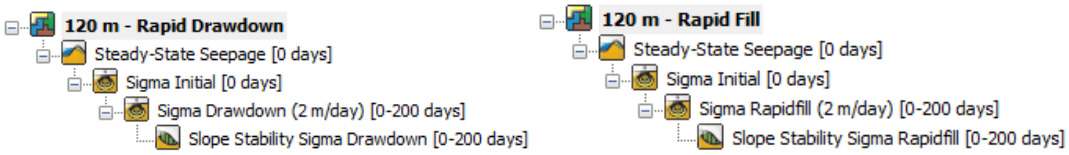

Figure 4.2. Analysis steps on GeoStudio software (Geo-Slope Int. Ltd. 2012a)

Since preliminary analyses are conducted only to observe the behaviour of slope stability of the embankments under different conditions related with pore water pressure, the default mesh size is used. The software automatically uses bigger meshes for bigger cross-sections. The mesh sizes range from 5 m to 25 m for cross-sections having height range from 40 m to 200 m.

For the purpose of examining the effect of mesh size, an analysis is conducted successively by using the mesh size as 2 m and 25 m without changing any other parameter. The outcoming safety factor distributions are almost the same (see Figure 4.3), because using smaller mesh sizes does not have significant effect on seepage and pore water pressure values (Yılmaz, 2017).

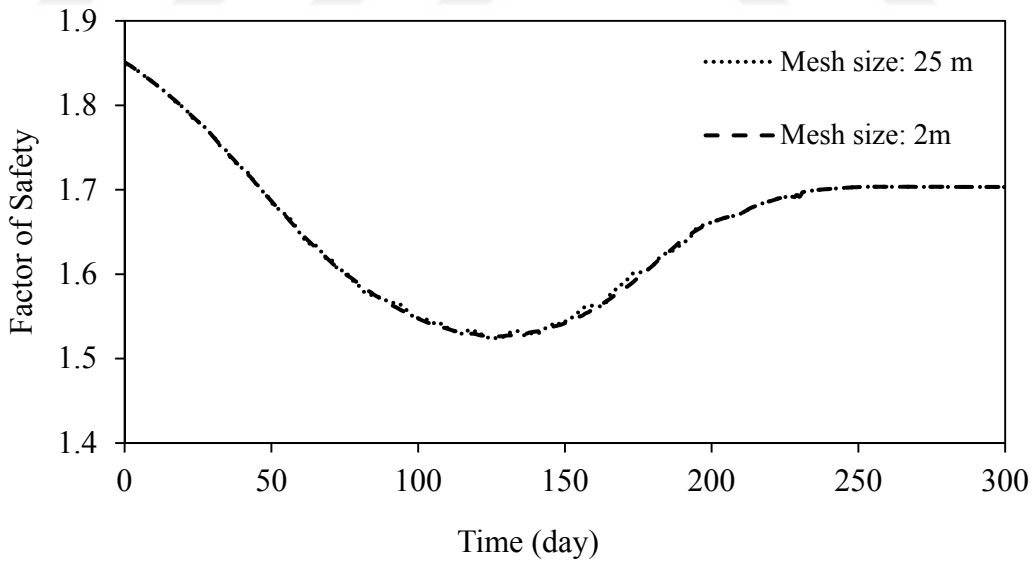

Figure 4.3. Comparison of safety factor results with respect to different mesh sizes

Several analyses have been conducted by designating sand filter zones at both upstream and downstream sides. Downstream filter is considered in form of chimney drain with 3 m thickness while the recommended minimum thickness is 1.5 m (FEMA, 2011). However, selecting thicker chimney drain keeps the phreatic line within the filter zone and provides a more stable downstream side against sloughing (Yılmaz, 2017). Similarly, the upstream filter is designed with the same thickness. Results are obtained as the distribution of safety factor with respect to time graph for all analyses. Then, the most critical safety factors corresponding to the minimum safety factor obtained among many assumed failure arcs with respect to time distributions, and their timing are sorted with the current water level in Table 4.6 in which critical stands for minimum safety factor.

When the results are compared with non-filtered analyses (see Figures 4.4 and 4.5), it is easy to admit that filter zone has no significant effect on the stability of the upstream face. Generally filter is used for preventing the material transfer between shell and core and downstream filter is preferred to improve the conditions of downstream face. Since the scope of this study is limited to upstream face as stated above, only two types of materials are used which are clay for the core and compacted sandy gravel with some clay for the shells.

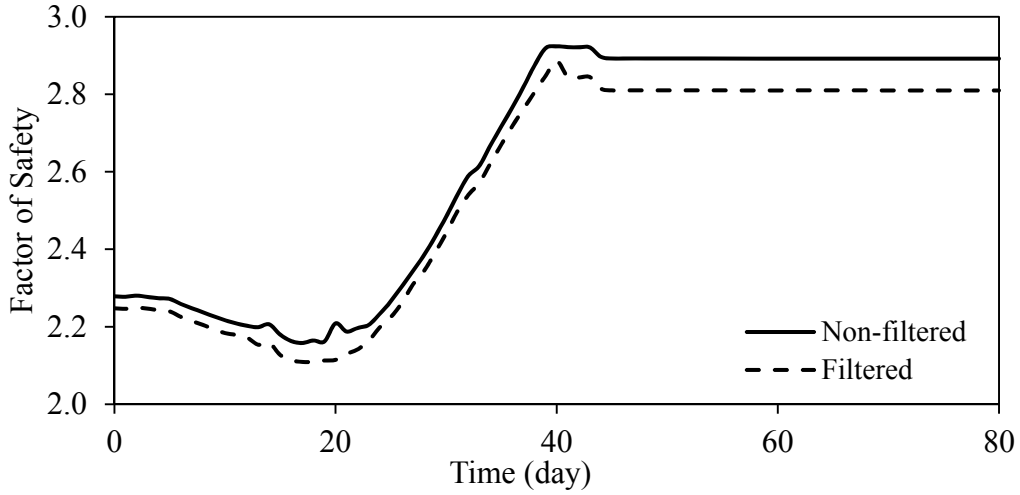

Figure 4.4. Typical factor of safety with respect to time graph for an arbitrary cross-section under rapid fill condition

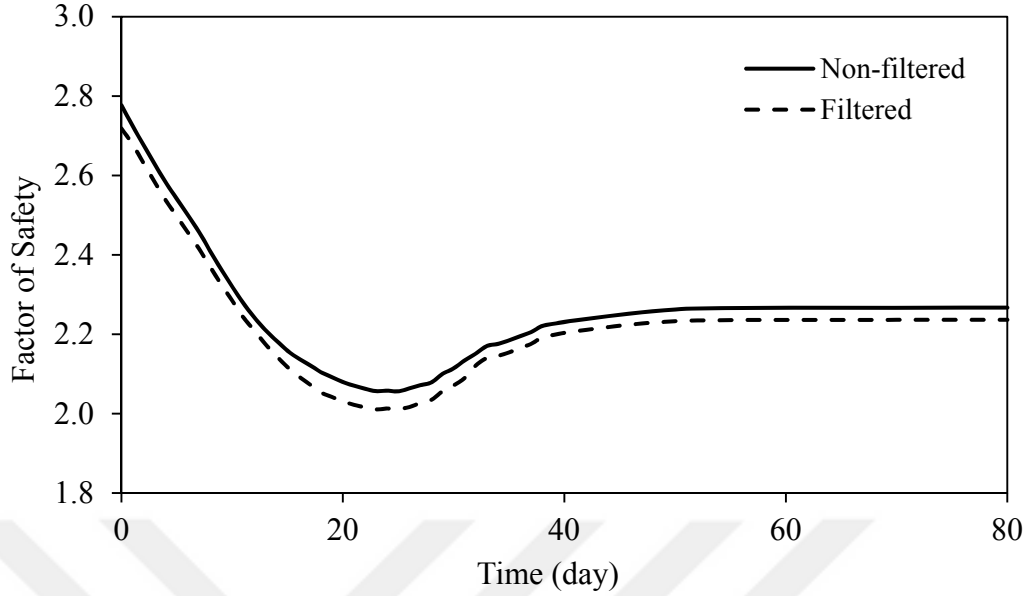

Figure 4.5. Typical factor of safety with respect to time graph for the same cross-section under rapid drawdown condition

Table 4.6 Analysis results for drawdown rate = 0.50 m/day, *c*=40 kPa, *Ø*=26°

Upstream Slope	1V:3H		1V:3.5H		1V:4H	
Dam Height (m)	**Critical Water Elevation (m)**	**Critical Duration (day)**	**Critical Water Elevation (m)**	**Critical Duration (day)**	**Critical Water Elevation (m)**	**Critical Duration (day)**
40	7.5	59	9	56	11.5	51
60	13	88	13	88	13	88
80	21.5	111	20	114	23.5	107
100	27.5	139	22.5	149	27	140
120	35.5	163	35	164	36	162
140	42	190	45.5	183	37.5	199
160	52	210	52.5	209	50.5	213
180	51.5	251	63	228	52.5	249
200	69.5	255	65.5	263	70.5	253

4.2 Rapid Fill Condition

During rapid fill the rising water level starts to build a resisting force in favor of slope stability such that safety factor increases. Subsequently, shell material gets saturated and driving force takes place. Therefore, safety factor decreases and remains constant as the pore water pressure reaches to the maximum level as already shown by Çalamak et al. (2020) (see Figure 4.4.).

4.3 Rapid Drawdown Condition

Hydrostatic pressure supports the upstream face in favor of stability in full reservoir condition but once this pressure starts to diminish due to drawdown, soil material of the dam body still remains saturated. This saturation requires some time to dissipate depending on the permeability of the soil. If drawdown rate is greater than it must be, water within the soil starts to seep towards the upstream face and negative pressure occurs. Negative pressure decreases the safety factor of the upstream face (see Figure 4.5). After a point, driving forces get bigger than the resisting forces and the upstream face loses its slope stability and consequently the failure occurs (Khassaf et al., 2013). After a while safety factor starts to increase. This behaviour comes into view by the relationship between pore water pressure and hydrostatic pressure of the stored water. As the stabilizer action of the water stored in the reservoir decreases due to the drawdown, pore water pressure keeps acting against. At a point, pore water pressure starts to dissipate and its action disappears as well. Eventually the slope gets capable of supporting itself with the absence of any undesirable force such that factor of safety starts to increase. This phenomenon is inherent for all earth-fill dams under drawdown condition.

Figures 4.4 and 4.5 show that the rapid drawdown leads to more critical situations when compared to the results of rapid fill condition. For this reason, results of rapid drawdown condition have been focused on while considering the most critical behaviour of the dam.

4.4 Dam Behaviour

Safety factor distributions obtained by the analyses are collected for all heights. The minimum safety factors obtained among several assumed failure arcs in the software for each analyses are considered as the critical state. Duration of the critical state and height of the water level at that time are termed as “critical duration” and “critical water elevation”. This process is also applied for all slopes and summarized for each value of drawdown rate as shown in Tables 4.6-4.10.

The variation of critical safety factor with respect to height for different slopes and drawdown rates is examined (see Figures 4.6-4.10) to comprehend their effect on the behaviour.

Table 4.7 Analysis results for drawdown rate = 0.75 m/day, c=40 kPa, $\emptyset$=26°

Upstream Slope	1V:3H		1V:3.5H		1V:4H	
Dam Height (m)	**Critical Water Elevation (m)**	**Critical Duration (day)**	**Critical Water Elevation (m)**	**Critical Duration (day)**	**Critical Water Elevation (m)**	**Critical Duration (day)**
40	9.25	37	8.5	38	12.25	33
60	15	56	12.75	59	18	52
80	24.5	70	23	72	21.5	74
100	32.5	86	31.75	87	23.5	98
120	41.25	101	36	108	32.25	113
140	44.75	123	52.25	113	38	132
160	55	136	52	140	52	140
180	63	152	51	168	52.5	166
200	68.75	171	56	188	70.25	169

Table 4.8 Analysis results for drawdown rate = 1.00 m/day, *c*=40 kPa, *Ø*=26°

Upstream Slope	1V:3H		1V:3.5H		1V:4H	
Dam Height (m)	**Critical Water Elevation (m)**	**Critical Duration (day)**	**Critical Water Elevation (m)**	**Critical Duration (day)**	**Critical Water Elevation (m)**	**Critical Duration (day)**
40	5	32	8	29	12	25
60	13	44	15	42	14	43
80	26	51	23	54	18	59
100	33	64	34	63	31	66
120	27	90	36	81	35	82
140	55	82	44	93	39	98
160	55	102	50	107	52	105
180	61	116	58	119	59	118
200	61	136	72	125	54	143

Table 4.9 Analysis results for drawdown rate = 1.50 m/day, *c*=40 kPa, *Ø*=26°

Upstream Slope	1V:3H		1V:3.5H		1V:4H	
Dam Height (m)	**Critical Water Elevation (m)**	**Critical Duration (day)**	**Critical Water Elevation (m)**	**Critical Duration (day)**	**Critical Water Elevation (m)**	**Critical Duration (day)**
40	7	20	8.5	19	7	20
60	15	28	12	30	21	26
80	24.5	35	21.5	37	18.5	41
100	32.5	43	25	48	23.5	51
120	33	56	36	54	33	58
140	42.5	63	42.5	63	51.5	59
160	59.5	65	50.5	71	49	74
180	54	82	66	74	52.5	85
200	66.5	87	63.5	89	69.5	87

Table 4.10 Analysis results for drawdown rate = 2.00 m/day, *c*=40 kPa, *Ø*=26°

Upstream Slope	1V:3H		1V:3.5H		1V:4H	
Dam Height (m)	**Critical Water Elevation (m)**	**Critical Duration (day)**	**Critical Water Elevation (m)**	**Critical Duration (day)**	**Critical Water Elevation (m)**	**Critical Duration (day)**
40	7	15	7	15	7	15
60	15	21	11	23	9	24
80	25	26	21	28	15	31
100	31	33	23	37	27	35
120	33	42	25	46	31	43
140	45	46	41	48	45	46
160	65	46	47	55	41	58
180	57	60	65	56	47	65
200	61	68	71	63	65	66

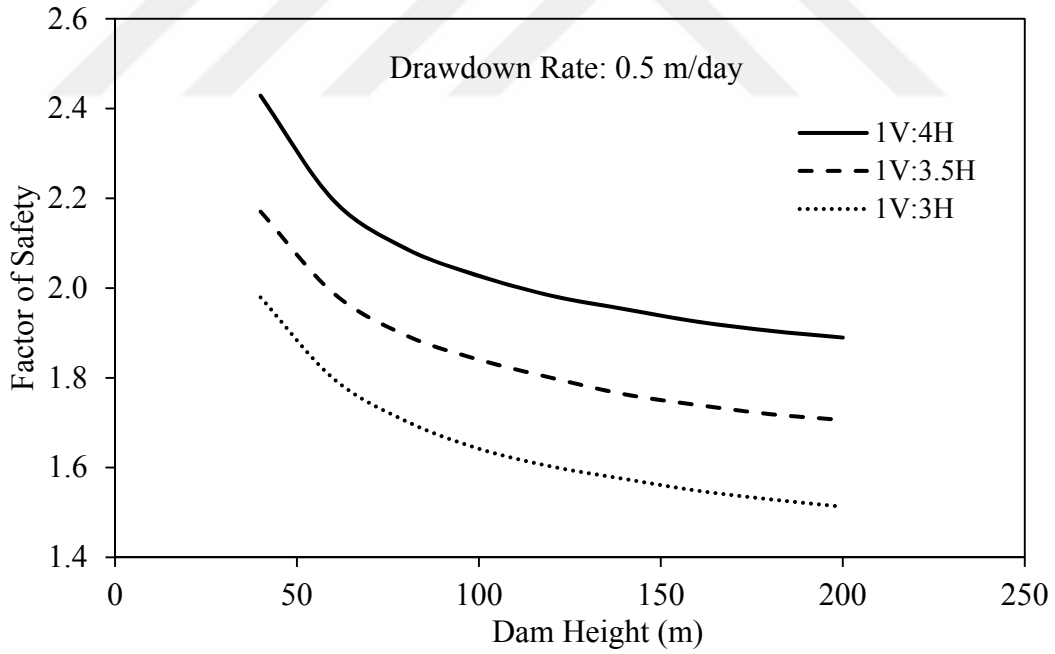

Figure 4.6. Critical safety factor of upstream slope with respect to height for drawdown rate = 0.50 m/day, *c*=40 kPa, *Ø*=26°

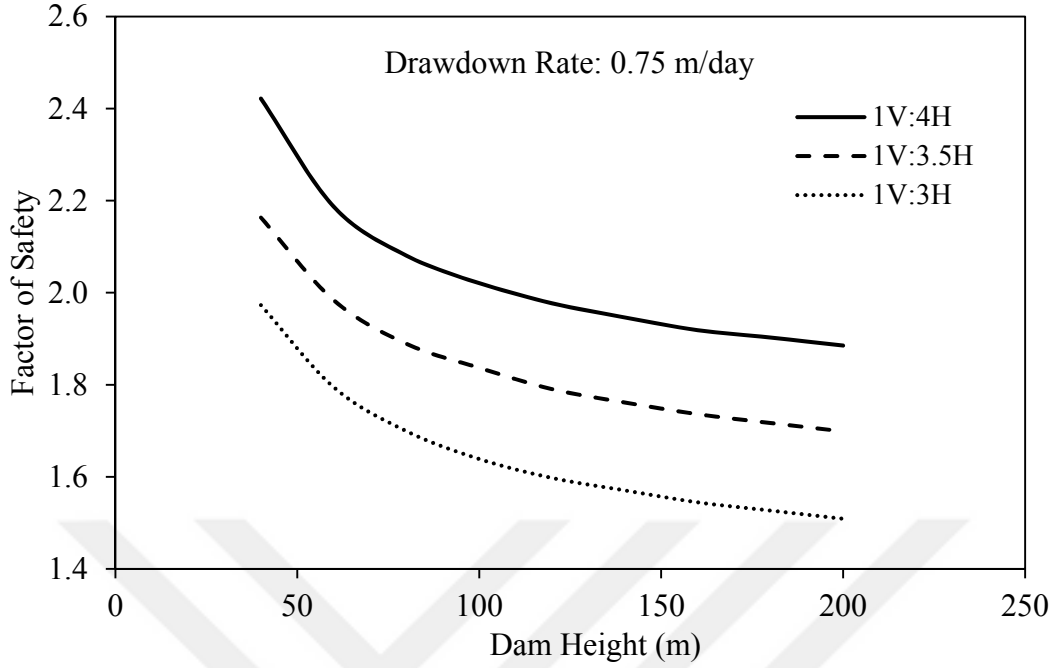

Figure 4.7. Critical safety factor of upstream slope with respect to height for drawdown rate = 0.75 m/day, c=40 kPa, $\emptyset$=26°

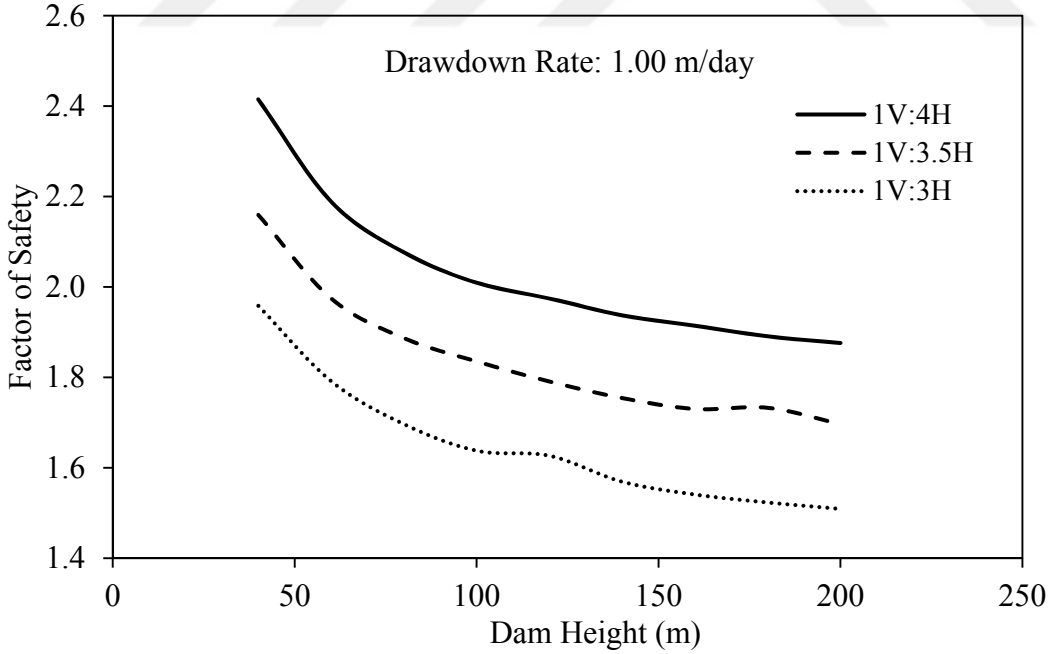

Figure 4.8. Critical safety factor of upstream slope with respect to height for drawdown rate = 1.00 m/day, c=40 kPa, $\emptyset$=26°

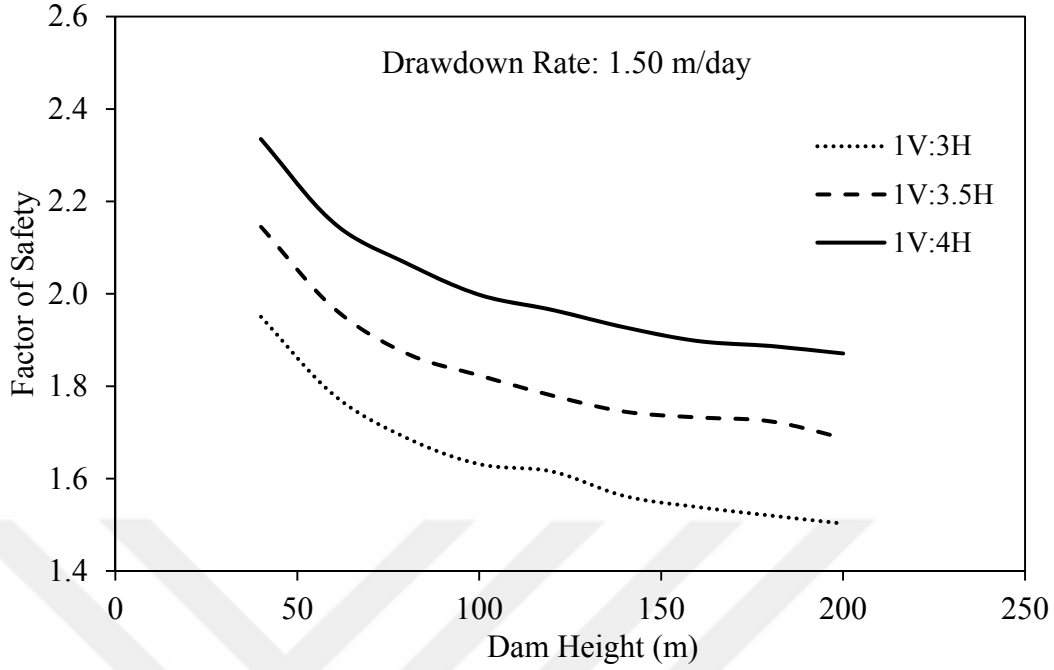

Figure 4.9. Critical safety factor of upstream slope with respect to height for drawdown rate = 1.50 m/day, c=40 kPa, $\emptyset$=26°

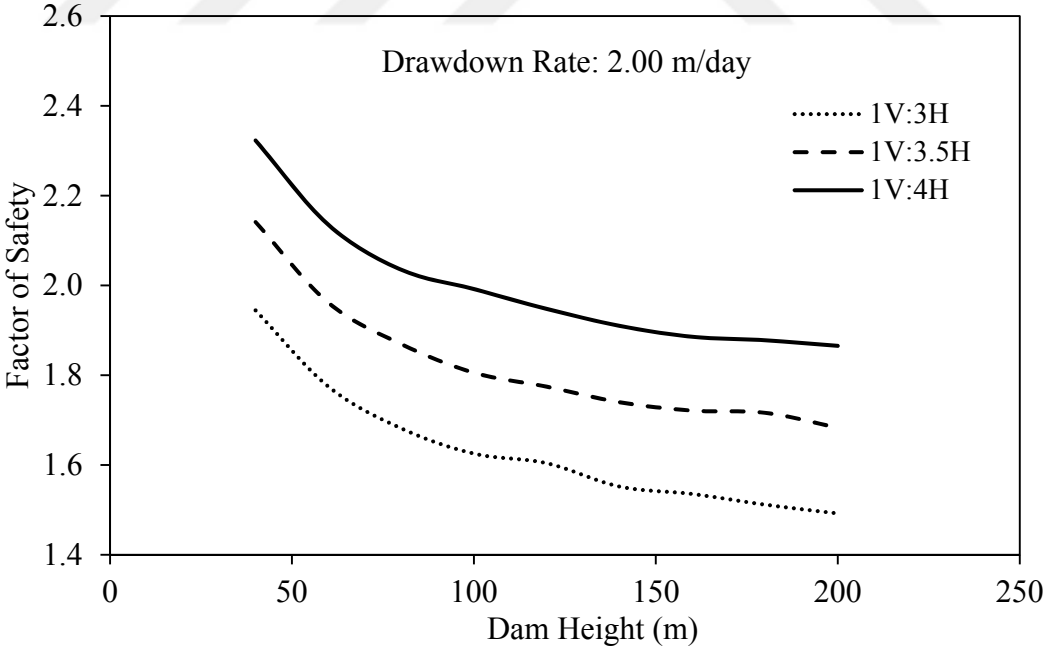

Figure 4.10. Critical safety factor of upstream slope with respect to height for drawdown rate = 2.00 m/day, c=40 kPa, $\emptyset$=26°

It can be seen in Figures 4.6-4.10 that safety factor decreases while dam height and slope of the upstream increases. Similarly, increasing the drawdown rate affects the stability in unfavorable way. Also it is obvious that the change in drawdown rate does not have significant effect on stability even when it is in rate of 2 m/day. Consequently, results of the analyses conducted in this chapter state that geometrical parameters, such as upstream slope angle and embankment height are more dominant and governing parameters for the stability when compared with drawdown rate.

The same analyses have been conducted for c=40 kPa, $\emptyset$=20° and c=40 kPa, $\emptyset$=35° successively to see the effect of friction angle on the behaviour. Similarly, variation of the critical safety factor is examined again by using different friction angle values (see Figures 4.11-4.20).

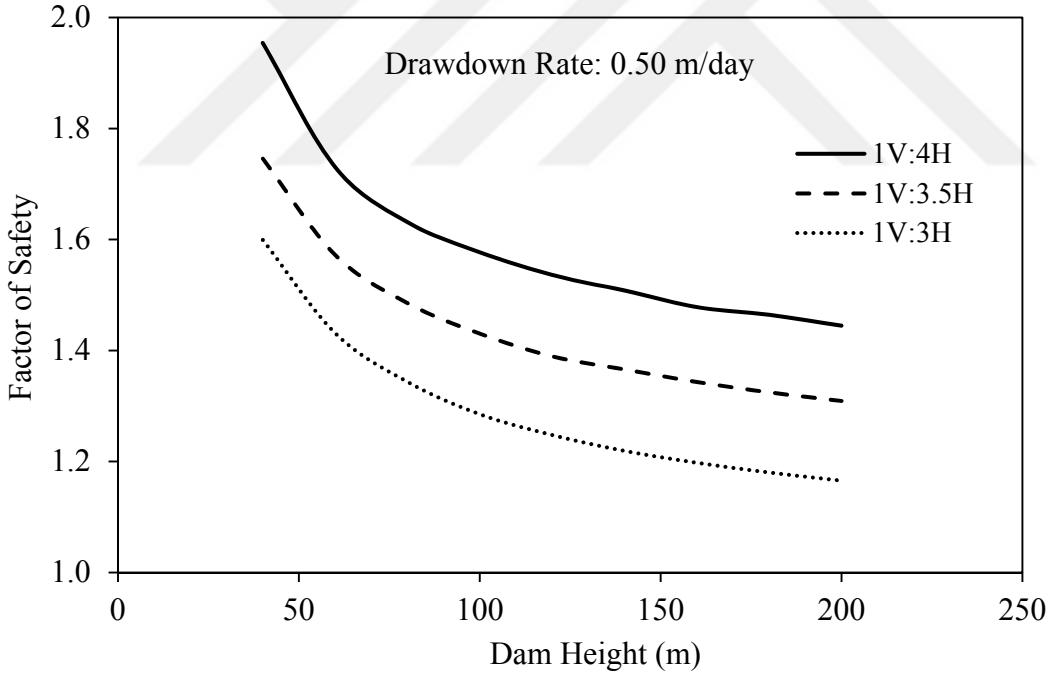

Figure 4.11. Critical safety factor of upstream slope with respect to height for drawdown rate = 0.50 m/day, c=40 kPa, $\emptyset$=20°

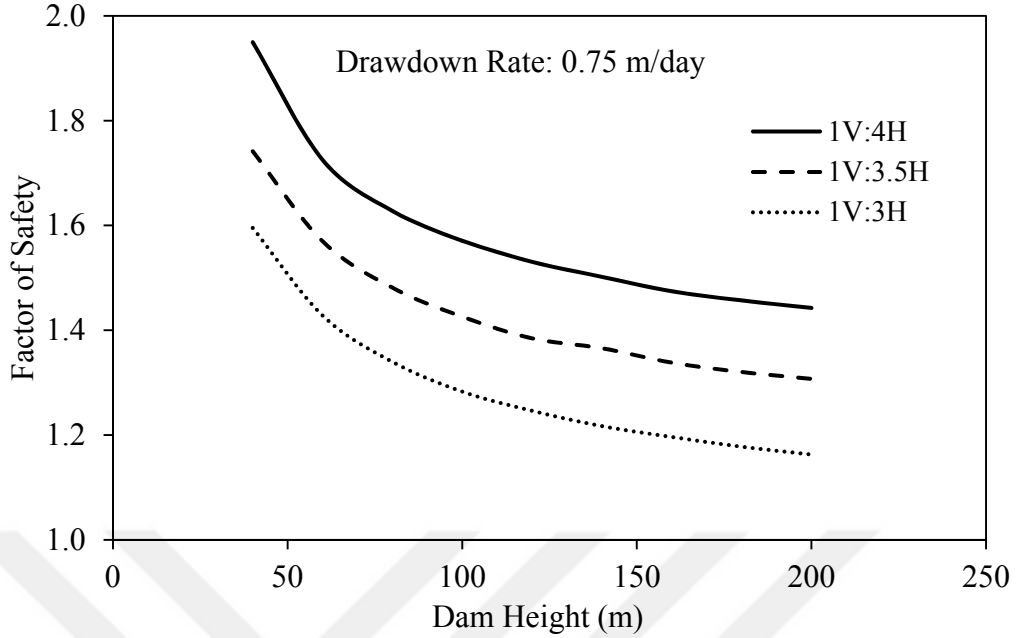

Figure 4.12. Critical safety factor of upstream slope with respect to height for drawdown rate = 0.75 m/day, c=40 kPa, $\emptyset$=20°

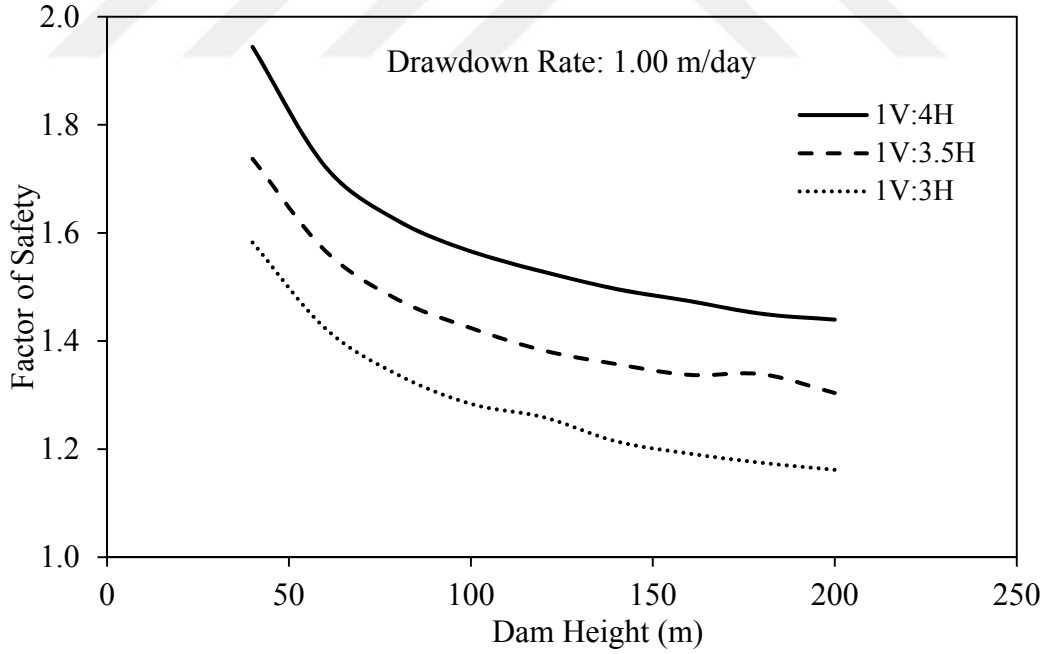

Figure 4.13. Critical safety factor of upstream slope with respect to height for drawdown rate = 1.00 m/day, c=40 kPa, $\emptyset$=20°

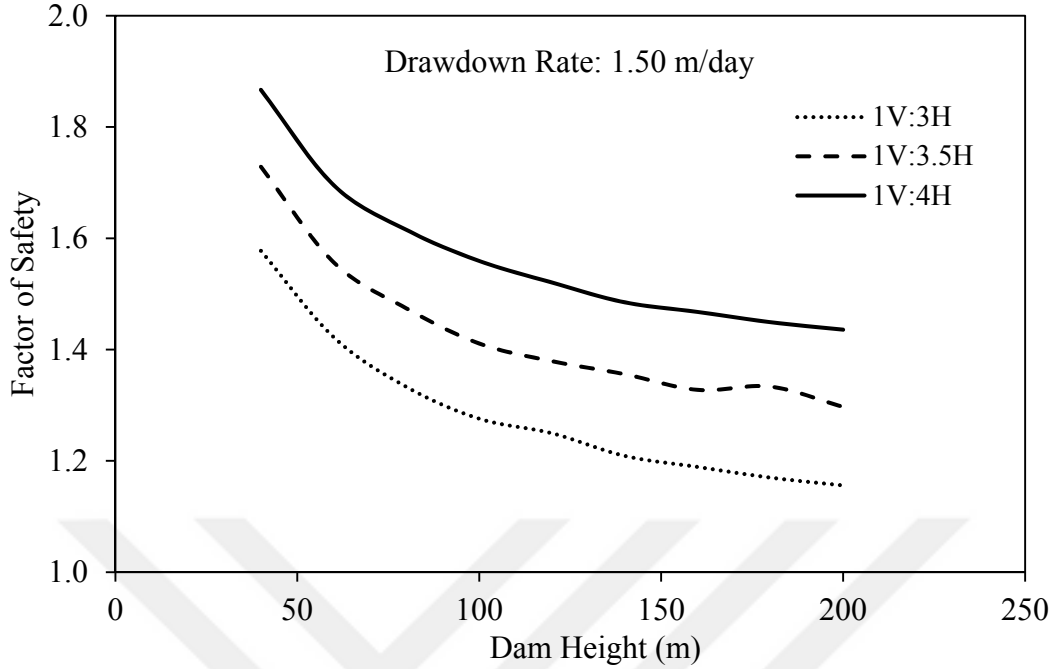

Figure 4.14. Critical safety factor of upstream slope with respect to height for drawdown rate = 1.50 m/day, c=40 kPa, $\emptyset$=20°

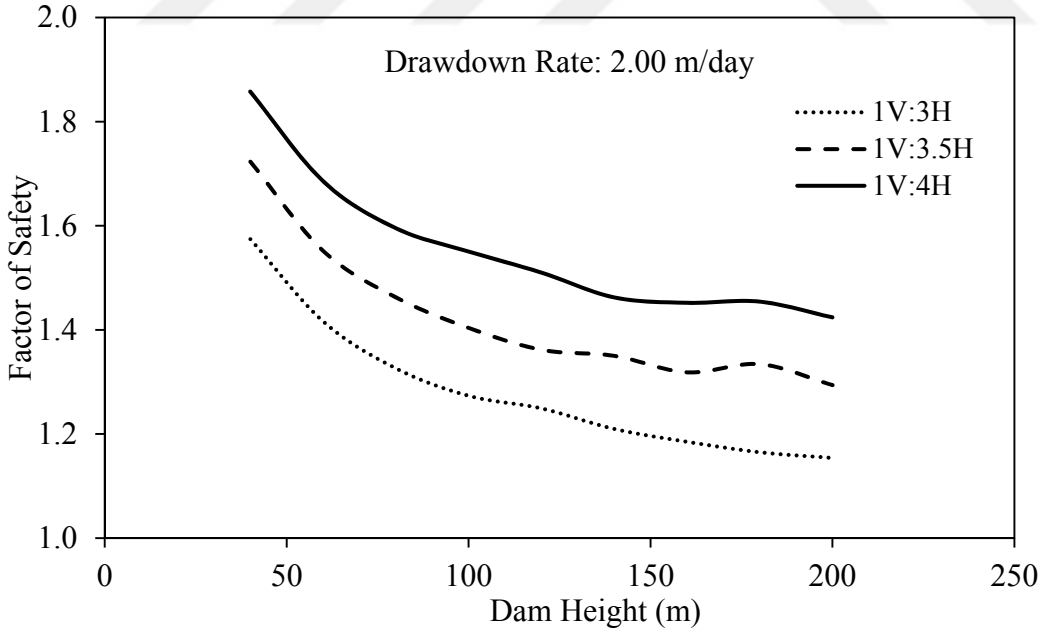

Figure 4.15. Critical safety factor of upstream slope with respect to height for drawdown rate = 2.00 m/day, c=40 kPa, $\emptyset$=20°

Figures 4.11-4.15 show that increasing the friction angle increases the stability.

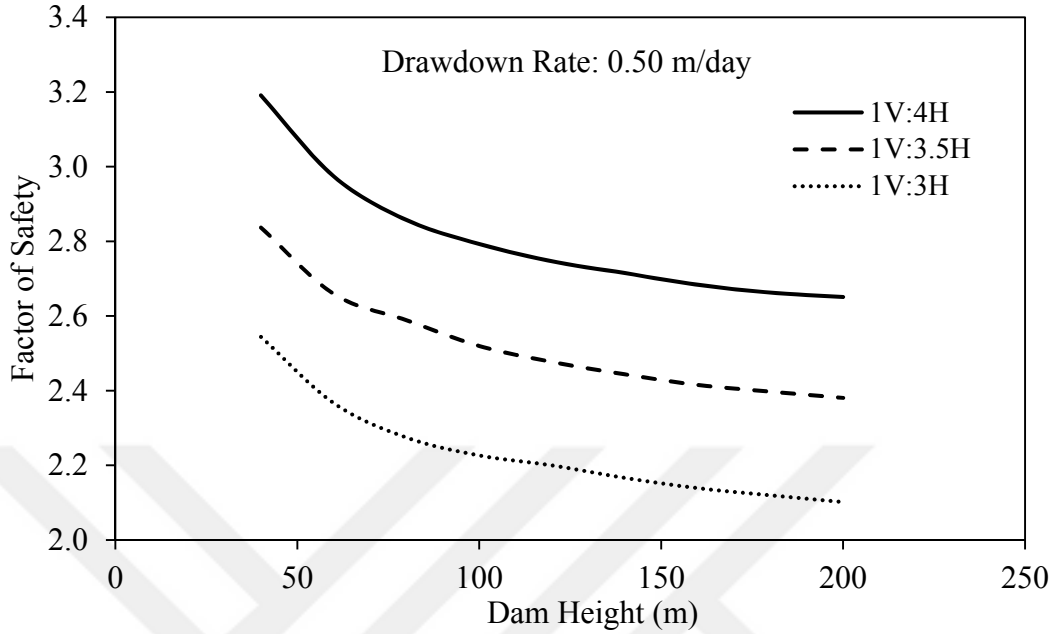

Figure 4.16. Critical safety factor of upstream slope with respect to height for drawdown rate = 0.50 m/day, *c*=40 kPa, *Ø*=35°

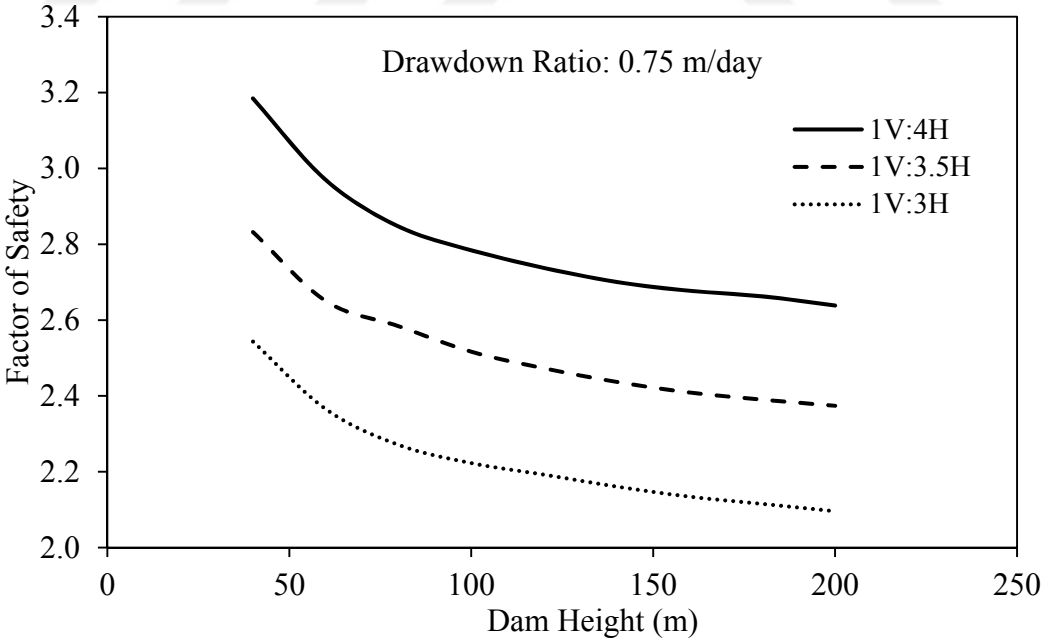

Figure 4.17. Critical safety factor of upstream slope with respect to height for drawdown rate = 0.75 m/day, *c*=40 kPa, *Ø*=35°

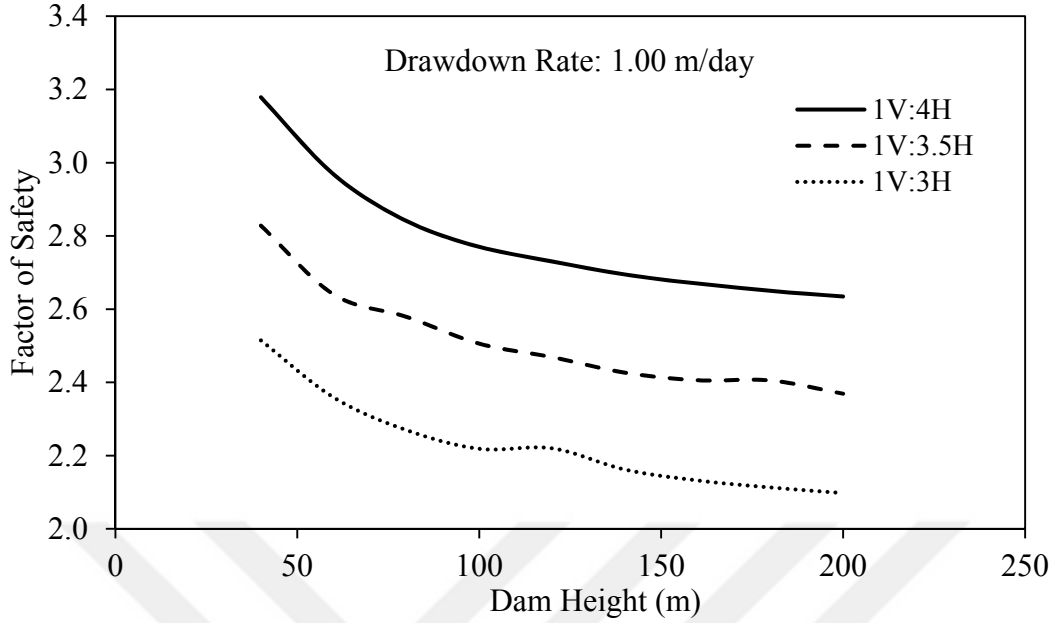

Figure 4.18. Critical safety factor of upstream slope with respect to height for drawdown rate = 1.00 m/day, *c*=40 kPa, *Ø*=35°

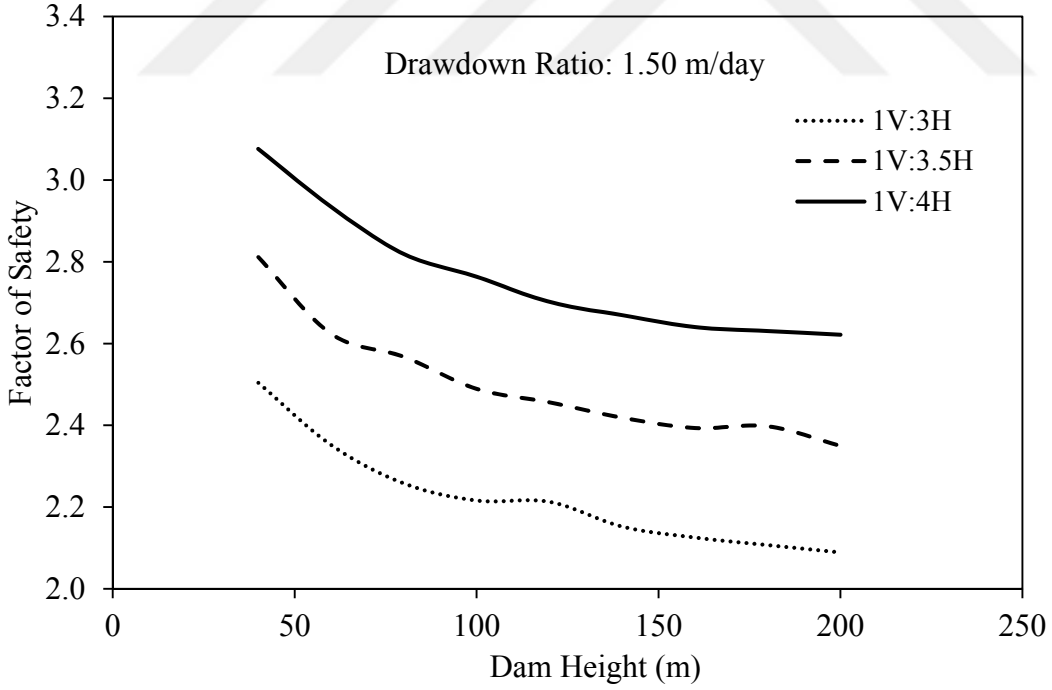

Figure 4.19. Critical safety factor of upstream slope with respect to height for drawdown rate = 1.50 m/day, *c*=40 kPa, *Ø*=35°

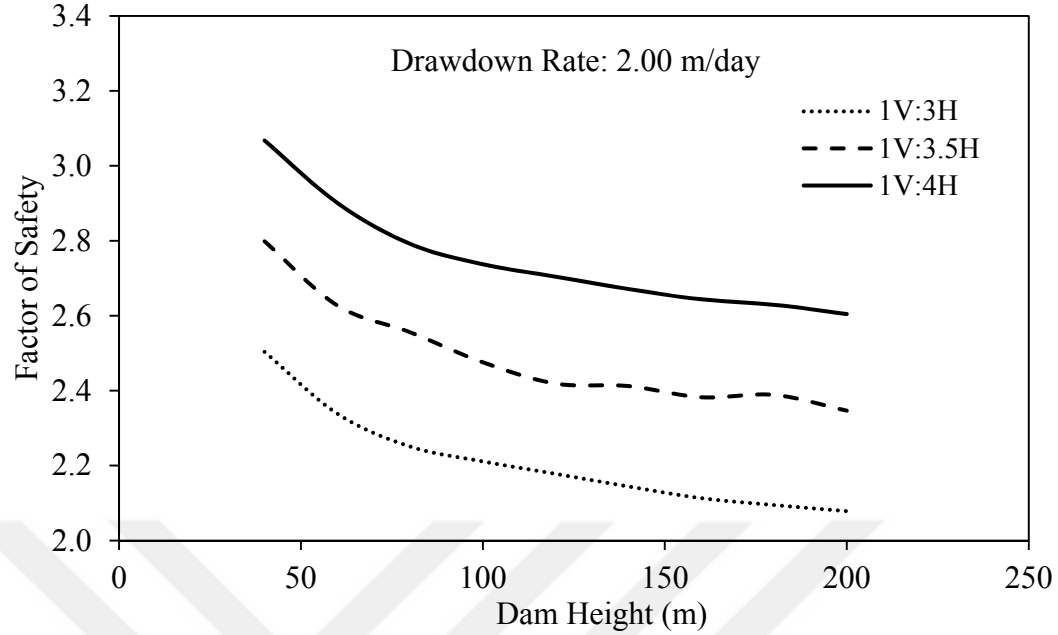

Figure 4.20. Critical safety factor of upstream slope with respect to height for drawdown rate = 2.00 m/day, c=40 kPa, $\emptyset$=35°

As can be seen from Figures 4.16-4.20, higher friction angle significantly increases the stability.

The results show that higher friction angle increases the slope stability. Since this parameter is essential for shear strength, any increment friction angle inherently increases the slope stability.

Slope of the upstream face also has significant effect on the stability as well as the friction angle, especially when compared with drawdown rate.

Inferentially, it must be noted that higher dams with steeper slopes are more risky due to having lower safety factors (see Figures 4.6-4.20). Therefore, it is obvious to conclude that monitoring higher structures is a crucial procedure that requires the best method to be used. Dam behaviour has been assessed with respect to some transient conditions using the software. During the operational conditions, similar analyses may be conducted using the actual pore water pressure values obtained from the piezometers.

CHAPTER 5

PIEZOMETER LAYOUT DETERMINATION

5.1 General

Many parameters need to be determined in design stage of embankment dams. In this prespective, field and laboratory measurements are conducted to evaluate the characteristics of the materials to be used in the dam body. Besides, some simplifying assumptions may also be made about some characteristics that cannot be identified easily because of highly heterogeneous composition of the fill materials and foundation soil. On the other hand, some uncertainties may be assocciated with the design, construction, controlling, and operation of the embankment dams. Therefore, it is of vital importance to assess the behaviour of such dams not only during the construction, filling process of their reservoirs, but also during the operational conditions along their physical lives. Dam instrumentation provide invaluable information about various parameters such that time-dependent dam behaviour can be assessed and design assumptions can be verified. Degree and type of instrumentation should be sufficient to have a realistic picture of the structure such that reliable assessments can be conducted and necessary remedial measures can be taken at the right time, if necessary. This study specifically focuses on determination of a reliable layout of vibrating wire piezometers in conventional earth-fill dams having clay cores. Throughout the chapter, the term “piezometer” stands for vibrating wire piezometer.

5.2 Piezometer Layout Determination

Improper design, use of problematic soil in dam body, and insuffient checks during construction may eventually lead to formation of concentrated seepage paths in the

body after the initial filling or during operational period of an embankment dam. As stated before, dam behavior should be monitored continuously by an integrated instrumentation system. As dam safety assessment based on proper instrumentation system is considered as an integral part of contemporary dam design, special attention should be paid on instrumentation layout design. However, there are no specified standards for determining the proper layout of such a system for monitoring of dams. As every dam is unique in terms of its site and design-specific conditions, such as hazard potential, material characteristics of the dam body and foundation, sophistication of the design procedures, degree of constructional care, etc., a proper configuration for an instrumentation system is suggested using engineering judgement and experience. Earth-fill dams should be supplemented with sufficient number of piezometers both at the foundation and dam body to collect local information, which will give an opportunity to check design assumptions during construction, initial filling, and for long-term monitoring during operation.

Piezometers yield pore water pressure measurements. Therefore, with the availability of sufficient number of piezometers, distributed throughout the dam body, the pore water pressure distribution within the embankment and phreatic line can be obtained. This information can be used for checking possibility of undesirable increase in pore water pressure value at a particular location or for computing instantaneous slope stability safety factor using real time data. Therefore, indicators of hazard potential of the embankment are highly based on availability of sufficient and reliable data obtained from piezometers.

One of the most critical conditions may be considered as upstream slope instability. Therefore, computing safety factors against the sliding under steady state, rapid fill, and rapid drawdown conditions need to be analyzed as handled in the previous chapter. A severe drawdown and fill rate is considered in this study to observe remarkable rapid changes in phreatic lines. Based on daily changes in regulation policies of reservoirs, a drawdown rate of 0.1 m/day is common; whereas a drawdown rate of 0.5 m/day is considered to be severe. On the other hand, drawdown rates exceeding 1 m/day are considered to be exceptional (Puigmarti et al. 2008). In

this study placement layout of piezometers is dictated according to the position of the phretaic line during the most critical condition. To this end, the phreatic lines corresponding to the minimum safety factor against sliding of the upstream slope during rapid drawdown and fill conditions are considered and a severe value, i.e. 2 m/day, is considered for both rapid drawdown and fill. Another assumption is made for the recession level of water in the reservoir. It is assumed that rapid drawdown takes place from the maximum reservoir level up to 70% of it. Rapid fill is assumed to start from the empty reservoir condition to the maximum reservoir level. However, as water level in the reservoir increases rapidly, the change in the phreatic line is quite low and the phreatic line corresponding to the critical safety factor remains at relatively low elevations in the dam body. Therefore, distribution of the piezometers throughout the dam body using this information would not be realistic as the piezometers in the upper layers will be subjected to very high negative pressures. That is why piezometer placement logic is decided to base on the more critical condition, i.e. the rapid drawdown case. As already explained in Chapter 4, this case also yields smaller safety factors as compared to the case of rapid fill.

In the analyses, heights of model earth-fill dams are chosen as 40 m, 60 m, 80 m, 100 m, and 120 m. As already explained in Chapter 4, the side slopes of both upstream and downstream shells are chosen as 1V:3H and the symmetrical side slopes of the clay core are 1V:0.5H. A filter zone, with a thickness of 3 m is used at both upstream and downstream sides of the clay core. The mesh size is used as 1 m to precisely obtain the geometry of the phreatic line.

The best piezometer placement configuration is to be searched for the aforementioned critical conditions. The following guidelines based on review of Turkish and international practice are applied in the development of piezometer layout scheme.

- One piezometer should be located at a low elevation in the filter, downstream of the core to monitor the effectiveness of the drainage system during filling

or operational process. Any unexpected increase in pore water pressure may be considered as a clogging problem of the filter.

- For highly compressible foundation material having low permeability, piezometers should also be placed in the foundation to measure seepage coming from the reservoir. However, foundation placement is not covered in this study.
- Trenches are drilled to install instruments and their appurtenaces. Drilling may damage the body, filter, and transition zones in close vicinity to the equipment and trigger internal erosion process. To offset this, a minimum of 5 m is to be placed between the piezometer and the core-filter interaction zone to eliminate possible increased openings during the installation. The same caution is also taken in the shell zone. This limitation leads to minimization of the number of piezometers or use of only sufficient number of piezometers that are enough to capture the phreatic line with the desired accuracy.
- Compaction quality is of utmost importance for embankment dams. Therefore, successive checks need to conducted for pore water pressures using the information obtained from piezometers. That is why probably more piezometers may be installed to monitor the construction process, especially during the initial filling than are required for long-term operation. It is to be aimed that some of the instruments used during the initial filling and construction should also be utilized for long-term monitoring upon completion of the dam.
- For long-term monitoring of embankment dams, at least one line of piezometers located along a transverse plane at the maximum section is recommended. However, considering various operational conditions throughout the physical life of an embankment dam, including rapid drawdown, unexpected increase of phreatic line due to clogging of the filter, etc., piezometers should also be located at higher elevations such that the quick response as a result of abrupt fluctuation in pore water pressure, is

easily obtained. The piezometers located at low elevations may be subject to a time-lag to get the information as a result of rapid change in phreatic line elevation. The time-lag may depend on the magnitude of the change of pore water pressure and type, characteristics, and degree of compaction of the fill material. An example to a multi-layer piezometer placement is shown in Figures 5.1 and 5.2. From economy viewpoint, minimum instrumentation should be installed provided that the information gathered from piezometers is enough to assess the behavior of the dam. Usually, minimum instrumentation (3 to 4) should be installed along a transverse section at a particular elevation of the dam concerned.

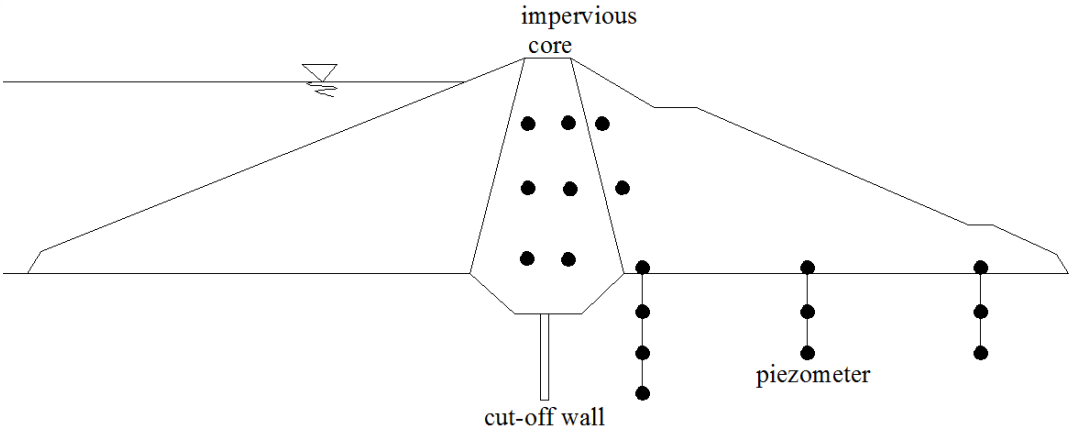

Figure 5.1. Typical piezometer application to an embankment dam (retrieved from: https://www.sisgeo.com/products/piezometers/item/vibrating-wire-piezometers.html)

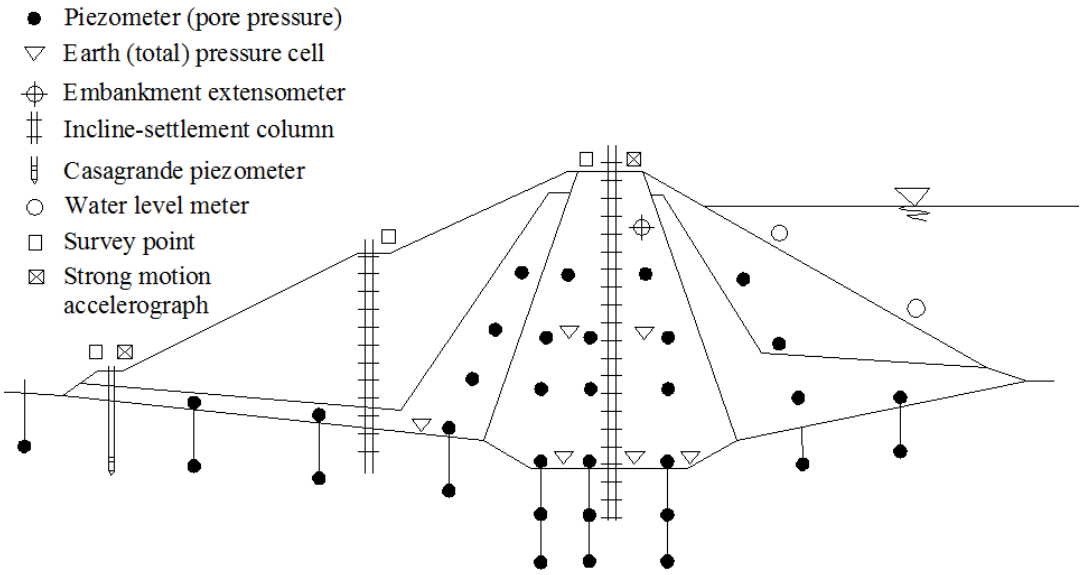

Figure 5.2 Typical instrumentation layout for an earth-fill dam (retrieved from: https://en.geotechnicsvn.com/supplying-installing-environmental-geotechnical-instrumentation-hydropower-dam-reservoir/)

It is advisable to install redundant piezometers considering the possibility of malfunction. If any sensor becomes inaccessible for replacement, the others located at different transverse sections may be used. Placement of more closely spaced piezometers or different instruments to measure the same feature may also be considered. For example, a piezometer may be accompanied by a total pressure cell in its close proximity (GILD, 2018).

Arı and Yanmaz (2018) proposed an optimum layout for pressure cells to be placed in CFRDs. As stated before, total pressure cells are normally placed in conjunction with vibrating wire piezometers (See Figure 5.3). Therefore, a similar layout as proposed by Arı and Yanmaz (2018) for total pressure cell configuration is assumed to be reasonable for piezometer placement in earth-fill dams. In other words, this configuration is accepted to be the starting point as maximum placement configuration for earth-fill dams and the reduction of piezometers one by one from this scheme is studied in view of the corresponding effect on the ability of the piezometers to capture the locus of the phreatic line with a reasonable accuracy. In

the analyses, it is assumed that the locus of phreatic line obtained by the software Geostudio is error-free and the piezometers are accepted to give exactly the same head value as the software.

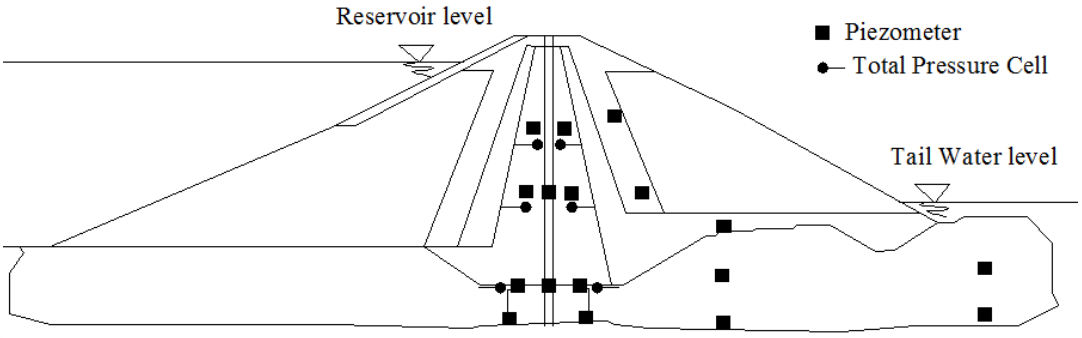

Figure 5.3 Total pressure cell and piezometer layout in an earth-fill dam (Konietzky, 2020)

According to the aforementioned information, the inital piezometer layouts for each dam height are selected as shown Figures 5.4-5.8. In these analyses, downstream shell is not taken into account because it is known that pore water pressure is a key variable for upstream and core sections under the aforementioned operating conditions, i.e. rapid fill and drawdown. On the other hand, effectively functioning cores reduces phreatic lines to very low elevations at the downstream shell for which placement of piezometers becomes unnecessary.

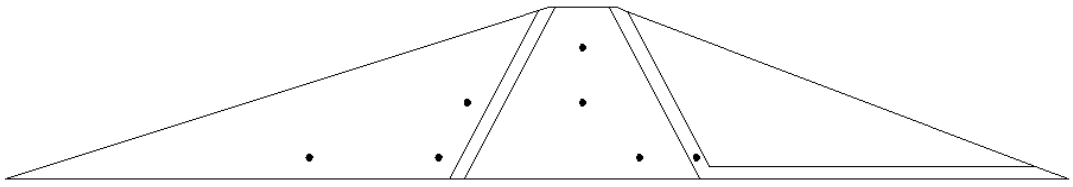

Figure 5.4. Layout scheme for H=40 m

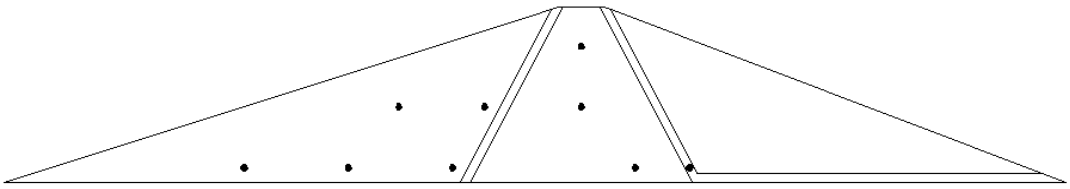

Figure 5.5. Layout scheme for H=60 m

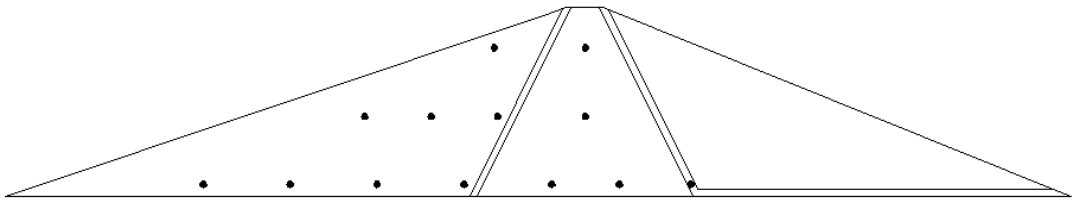

Figure 5.6. Layout scheme for H=80 m

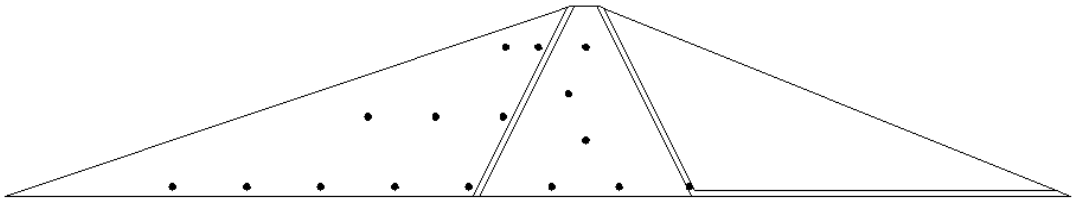

Figure 5.7. Layout scheme for H=100 m

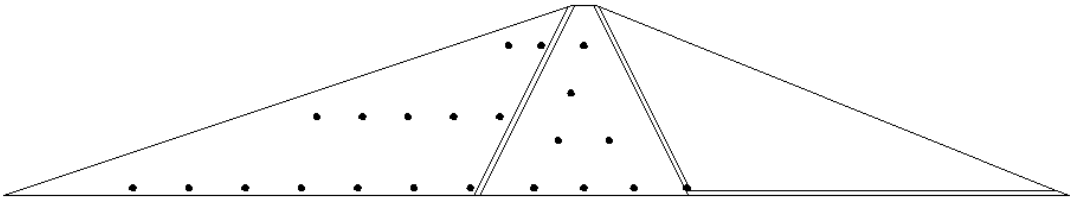

Figure 5.8. Layout scheme for H=120 m

Since these layouts are all obtained for the most critical condition, i.e. up to 70% lowering of the reservoir level under rapid drawdown condition, performance of these piezometers with respect to different conditions need to be assessed as well. To this end, first, accuracies of the layouts of the piezometers are evaluated with respect to their ability in capturing the pore water pressure distribution. For this reason, the area under the phreatic line in the most critical condition is focused.

At the beginning, the layout for H=120 m is examined. The actual area under the phreatic line is compared with the area calculated by the piezometers. In the maximum layout, there are 12 piezometers under the phreatic line (see Figure 5.9). Therefore, the data taken only from these piezometers will provide the information about the locus of the phreatic line.

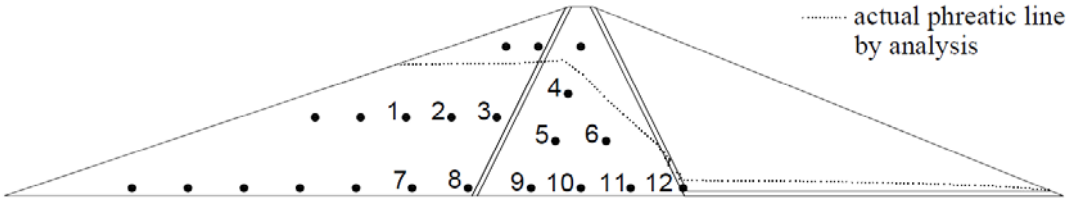

Figure 5.9. Piezometers under the phreatic line for H=120 m

The piezometers record the pore water pressure in the form of lines in vertical direction. These lines start from the point where devices are placed on and extend to the phreatic line. Intersection points of the vertical lines and the phreatic line represent the measurements of the piezometers. The calculated area is created by connecting these measurement points of the piezometers. When these points are connected with straight lines, the phreatic line is approximately obtained as shown in Figure 5.10.

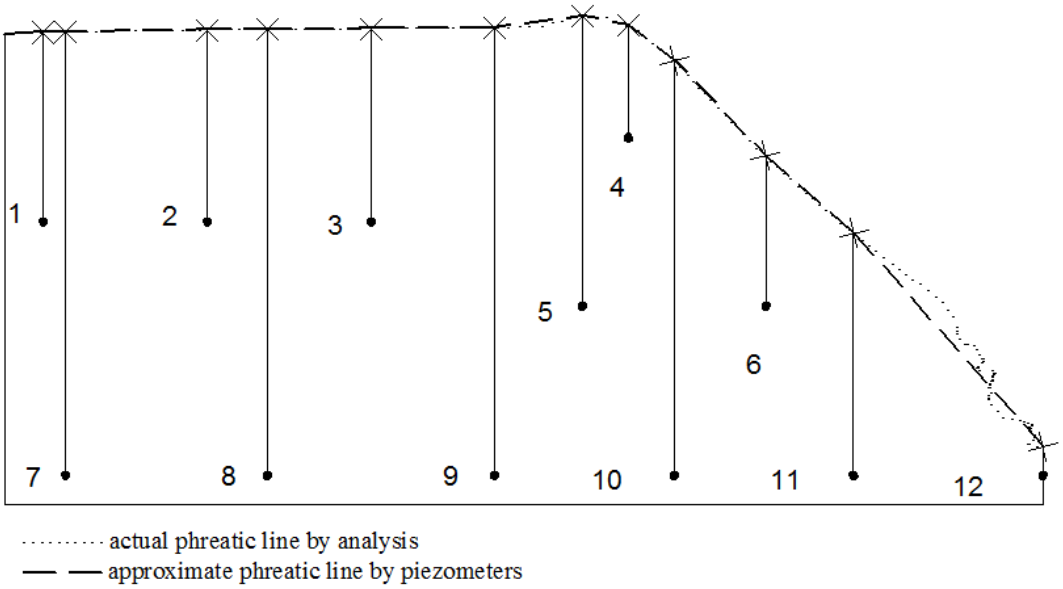

Figure 5.10. Comparison of actual and approximate phreatic lines for H=120 m

In the maximum placement, the area under approximate phreatic line is calculated as 12876.35 m² while the area under the actual phreatic line is 12938.70 m². This means that this layout provides 99.518% of the actual information about the pore water pressure distribution. However, since a designer may search for a more economical

layout, then the performance obtained from less piezometers should also be observed. To this end, decreasing the number of piezometers one by one can be evaluated as explained below.

To use 11 piezometers, there will be 11 alternatives to decide on those to be utilized out of 12 piezometers. For this reason, every alternative with 11 piezometers are to be examined separately. Each piezometer has been successively taken out from the initial maximum configuration and the area under the approximate phreatic line is calculated by the remaining piezometers. The best alternative is obtained as the one giving the maximum area which is closest but smaller than the area calculated by 12 piezometer-configuration. The alternatives that give greater areas than the area calculated by 12 piezometers are ignored because when some of the piezometers are taken out, the approximate line stays above the actual line, which is contrary to the accepted practice. Therefore, any alternative that gives area ratio greater than 99.518% is ignored. The maximum area ratio, closest but smaller than the 99.518%, is then selected. The comparisons of each alternative are given in Figures 5.11-5.21.

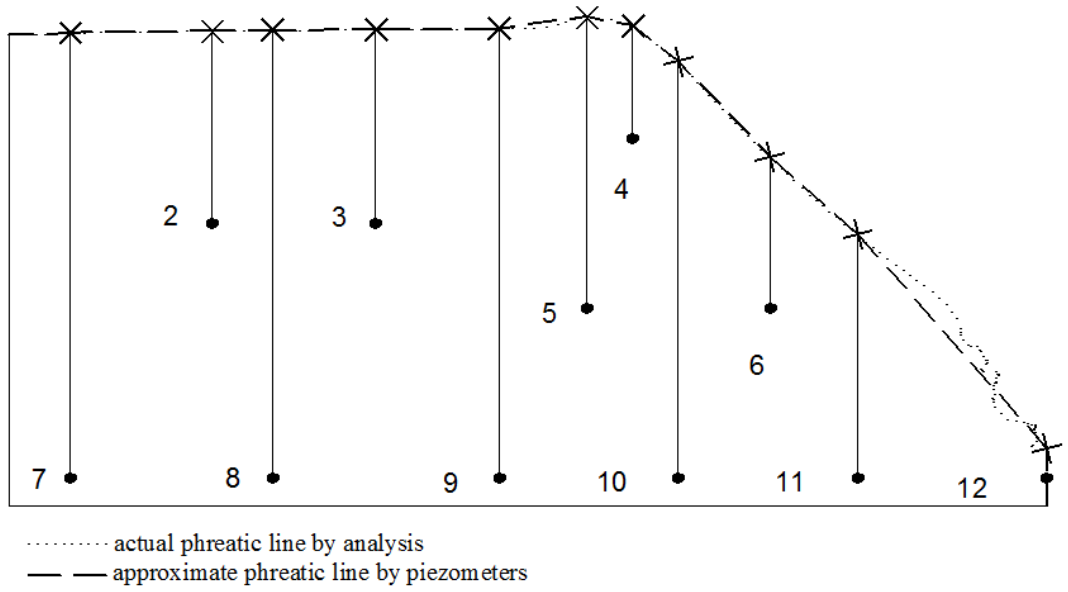

Figure 5.11. Comparison of actual and approximate phreatic lines when piezometer 1 is taken out for H=120 m (area ratio: 99.517%)

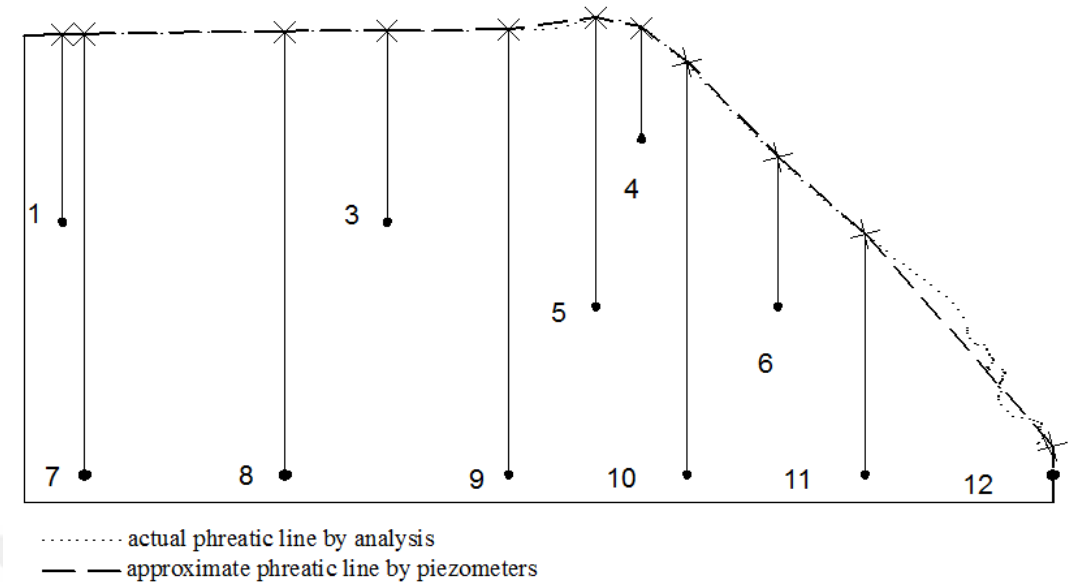

Figure 5.12. Comparison of actual and approximate phreatic lines when piezometer 2 is taken out for H=120 m (area ratio: 99.513%)

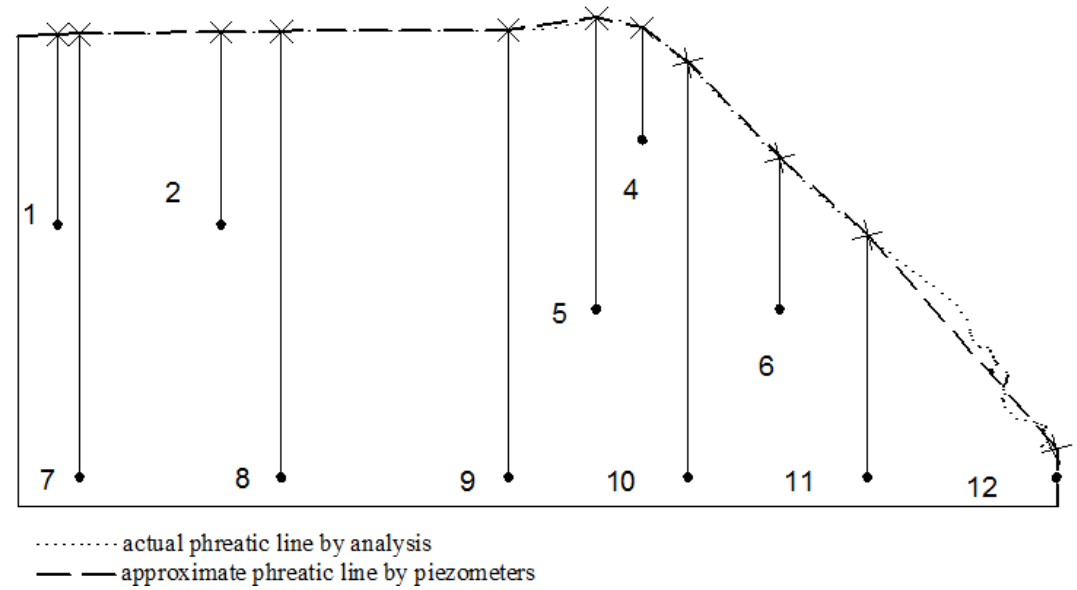

Figure 5.13. Comparison of actual and approximate phreatic lines when piezometer 3 is taken out for H=120 m (area ratio: 99.517%)

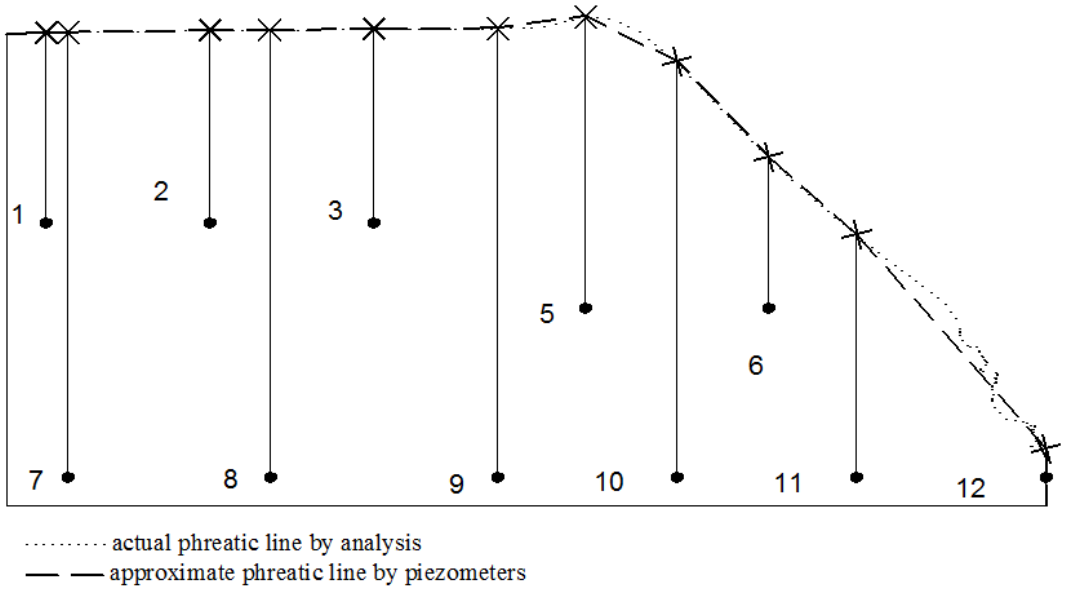

Figure 5.14. Comparison of actual and approximate phreatic lines when piezometer 4 is taken out for H=120 m (area ratio: 99.374%)

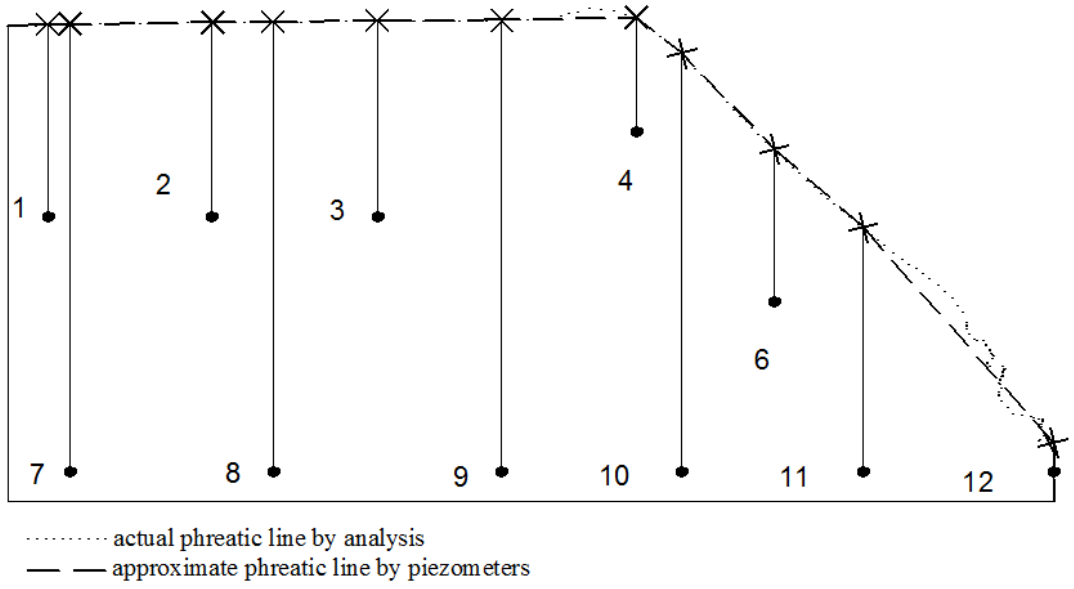

Figure 5.15. Comparison of actual and approximate phreatic lines when piezometer 5 is taken out for H=120 m (area ratio: 99.353%)

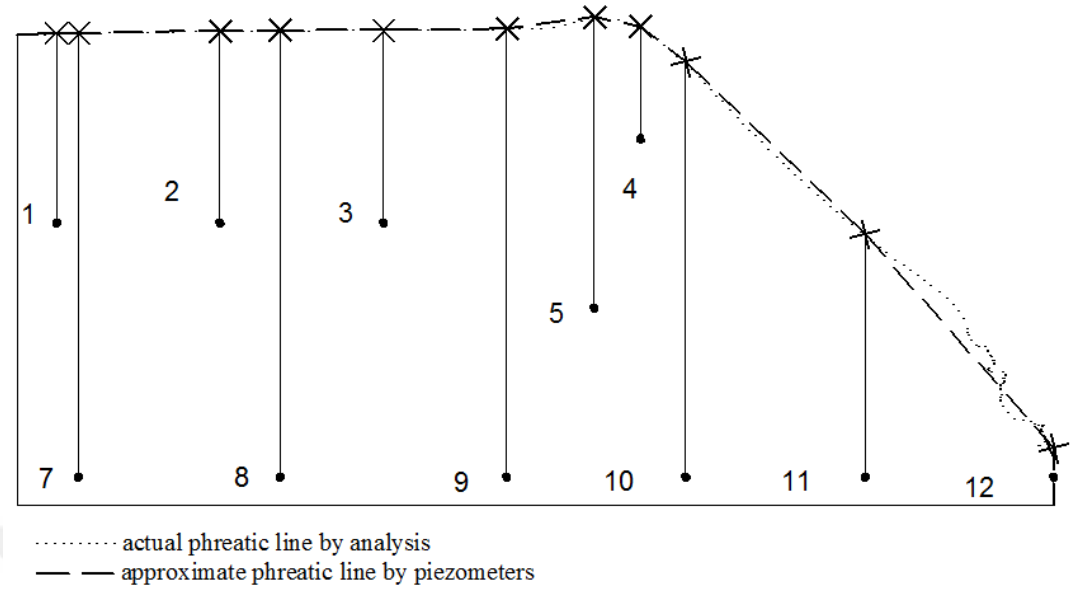

Figure 5.16. Comparison of actual and approximate phreatic lines when piezometer 6 is taken out for H=120 m (area ratio: 99.676%)

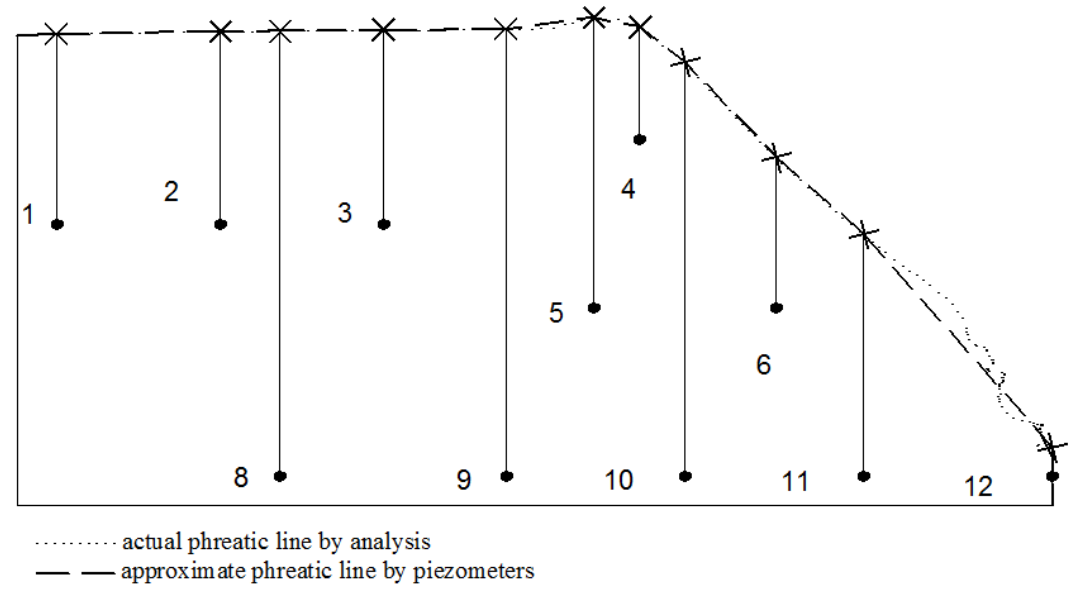

Figure 5.17. Comparison of actual and approximate phreatic lines when piezometer 7 is taken out for H=120 m (area ratio: 99.515%)

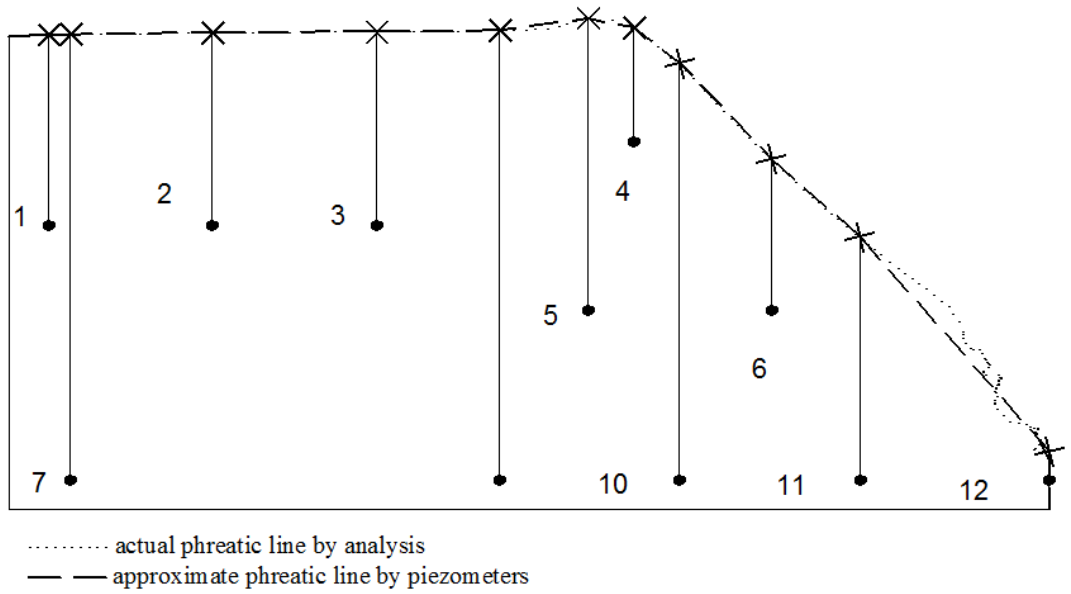

Figure 5.18. Comparison of actual and approximate phreatic lines when piezometer 8 is taken out for H=120 m (area ratio: 99.517%)

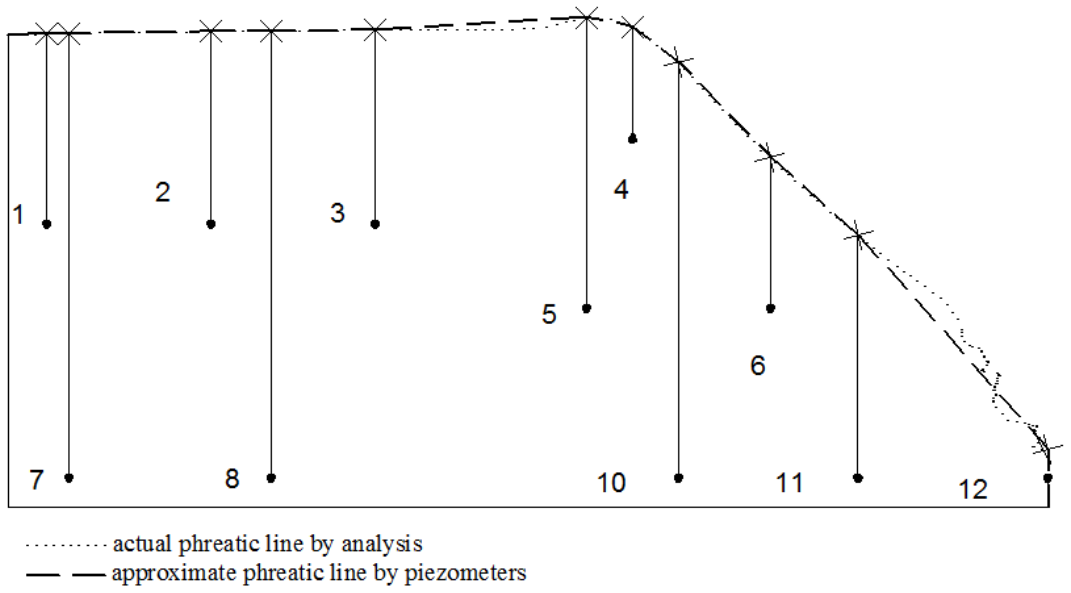

Figure 5.19. Comparison of actual and approximate phreatic lines when piezometer 9 is taken out for H=120 m (area ratio: 99.684%)

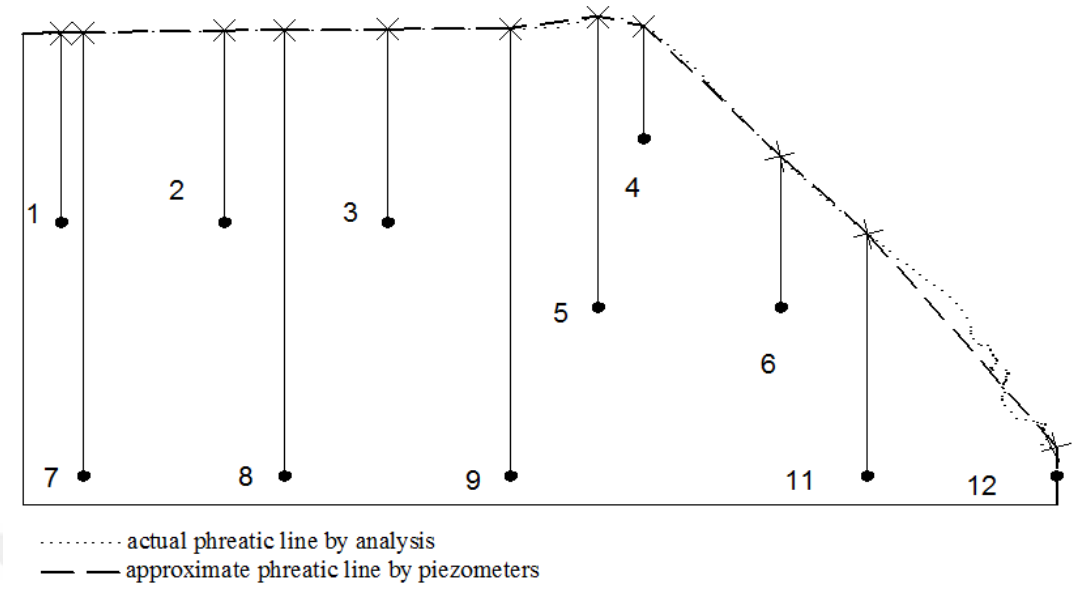

Figure 5.20. Comparison of actual and approximate phreatic lines when piezometer 10 is taken out for H=120 m (area ratio: 99.382%)

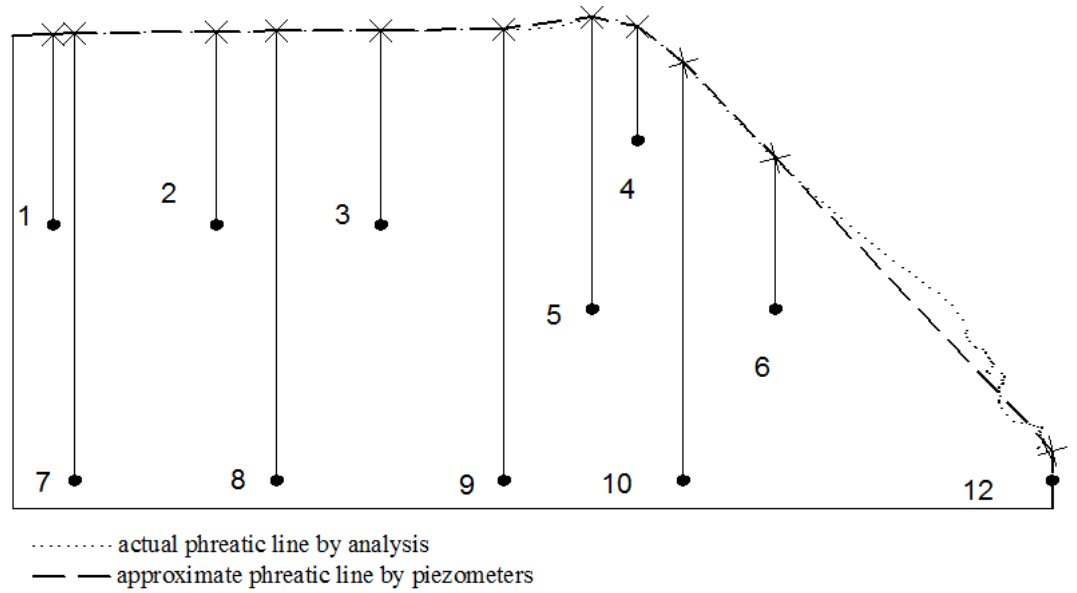

Figure 5.21. Comparison of actual and approximate phreatic lines when piezometer 11 is taken out for H=120 m (area ratio: 99.011%)

The comparisons show that taking Piezometer 3 out of the configuration is the best alternative for using 11 piezometers option. When Piezometer 3 is taken out, the remaining piezometers can calculate the maximum area that can be calculated by 11 piezometers.

This procedure is repeated successively for using even less piezometers from 10 to 2 and the order of taking out the piezometers is found as 3-1-8-7-2-10-5-11-6-4. The alternatives for H=120 m are shown as Figures 5.22-5.32. The piezometers in the upstream shell, which are not numbered, are considered to be redundant ones at this stage. However, they may give information under different operational conditions not considered herein.

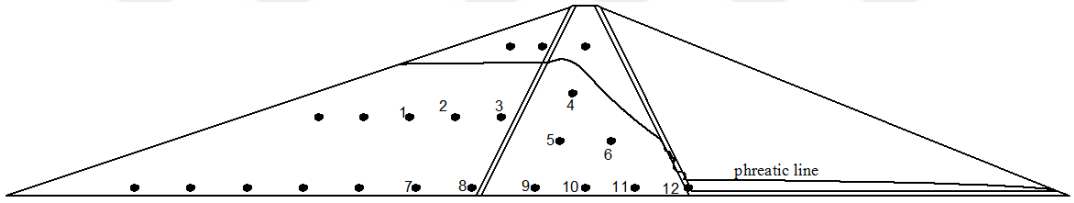

Figure 5.22. Alternative to use 12 piezometers under the phreatic line for H=120 m

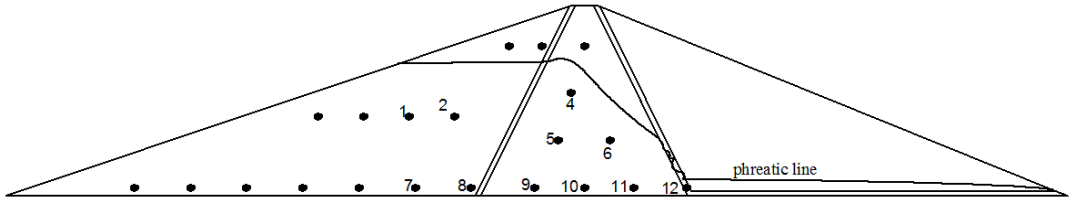

Figure 5.23. Alternative to use 11 piezometers under the phreatic line for H=120 m

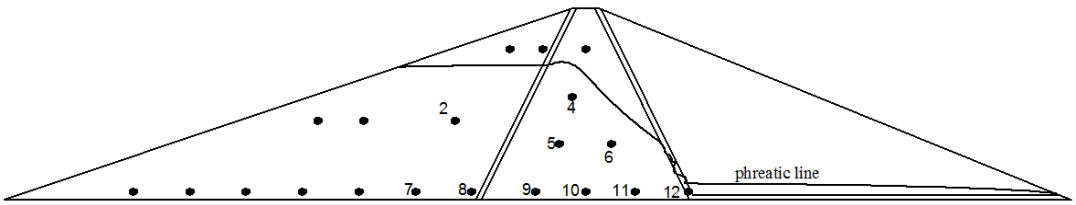

Figure 5.24. Alternative to use 10 piezometers under the phreatic line for H=120 m

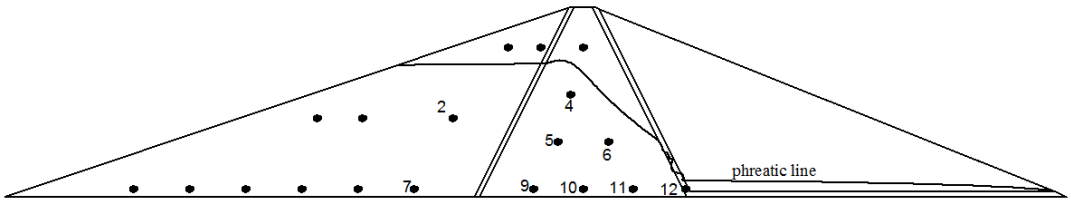

Figure 5.25. Alternative to use 9 piezometers under the phreatic line for H=120 m

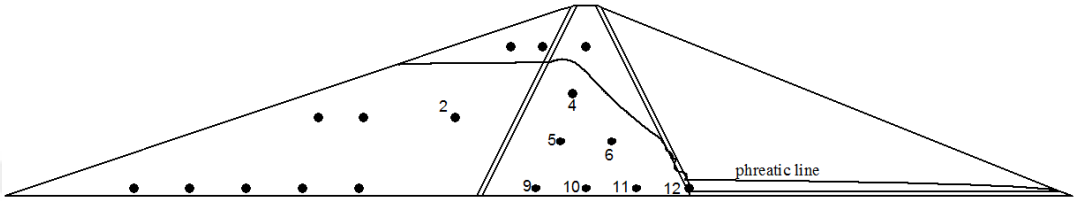

Figure 5.26. Alternative to use 8 piezometers under the phreatic line for H=120 m

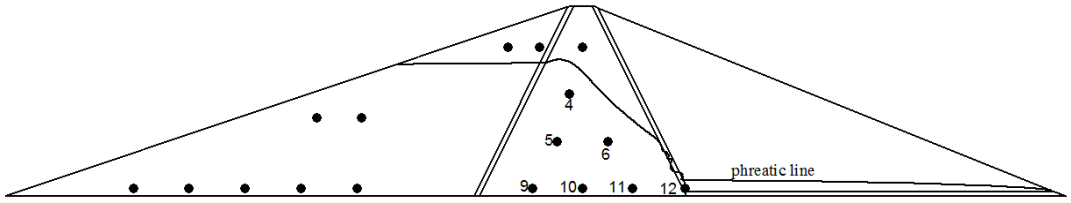

Figure 5.27. Alternative to use 7 piezometers under the phreatic line for H=120 m

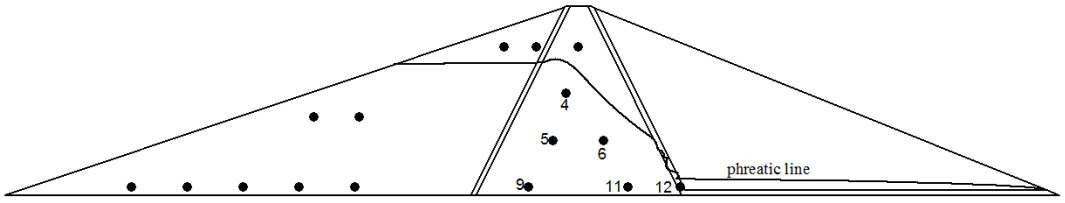

Figure 5.28. Alternative to use 6 piezometers under the phreatic line for H=120 m

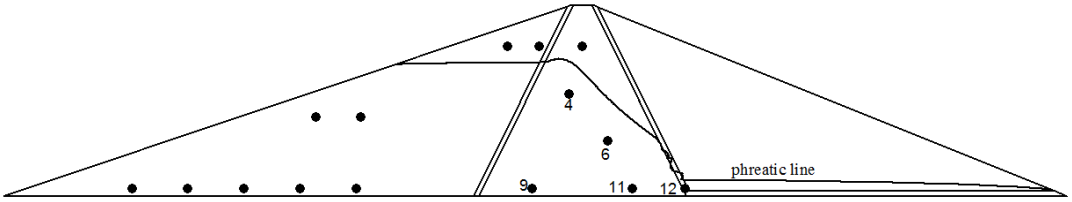

Figure 5.29. Alternative to use 5 piezometers under the phreatic line for H=120 m

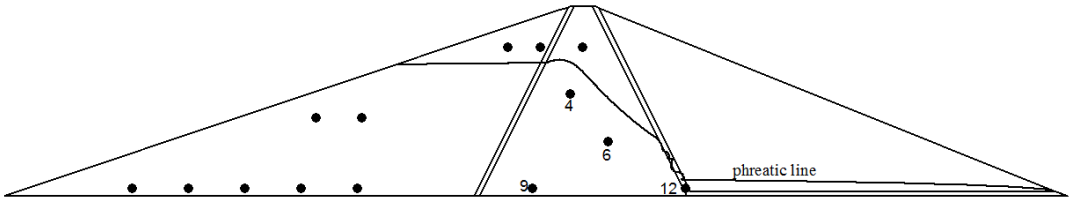

Figure 5.30. Alternative to use 4 piezometers under the phreatic line for H=120 m

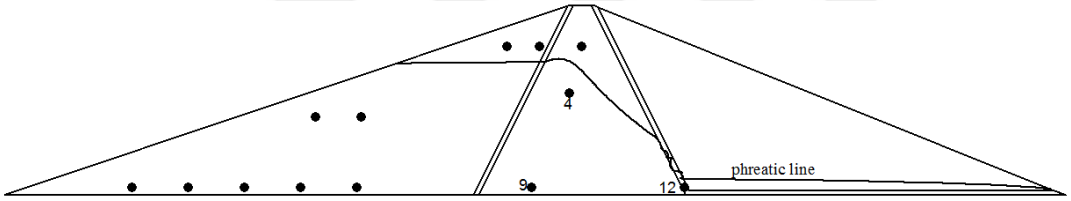

Figure 5.31. Alternative to use 3 piezometers under the phreatic line for H=120 m

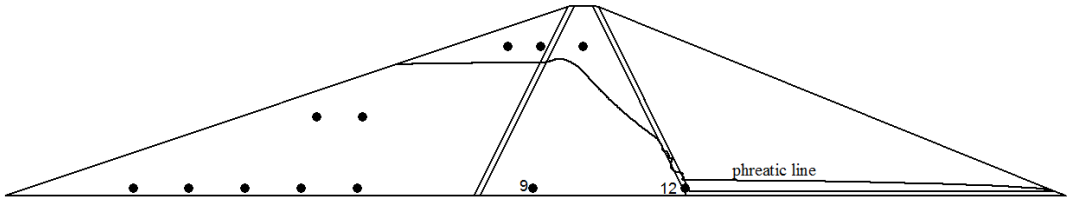

Figure 5.32. Alternative to use 2 piezometers under the phreatic line for H=120 m

Collecting the aforementioned information presented in Figures 5.22-5.32, in a single figure would be helpful in decision-making. To this end, Figure 5.33 is generated to present the relationship between the number of piezometers and the

corresponding area ratio. As expected, the area ratio tends to unity as number of piezometers increases. However, percent increase of area ratio is almost negligible after 9 piezometers, i.e. less than 0.02% (See Figure 5.33). Therefore, selection of more than 9 piezometers does not improve the information obtained from the layout configuration with 9 instruments. In fact, selection of the required number of piezometers for an actual dam project is based on the allocated budget for instrumentation system.

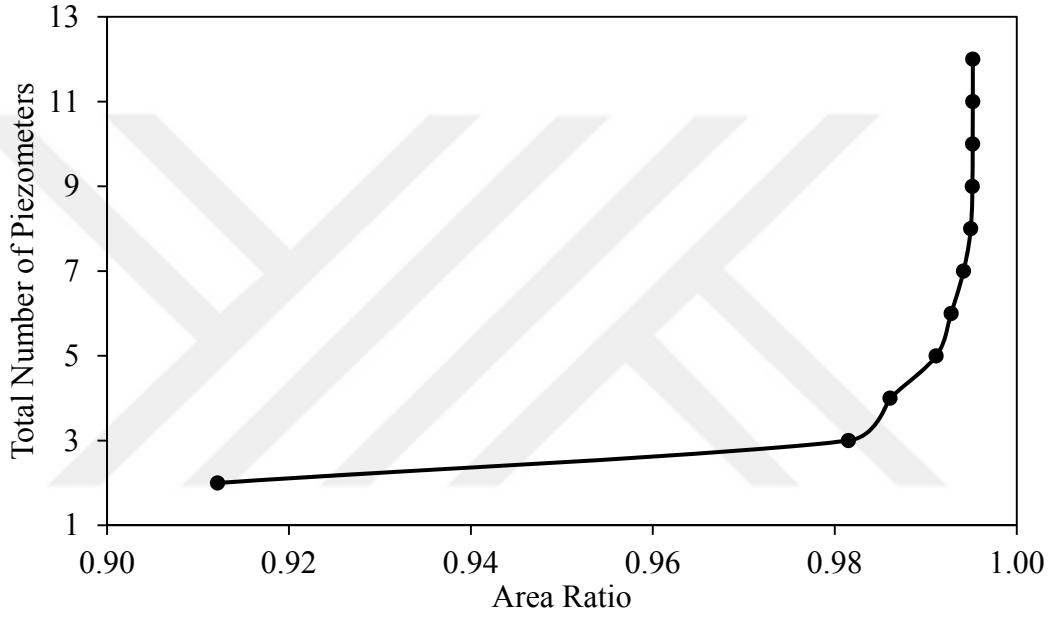

Figure 5.33. Total number of piezometers with respect to area ratio for H=120 m

Performance of piezometer layout for H=120 m is also observed under the condition of rapid drawdown from the maximum reservoir level to the half of the reservoir. In that case, the phreatic line in the most critical condition gets lower and more piezometers become enable to measure pore water pressure (see Figure 5.34). This means that the proposed layout for the previous condition, i.e. up to 70% lowering of the reservoir level, performs even better for the new pronounced drawdown condition.

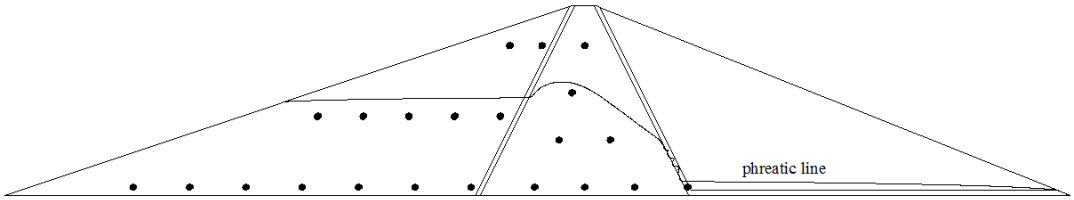

Figure 5.34. Maximum placement under 50% of rapid drawdown condition for H=120 m

The higher levels are proposed to measure negative pressures which may occur at the early times of rapid drawdown conditions. Therefore they can be operated to measure the suction region under drawdown condition. Also, data collection under steady condition is operated by the piezometers at higher layers (see Figure 5.35).

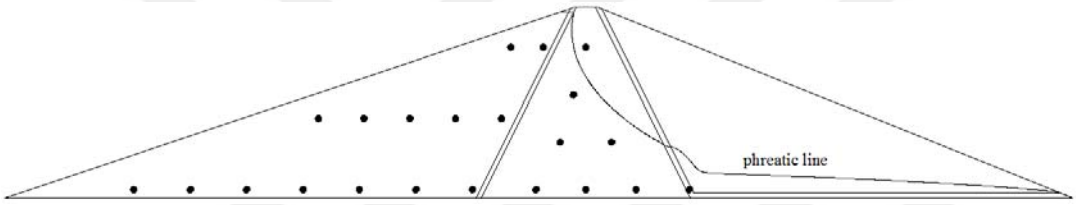

Figure 5.35. Maximum placement under steady state condition for H=120 m

After finding the best placement for H=120 m, the same procedure is also repeated for other embankment heights.

5.2.1 Piezometer Placement Details for H=100 m

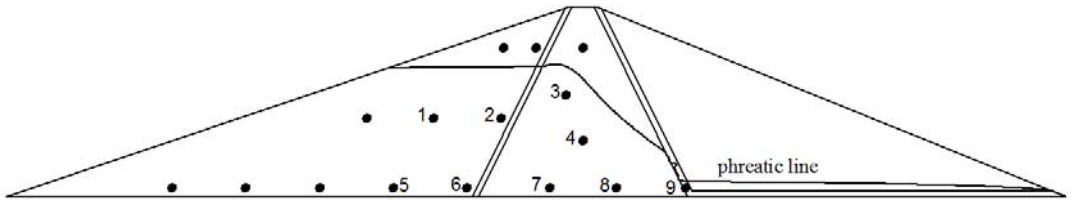

Figure 5.36. Alternative to use 9 piezometers under the phreatic line for H=100 m

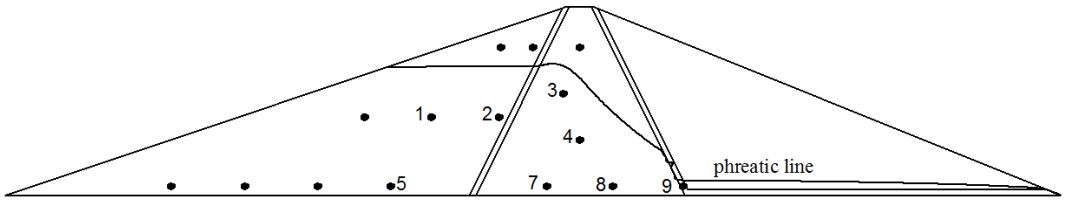

Figure 5.37. Alternative to use 8 piezometers under the phreatic line for H=100 m

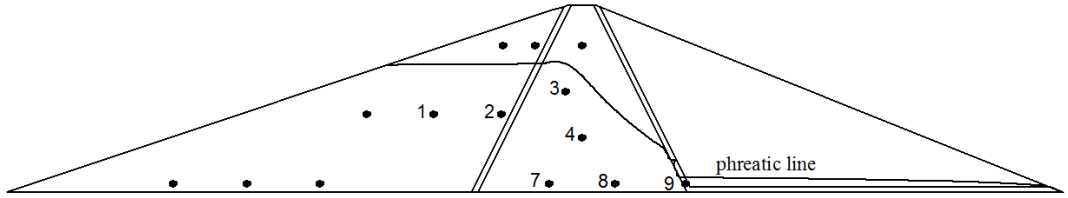

Figure 5.38. Alternative to use 7 piezometers under the phreatic line for H=100 m

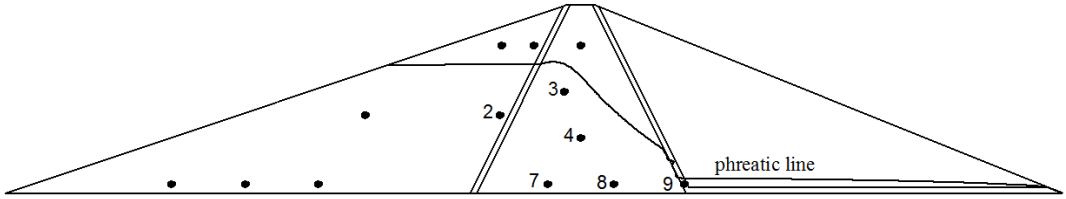

Figure 5.39. Alternative to use 6 piezometers under the phreatic line for H=100 m

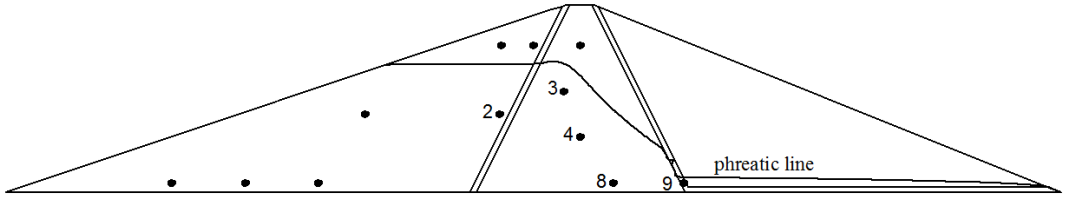

Figure 5.40. Alternative to use 5 piezometers under the phreatic line for H=100 m

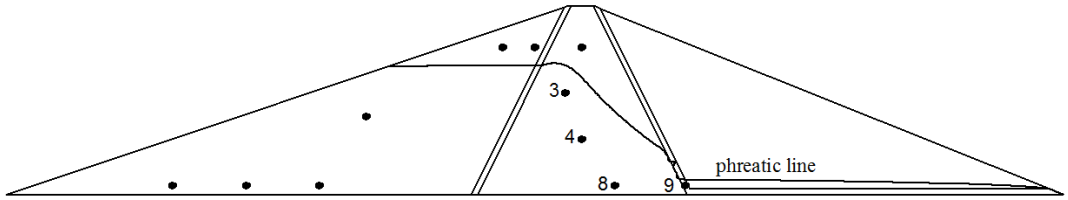

Figure 5.41. Alternative to use 4 piezometers under the phreatic line for H=100 m

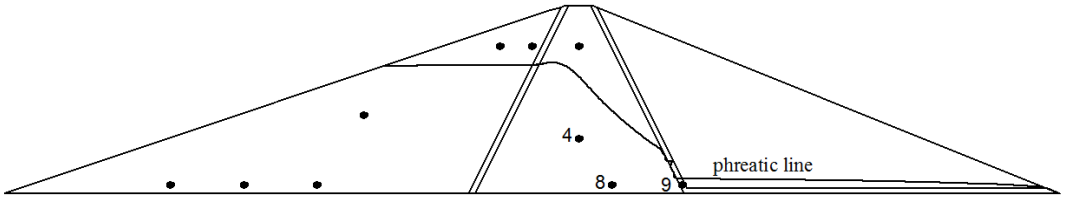

Figure 5.42. Alternative to use 3 piezometers under the phreatic line for H=100 m

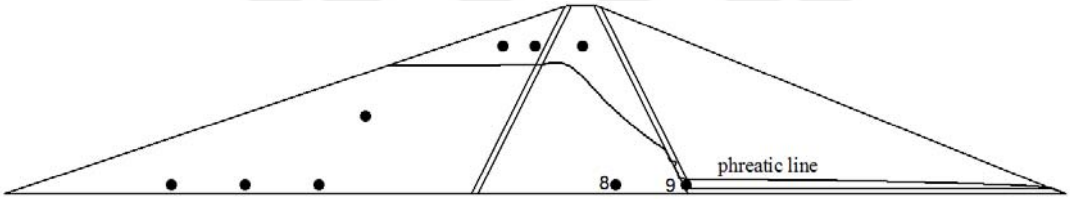

Figure 5.43. Alternative to use 2 piezometers under the phreatic line for H=100 m

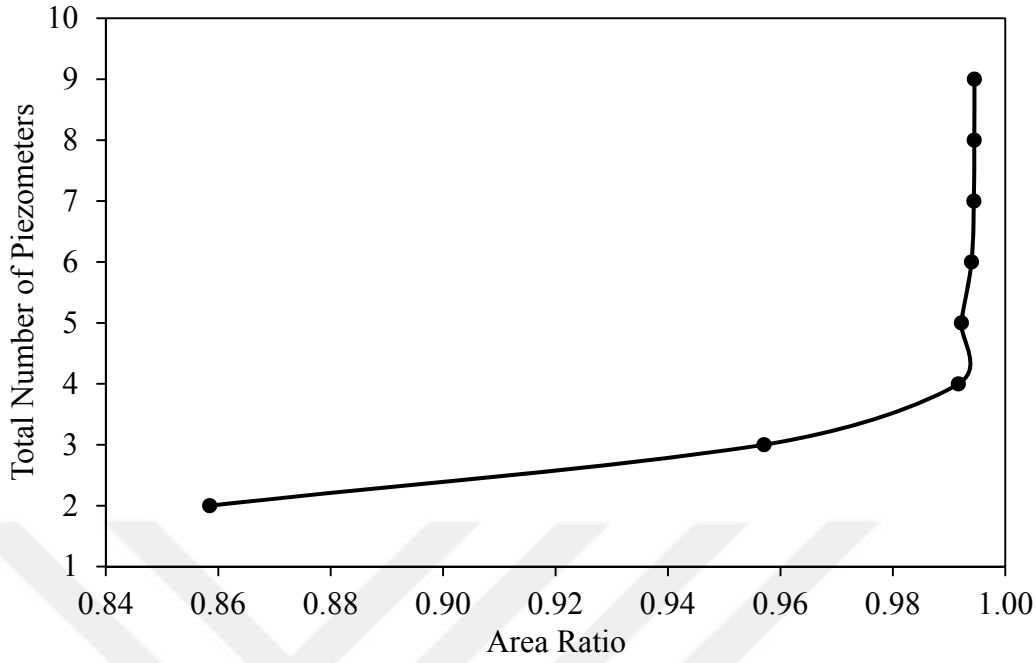

Figure 5.44. Total number of piezometers with respect to area ratio for H=100 m

Using a similar reasoning, selection of 7 piezometers will be enough for H=100 m. Furthermore, 50% lowering during drawdown and steady state case at the maximum reservoir level effects are also observed in Figures 5.45 and 5.46. The proposed layout is accepted to be applicable to these cases as well.

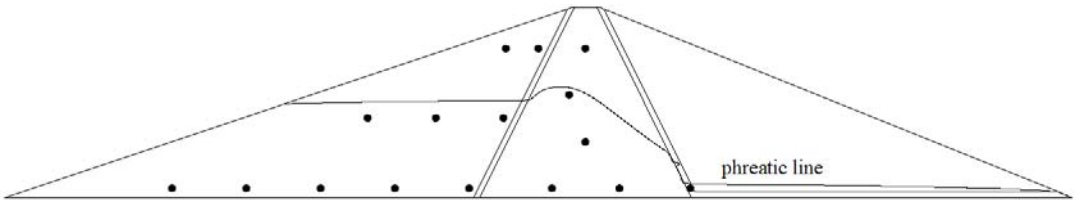

Figure 5.45. Maximum placement under 50% of rapid drawdown condition for H=100 m

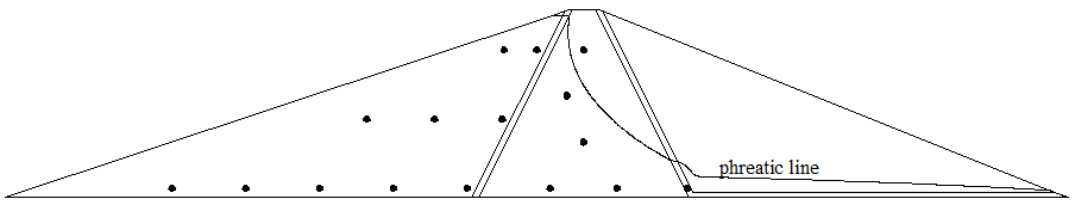

Figure 5.46. Maximum placement under steady state condition for H=100 m

5.2.2 Piezometer Placement Details for H=80 m

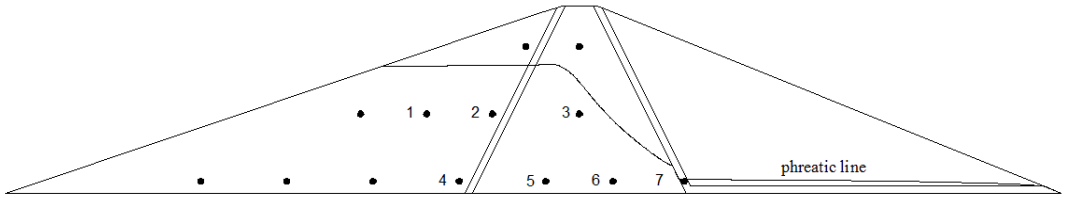

Figure 5.47. Alternative to use 7 piezometers under the phreatic line for H=80 m

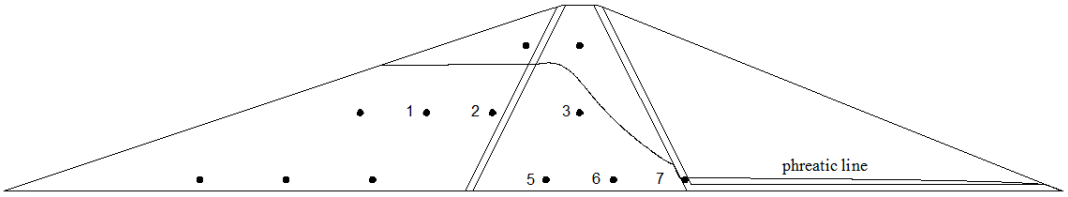

Figure 5.48. Alternative to use 6 piezometers under the phreatic line for H=80 m

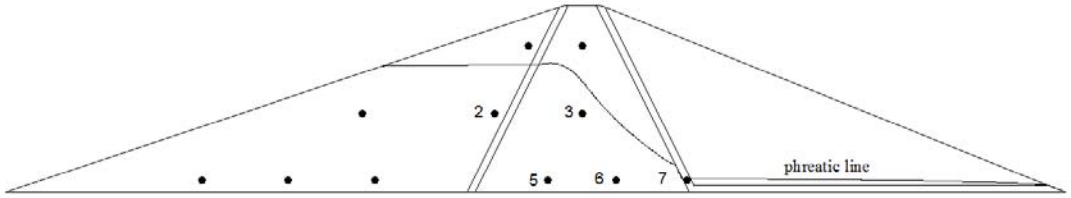

Figure 5.49. Alternative to use 5 piezometers under the phreatic line for H=80 m

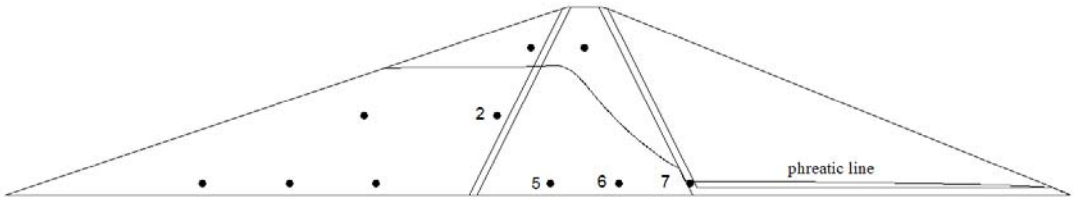

Figure 5.50. Alternative to use 4 piezometers under the phreatic line for H=80 m

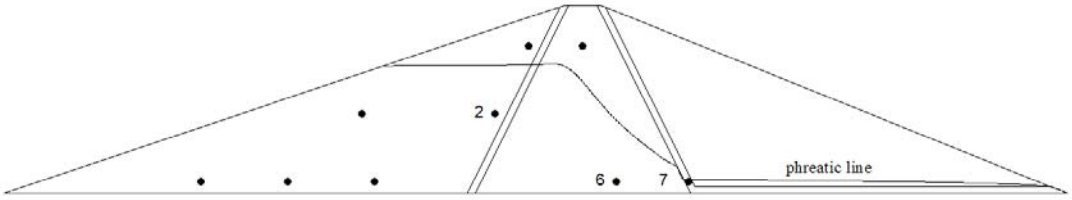

Figure 5.51. Alternative to use 3 piezometers under the phreatic line for H=80 m

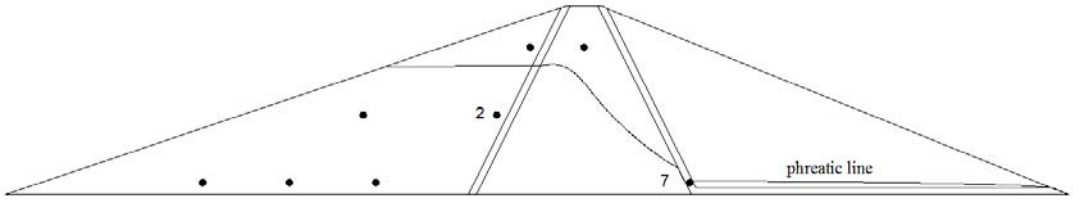

Figure 5.52. Alternative to use 2 piezometers under the phreatic line for H=80 m

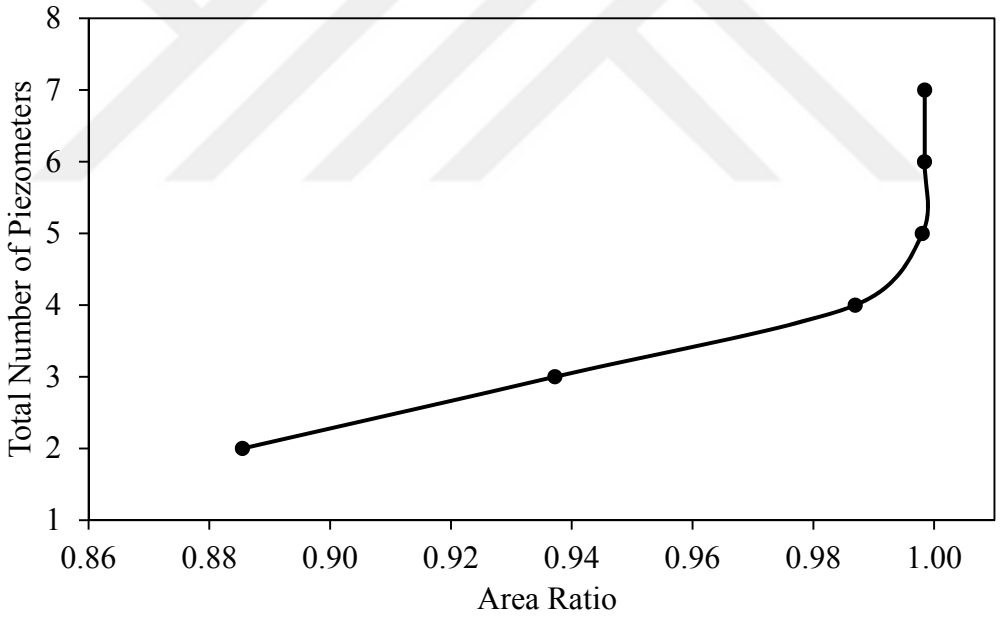

Figure 5.53. Total number of piezometers with respect to area ratio for H=80 m

In a similar manner, selection of 5 piezometers will be enough for H=80 m. Furthermore, 50% lowering during drawdown and steady state case at the maximum reservoir level effects are also observed in Figures 5.54 and 5.55. The proposed layout is accepted to be applicable to these cases as well.

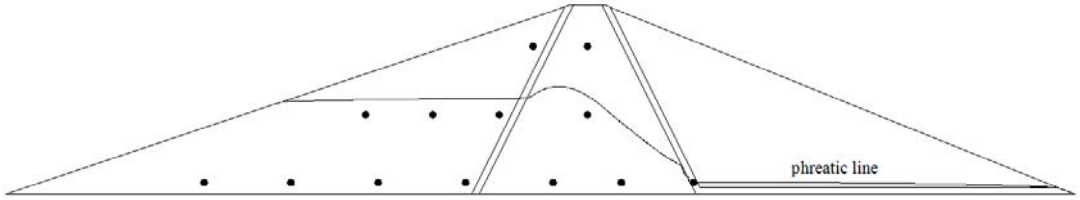

Figure 5.54. Maximum placement under 50% of rapid drawdown condition for H=80 m

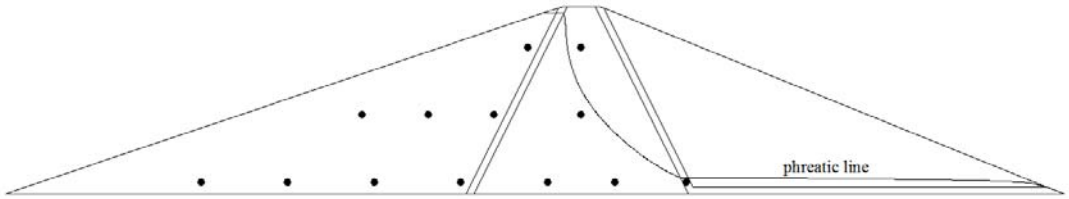

Figure 5.55. Maximum placement under steady state condition for H=80 m

5.2.3 Piezometer Placement Details for H=60 m

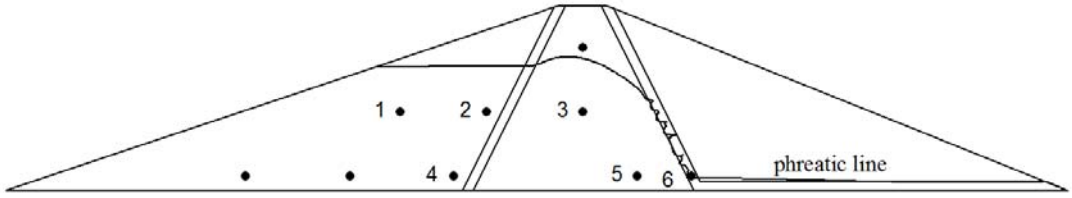

Figure 5.56. Alternative to use 6 piezometers under the phreatic line for H=60 m

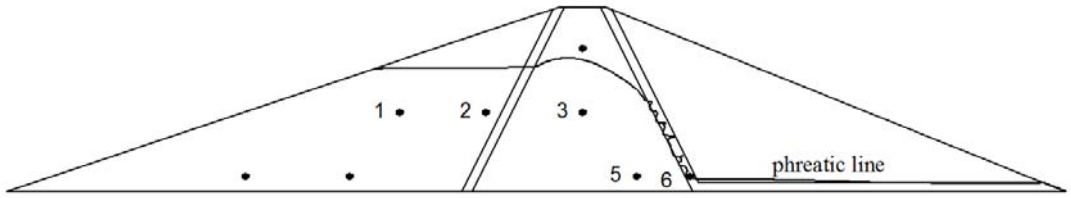

Figure 5.57. Alternative to use 5 piezometers under the phreatic line for H=60 m

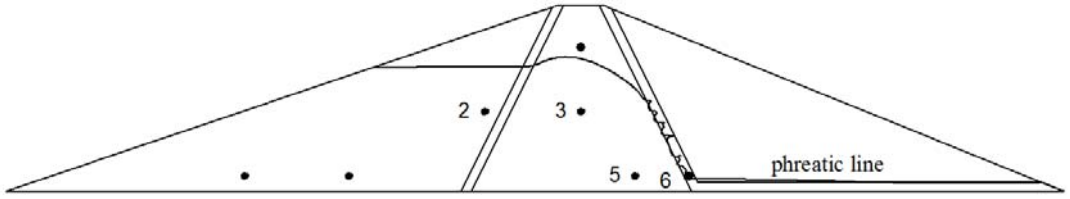

Figure 5.58. Alternative to use 4 piezometers under the phreatic line for H=60 m

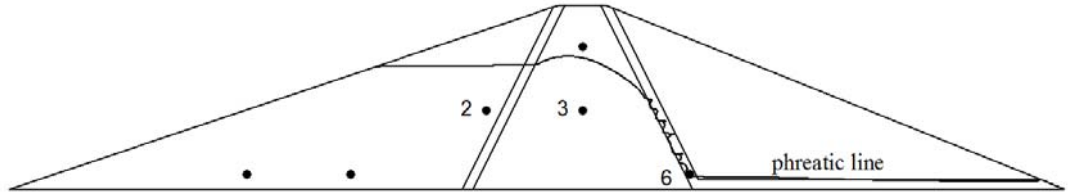

Figure 5.59. Alternative to use 3 piezometers under the phreatic line for H=60 m

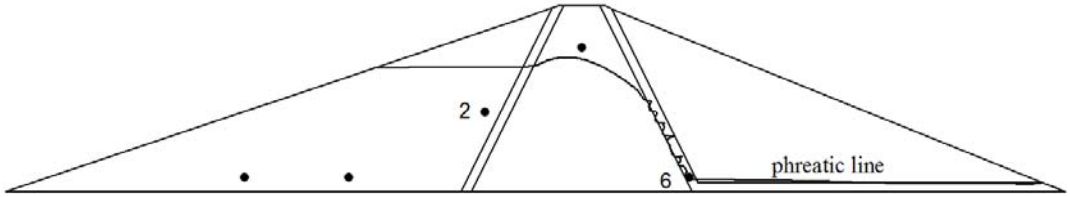

Figure 5.60. Alternative to use 2 piezometers under the phreatic line for H=60 m

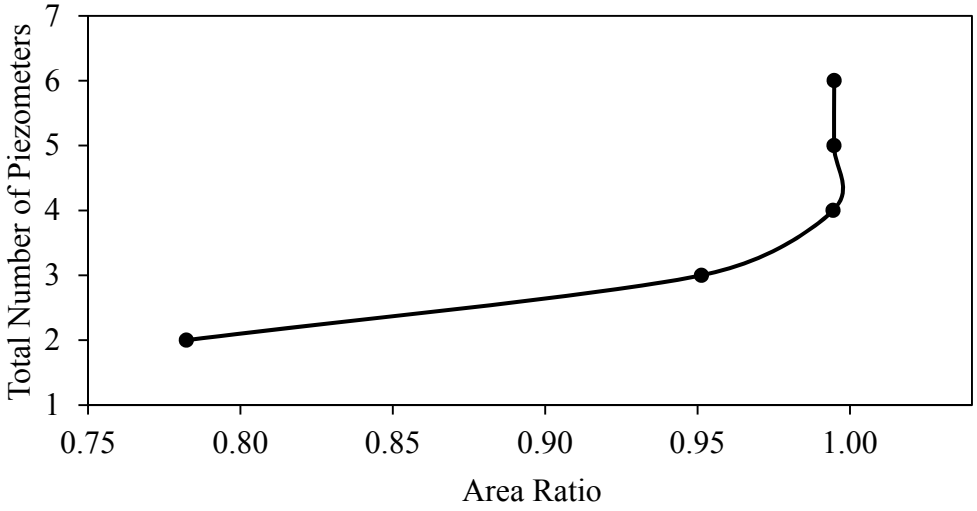

Figure 5.61. Total number of piezometers with respect to area ratio for H=60 m

Selection of 4 piezometers will be enough for H=60 m. Furthermore, 50% lowering during drawdown and steady state case at the maximum reservoir level effects are also observed in Figures 5.62 and 5.63. The proposed layout is accepted to be applicable to these cases as well.

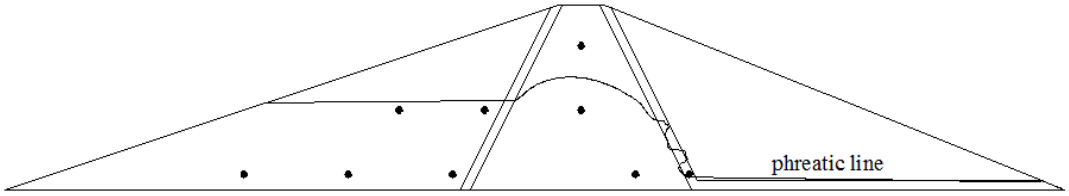

Figure 5.62. Maximum placement under 50% of rapid drawdown condition for H=60 m

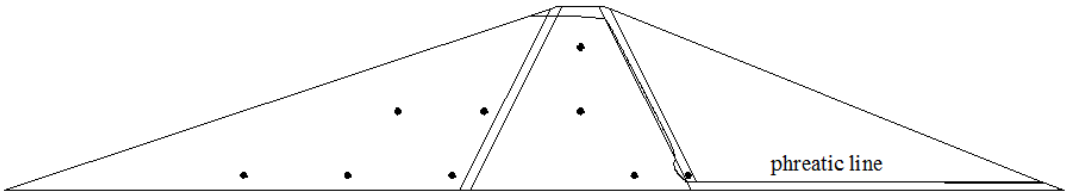

Figure 5.63. Maximum placement under steady state condition for H=60 m

5.2.4 Piezometer Placement Details for H=40 m

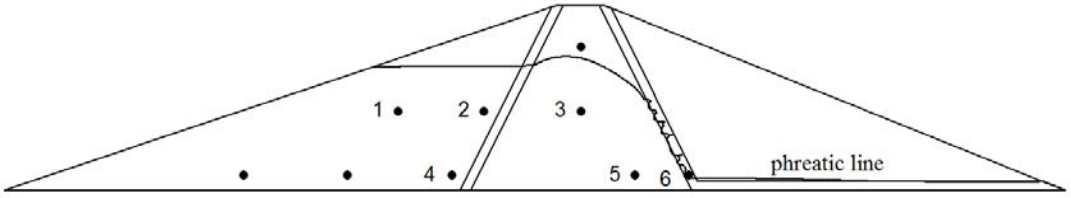

Figure 5.64. Alternative to use 6 piezometers under the phreatic line for H=40 m

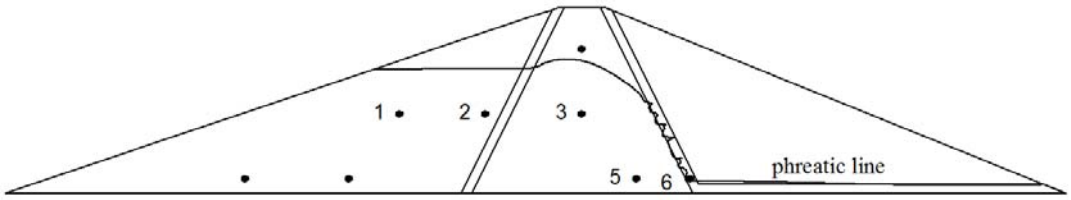

Figure 5.65. Alternative to use 5 piezometers under the phreatic line for H=40 m

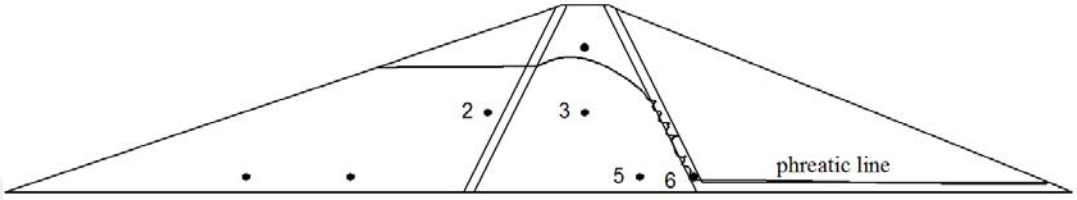

Figure 5.66. Alternative to use 4 piezometers under the phreatic line for H=40 m

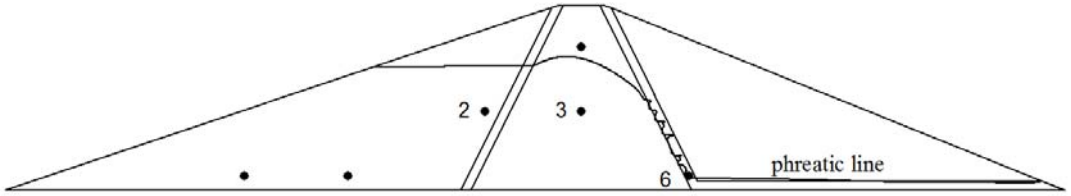

Figure 5.67. Alternative to use 3 piezometers under the phreatic line for H=40 m

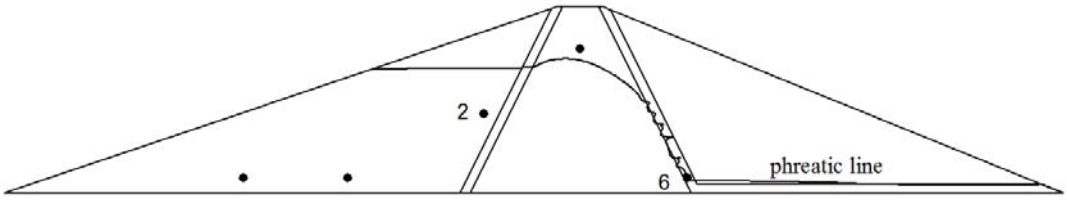

Figure 5.68. Alternative to use 2 piezometers under the phreatic line for H=40 m

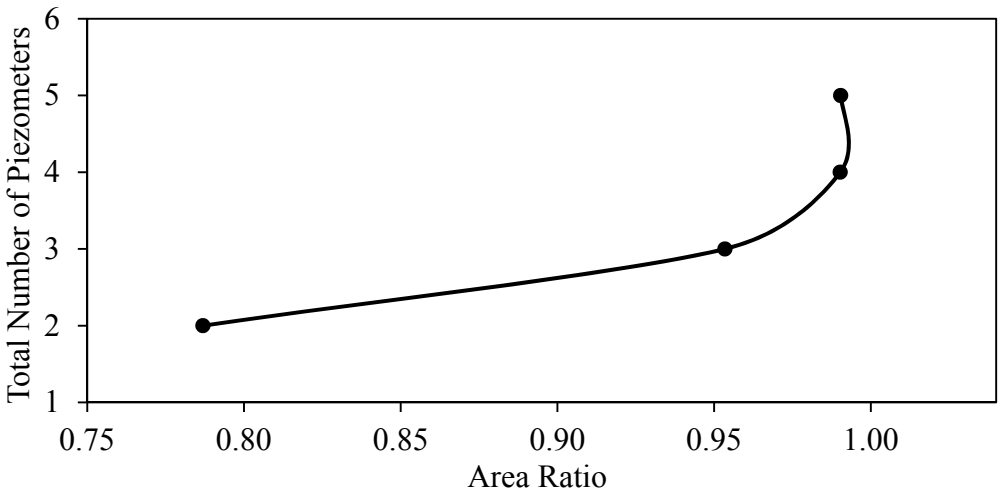

Figure 5.69. Total number of piezometers with respect to area ratio for H=40 m

Selection of 4 piezometers will be enough for H=40 m. Furthermore, 50% lowering during drawdown and steady state case at the maximum reservoir level effects are also observed in Figures 5.70 and 5.71. The proposed layout is accepted to be applicable to these cases as well.

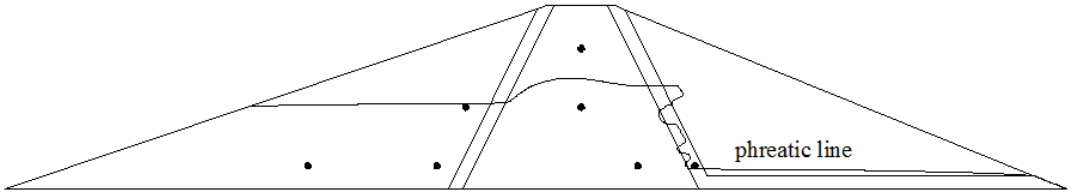

Figure 5.70. Maximum placement under 50% of rapid drawdown condition for H=40 m

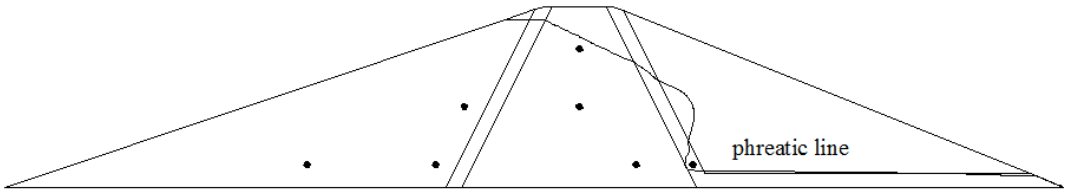

Figure 5.71. Maximum placement under steady state condition for H=40 m

Horizontal and vertical coordinates of all the piezometers are given in Appendix A to show their exact locations within the embankment.

Time-dependent phreatic lines are illustrated in the figures in Appendix B to highlight the propagation of the phreatic line with respect to time for the transient conditions.

5.3 Application to Some Existing Dams

Although the proposed layouts are valid for dams having certain upstream slope, crest width, material zones and material characteristics under specific conditions as stated in Chapter 5, they are applied on some existing dams to discuss the differences.

5.3.1 Mornos Dam, Greece

Mornos Dam is 139 m high clay cored earth-fill dam. It is monitored with various types of instruments. The existing and recommended piezometer layouts are shown in Figure 5.72.

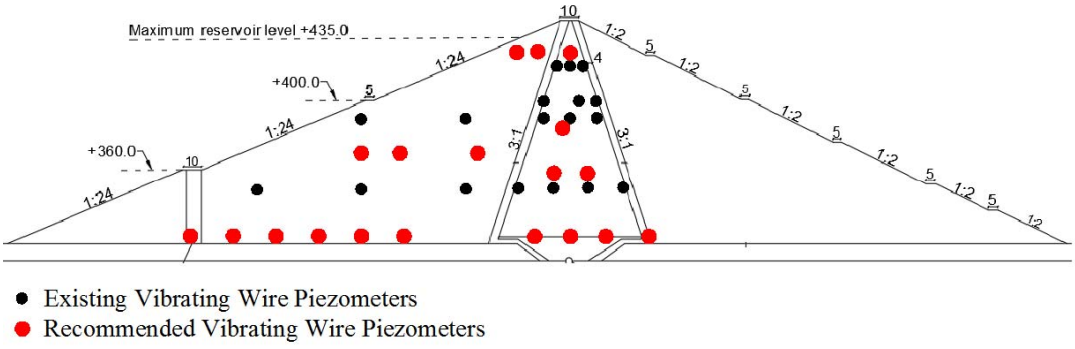

Figure 5.72. Mornos Dam piezometer locations (retrieved from: Toromanovic et al., 2017)

In the existing case, for the maximum cross-section of Mornos Dam, totally 18 piezometers are used and they are distributed as 13 for the core section in 4 layers and 5 for the shell section in 2 layers. It seen that there is not any piezometer in filter zones. On the other, when the best layout proposed for 120 m height of embankment is applied on Mornos Dam, it is stated that there must be more piezometers in the

shell section while less piezometers are recommended for the core section and using totally 19 piezometers are satisfactory.

5.3.2 Sahand Dam, Iran

Sahand Dam is 60 m high clay cored earth-fill dam. The existing and recommended piezometer layouts are shown in Figure 5.73.

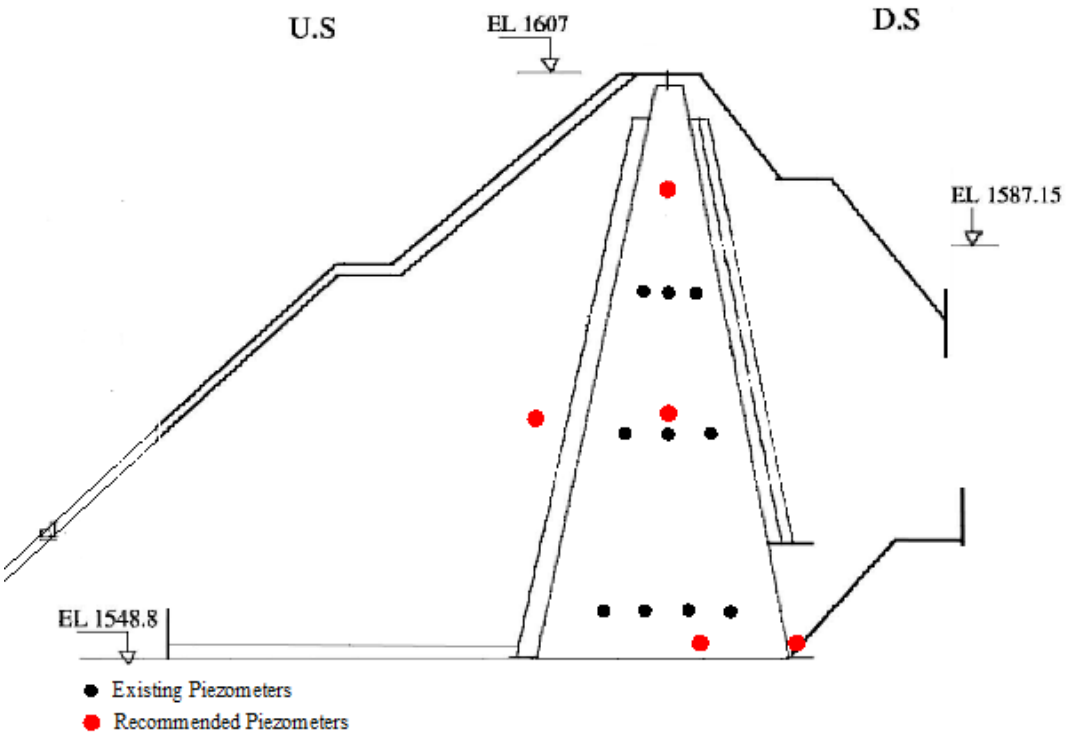

Figure 5.73. Sahand Dam piezometer locations (retrieved from: Nourani and Babakhani, 2013)

The dam includes 10 piezometers in 3 layers within the core section while the shell sections are not placed with piezometers. However, when the best layout proposed for 60 m height of embankment is applied on Sahand Dam, there must be at least one piezometer in the upstream shell section and 3 piezometers in the core section. Also, a piezometer is recommended in the downstream filter.

These situation can inherently be caused by difference of parameters used in the design of Mornos Dam and the parameters used in this thesis.

It must be noted that comparisons of the existing and recommended layouts are only based on location and number of the piezometers. No any other parameter is considered while comparing the relevant layouts. Design criteria of the existing dams can inherently be different and much more complicated than the conditions considered in this thesis. This may be the main reason of the differences between the existing and recommended layouts. However, the recommended layouts in this thesis are obtained by considering some fundamental conditions which can be valid for majority of earth-fill dams. Therefore, the recommended layouts are presented as optimum layout design of earth-fill dams, which is the scope of the thesis.

CONCLUSIONS

6.1 Summary

Instrumentation layout of piezometers within a dam body is generally applied by adhering to the previous practices or experiences because there is no any rule or certified regulation. This deficiency generates the necessity of developing reliable piezometer layout for clay cored earth-fill dams. By focusing on this necessity, this study motivated to develop the ideal piezometer layout which can be used as a supportive principle while designing the instrumentation system.

The software Geo Studio is used throughout the study. Dam model cross-sections having different heights ranging from 40 m to 200 m with 20 m increments are analyzed in terms of pore water pressure and slope stability in steady state, rapid drawdown, and rapid fill conditions.

The cross-sections used for preliminary analyses are modeled without filter zones with bigger sized meshes. Besides, the cross-sections used for the verification analyses are modeled with filter zones and meshes having 1 m size. No significant effect on upstream slope stability was observed with the inclusion of filter layer.

Phreatic line developing in the dam body is visualized by placing the piezometers in a tolerable configuration, sufficient to capture the locus of the phreatic line. Cross-sections having different heights are analyzed and reliable piezometer layouts have been found.

6.2 Major Findings of the Study

Best piezometer configuration layout is obtained for earth-fill dam models having heights ranging from 40 m to 120 m in 20 m increments. Interpolation may be applied for determining number of piezometers having different heights in the specified height range. The conclusions stated below are valid for earth-fill dams having heights in the specified range with the side slopes for both faces (1V:3H) and core section (1V:0.5H) stated in the text. The following conclusions have been derived throughout the study:

- The searching for best placement aims to minimize the number of piezometers and maximize the area that can be read by the piezometers. Number of piezometers for a particular height is selected according to the area ratio. When the percent increase of the area ratio is less than about 0.02%, further increase of number of piezometers is accepted to be uneconomical.
- Outcome allows the designer to have sufficient number of points on the phreatic line. The points provided by the ideal instrumentation layout safely presents the most sufficient information. Whoever desires to have more information can costly use more devices.
- Total number of piezometers with respect to area ratio distributions state that the proposed layouts perform successfully under specified conditions.
- Piezometer layout of the existing dams can be very different than the proposed layouts. Operative demands cannot be the same for all dams or design criteria such as material characteristics, geometry of the embankment, foundation conditions, etc., may change for each dam. Therefore, the best piezometer layout of dams must be designed by considering their individual conditions.

6.3 Recommendations for Further Studies

- In this study, effect of some parameters on pore water pressure is examined. These parameters are friction angle of the shell material, rate of drawdown, rate of fill, height of dam, and angle of the upstream face. Effect of other parameters, such as hydraulic conductivity and unit weight of the shell material can also be examined in a future research. Additionally, effect of material properties of the clay core can be observed by changing slope and material properties.
- Best piezometer layout is studied on cross-sections having constant upstream slope and crest width. Piezometer layout according to changing side slopes and crest width can also be studied.
- Conditions that may require monitoring the pore water pressure at downstream shell, such as performance of filters, drain or relief wells can be further studied.
- This study is focused on instrumentation of the earth-fill dam. Monitoring the pore water pressure of soil layer below the embankment can be studied for changing conditions.
- Vibrating wire piezometer is used in this study because of its popularity and reliability. Optimum placing of other types of piezometers or placing various types together may end up with a suitable recommendation as well.
- Embankments having combined cofferdams or different types of impervious zones, such as inclined clay cores or asphalt cores can also be observed.

REFERENCES

Arı, O., and Yanmaz, A.M. "A Methodology for Optimal Layout Design of Pressure Cells for Concrete Face Rockfill Dams", Journal of Civil Engineering, KSCE, doi: 10.1007/s12205-017-1991-x, 2018

Arı, O., and Yanmaz, A.M. "Monitoring of Existing Dams with Retrofitted Instruments", Yapı Dünyası, No:157, 16-20, 2009 (in Turkish).

ASCE (1989). *Conventional Hydro Guidelines, Division II. Design.* New York, NY: ASCE.

ASCE (American Society of Civil Engineers). (2000). *Task Committee on Instrumentation and Monitoring Dam Performance. Guidelines for Instrumentation and Measurements for Monitoring Dam Performance*; American Society of Civil Engineers: Reston, VA,USA.

Bartholomew, C.L. and Murray, B.C. (1987). *Embankment Dam Instrumentation Manual*; US Department of the Interior, Bureau of Reclamation: Denver, CO, USA (pp. 71–83).

Beenenga, C., Deichert, A., Saber, R. (2016). *Rapid drawdown at embankment dams, is it a real concern?* Association of State Dam Safety Officials, Inc.

Bilgi, V. (1990). *Toprak ve Kaya Dolgu Barajların Projelendirme Kriterleri.* Devlet Su İşleri Genel Müdürlüğü.

Bowles, J. E. (1996). *Foundation Analysis and Design*. New York, McGraw-Hill.

Carsel, R.F. ve Parrish, R.S. (1988). "Developing Joint Probability Distributions of Soil Water Retention Characteristics." Water Resources Research, Vol. 24, No. 5, 755–769.

Carter, M. and Bentley, S. P. (1991). *Correlations of Soil Properties.* London, Pentech Press.

Çalamak, M., Selamoğlu, M. and Yanmaz, A.M. (2015). Assessment of the Effects of Rapid Drawdown Study on Slope Stability of Earth-fill Dams. *4th National Symposium on Hydraulic Structures*, 1, s.278-287. doi: 10.13140/RG.2.1.2084.7448

Çalamak, M., Kılıç, Y. and Yanmaz, A. M. (2020). *On the Stability of Moderate Height Berm-Type Earthen Dams: The Hancağız Dam Example.* Geotechnical and Geological Engineering, 38(4), 4169–4179. doi: 10.1007/s10706-020-01286-6

Dunnicliff, J. (1993). *Geotechnical Instrumentation for Monitoring Field Performance;* John Wiley and Sons: Hoboken, NJ, USA, (pp. 97–108).

FEMA. (2011). *Filters for Embankment Dams Best Practices for Design and Construction*. Federal Emergency Management Agency.

FERC (Federal Energy Regulatory Commission). (1991). *Chapter IV, Embankment Dams*, Federal Energy Regulatory Commission available at: https://www.ferc.gov/sites/default/files/2020-04/chap4.pdf

FERC (Federal Energy Regulatory Commission). (1991). *Chapter IX, Instrumentation and Monitoring*, Federal Energy Regulatory Commission. available at: https://www.ferc.gov/sites/default/files/2020-04/chap9.pdf

Geosense. (2021). *Application Guide – Piezometers*. Retrieved from https://www.geosense.co.uk/wp-content/uploads/2021/05/Piezometers-Application-Guide-V1.1.pdf

Geo-Slope Int. Ltd. (2012a). Seepage Modeling with SEEP/W. Geo-Slope International Ltd., Calgary, Alberta, Canada.

Geo-Slope Int. Ltd. (2012b). Stability Modeling with SLOPE/W. Geo-Slope International Ltd., Calgary, Alberta, Canada.

Geo-Slope Int. Ltd. (2013). Stress-Deformation Modeling with SIGMA/W. Geo-Slope International Ltd., Calgary, Alberta, Canada.

Geo-Slope Int. Ltd. (2014a). “Groundwater Seepage Analysis with SEEP/W.” Calgary, Alberta, Canada.

GILD. 2018. *Guidelines for instrumentation of large dams*, Central Water Commission, Central Dam Safety Organization, Doc. No. CDSO_GUD_DS_02_v1.0., New Delhi.

ICOLD (International Commission on Large Dams). (1983). *Deterioration of dams and reservoirs*. International Commission on Large Dams, LNEC, Lisboa, Portugal (pp. 1-312).

INDNR (Indiana Department of Natural Resources). (2003). *Dam Safety Inspection Manual.*

Jansen, R.B. (2012). *Advanced Dam Engineering for Design, Construction, and Rehabilitation*; Springer Science and Business Media: Berlin/Heidelberg, Germany.

Johnson, F.A. and Illes, P. (1976). *A Classification of Dam Failures*. Water Power and Dam Construction, U.S.A., 43–45.

Khassaf, S., Hameed, M.R. and Al-deen, N.N. (2013). *Slope Stability Analysis under Rapid rawdownCndition and Siesmic Loads of Earth Dam (Case Study: Mandali Dam)*. International Journal of Innovative Research in Science, Engineering and Technology, 2, 7114-7118.

Kılıç, Y., (2017). “Effects of Berm Characteristics on Earth-fill Dam Stability.” Master Thesis, Middle East Technical University, Department of Civil Engineering.

Konietzky, H.H. “Dam Construction”, Doc.Playernet, TU Bergakademie Freiberg. Retrieved from: http://docplayer.net/190166206-Dam-constructions-editor-prof-dr-ing-habil-heinz-konietzky-tu-bergakademie-freiberg-geotechnical-institute.html

Majoros, M. and Sneed, H. M. (1981). *The softest program test system*. Journal of Systems and Software, 2(4), 289–296. doi: 10.1016/0164-1212(81)90003-0

Mancebo Piqueras, J. A., Sanz Pérez, E. and Menéndez-Pidal, I. (2012). *Water seepage beneath dams on soluble evaporite deposits: a laboratory and field study (Caspe Dam, Spain)*. Bulletin of Engineering Geology and the Environment, 71(2), 201–213. Springer Science and Business Media LLC.

Masoumi, I., Ahangari, K., and Noorzad, A. (2018). *Integrated fuzzy decision approach for reliability improvement of dam instrumentation and monitoring*. Journal of Structural Integrity and Maintenance, 3(2), 114–125. doi: 10.1080/24705314.2018.1461546

Mizuno, M., Hirose, T. (2009). *Instrumentation and monitoring of dams and reservoirs*, 1, 1–8, Water Storage Transp. Distrib.

Nourani, V. and Babakhani, A. (2013*). Integration of Artificial Neural Networks with Radial Basis Function Interpolation in Earthfill Dam Seepage Modeling*. Journal of Computing in Civil Engineering, 27(2), 183–195. doi: 10.1061/(asce)cp.1943-5487.0000200

NRCS. (2005). *Technical Release No. 60, Earth Dams and Reservoirs.* Natural Resources Conservation Service.

Persson, V. H. (1997). "Response to Analysis and Static Strength of Embankment Materials." California Department of Water Resources, Division of Safety of Dams.

Puigmarti, N.M.P., Alonso, E., and Olivella, S. (2008). Rapid drawdown in slopes and embankments, Water Resources Research, 44(5).

Rashidi, M. and Haeri, S. M. (2017). *Evaluation of behaviors of earth and rockfill dams during construction and initial impounding using instrumentation data and numerical modeling*. Journal of Rock Mechanics and Geotechnical Engineering, 9(4), 709–725. doi: 10.1016/j.jrmge.2016.12.003

Seyed-Kolbadi, S. M., Hariri-Ardebili, M. A., Mirtaheri, M., and Pourkamali-Anaraki, F. (2020). *Instrumented Health Monitoring of an Earth Dam.* Infrastructures, 5(3), 26. doi: 10.3390/infrastructures5030026

Shi, Z.-M., Wang, Y.-Q., Peng, M., Chen, J.-F. and Yuan, J. (2015). *Characteristics of the landslide dams induced by the 2008 Wenchuan earthquake and dynamic behavior analysis using large-scale shaking table tests. Engineering Geology*, 194, 25–37. Elsevier BV. doi: 10.1016/j.enggeo.2014.10.009

Soil Instruments. (2013). *Pneumatic Piezometer*. Retrieved from http://www.itmsoilsupport.com/manuals/Man014_Pneumatic_Piezometer.pdf

Soil Instruments. (2021). *Standpipe Piezometer*. Retrieved from http://www.itmsoilsupport.com/manuals/Man052_Standpipe_Piezometer.pdf

Toromanovic, J., Laue, J., and Knutsson, S. (2017). *Assessment of Arching and Cracking Potential by Numerical Modelling: A Case Study of the Mornos Dam.*

USACE. (2003). *Slope Stability, Engineering Manual* 1110-2-1902, Department of the Army, Corps of Engineers, Washington, D. C.

USBR. (1987). *Design of Small Dams*. United States Department of the Interior, Bureau of Reclamation, Washington, DC.

USGS (U.S. Geological Survey). (2005). *Ground and Surface Water Interactions and Quality of Discharging Ground Water*, Lower Nooksack River Basin, WA. Scientific Investigations Report 2005-5255. available at: https://pubs.usgs.gov/sir/2005/5255/section4.html

Wang, H., and Anderson, M. P. (1982). *Introduction to Groundwater Modelling : Finite Difference and Finite Element Method*. (L. Olsen, ed.), W. H. Freeman and Company, San Francisco.

Yanmaz, A.M., and Arı, O. “An Overview of the Role of Retrofitted Instruments in Dam Safety”, Proceedings of Eighth International Congress on Advances in Civil Engineering, Vol. 1, 311-318, North Cyprus, 2008.

Yanmaz, A.M., and Sezgin, Ö.İ. “An Evaluation Study on Instrumentation System of Cindere Dam”, Journal of Performance of Constructed Facilities, ASCE, Vol. 23, No. 6, 415-422, 2009.

Yanmaz, A.M., and Arı, O. “A Case Study on Dam Instrumentation Retrofitting”, Journal of Civil Engineering, KSCE, Vol. 15, No.2, 317-325, 2011.

Yanmaz, A.M., (2018). Applied Water Resources Engineering. Fifth edition, Ankara: METU Press Publishing Company.

Yılmaz, A.N. (2017). “Assessment of Performance of Drainage Systems in Earth-Fill Dams.” Master Thesis, Middle East Technical University, Department of Civil Engineering.

Zhu, P., Leng, Y. B., Y.Zhou, and Jiang, G. L. (2011). *Safety Inspection Strategy for Earth Embankment Dams using Fully Distributed Sensing*. Procedia Engineering, 8, 520–526. doi: 10.1016/j.proeng.2011.03.094

APPENDICES

A. Maximum Piezometer Layouts and Coordinate Tables

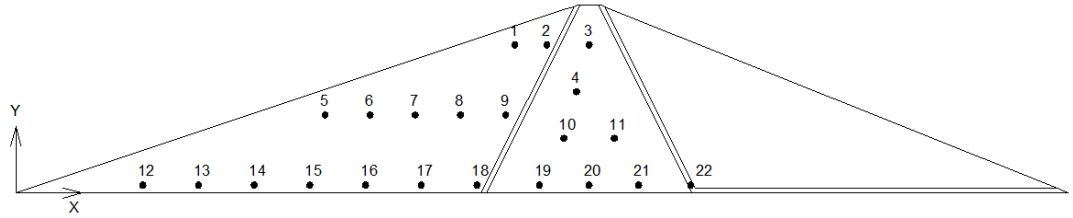

Figure A.1. Maximum piezometer layout for H=120 m

Table A.1 Coordinates of the piezometers for H=120 m

POINT	X (m)	Y (m)
1	319.897	94.600
2	340.446	94.600
3	367.500	94.600
4	359.436	64.733
5	198.210	49.800
6	227.151	49.800
7	256.092	49.800
8	285.033	49.800
9	313.974	49.800
10	351.311	34.867
11	383.689	34.867
12	81.412	5.000
13	117.118	5.000
14	152.823	5.000
15	188.529	5.000
16	224.234	5.000
17	259.940	5.000
18	295.646	5.000
19	335.750	5.000
20	367.500	5.000
21	399.250	5.000
22	432.677	5.000

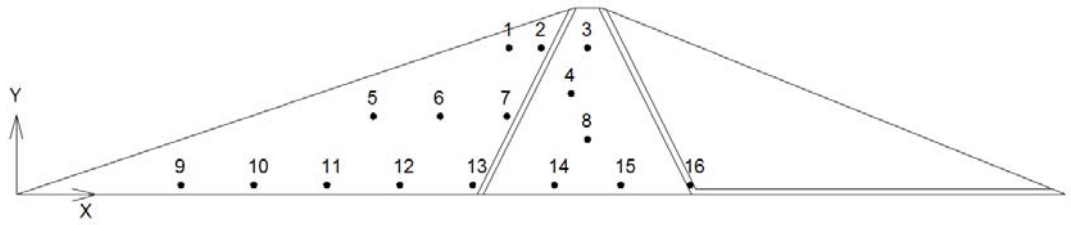

Figure A.2. Maximum piezometer layout for H=100 m

Table A.2 Coordinates of the piezometers for H=100 m

POINT	X (m)	Y (m)
1	265.231	78.600
2	282.446	78.600
3	307.500	78.600
4	298.583	54.067
5	192.223	41.800
6	228.134	41.800
7	264.046	41.800
8	307.500	29.533
9	88.5486	5.000
10	127.823	5.000
11	167.097	5.000
12	206.372	5.000
13	245.646	5.000
14	289.667	5.000
15	325.333	5.000
16	362.677	5.000

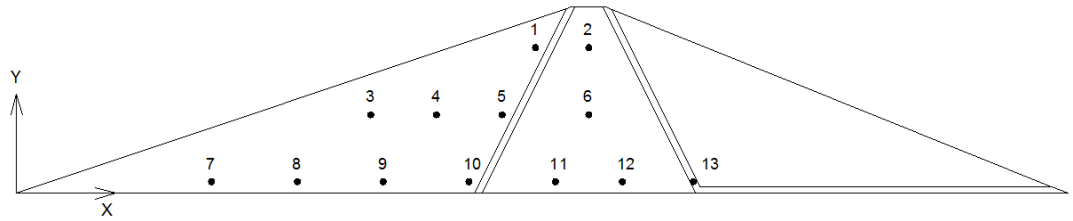

Figure A.3. Maximum piezometer layout for H=80 m

Table A.3 Coordinates of the piezometers for H=80 m

POINT	X (m)	Y (m)
1	224.446	62.600
2	247.500	62.600
3	153.223	33.800
4	181.634	33.800
5	210.046	33.800
6	247.500	33.800
7	84.258	5.000
8	121.388	5.000
9	158.517	5.000
10	195.646	5.000
11	233.000	5.000
12	262.000	5.000
13	292.677	5.000

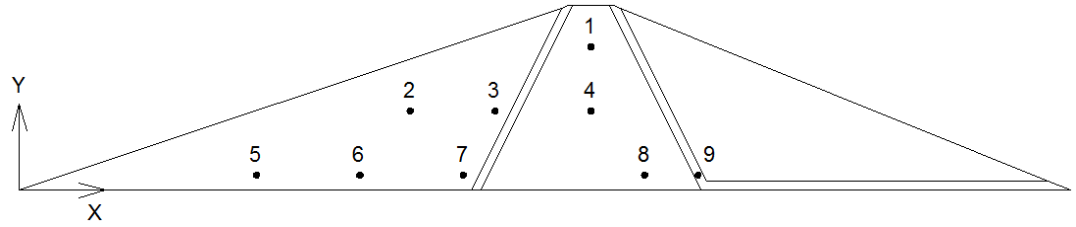

Figure A.4. Maximum piezometer layout for H=60 m

Table A.4 Coordinates of the piezometers for H=60 m

POINT	X (m)	Y (m)
1	187.508	46.617
2	128.175	25.809
3	156.050	25.809
4	187.508	25.809
5	77.823	5.000
6	111.734	5.000
7	145.646	5.000
8	205.093	5.000
9	222.677	5.000

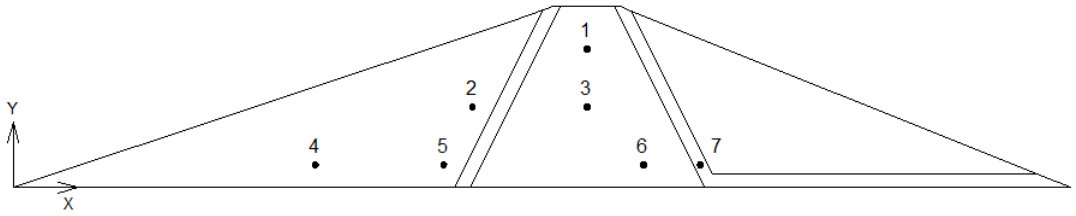

Figure A.5. Maximum piezometer layout for H=40 m

Table A.5 Coordinates of the piezometers for H=40 m

POINT	X (m)	Y (m)
1	127.500	30.600
2	102.046	17.800
3	127.500	17.800
4	67.097	5.000
5	95.646	5.000
6	140.090	5.000
7	152.677	5.000

B. Time-Dependent Phreatic Lines Under 70% of Rapid Drawdown Condition

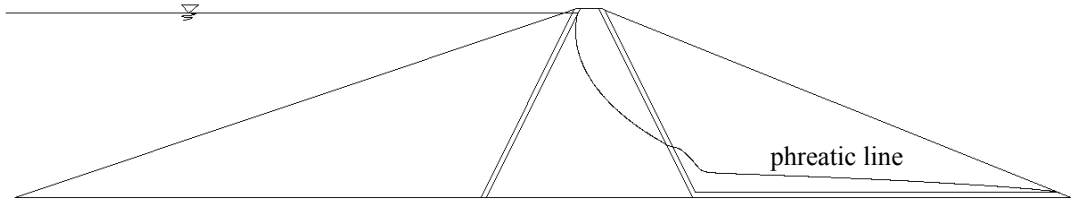

Figure B.6. Phreatic line at day 0 (steady state) for H=120 m

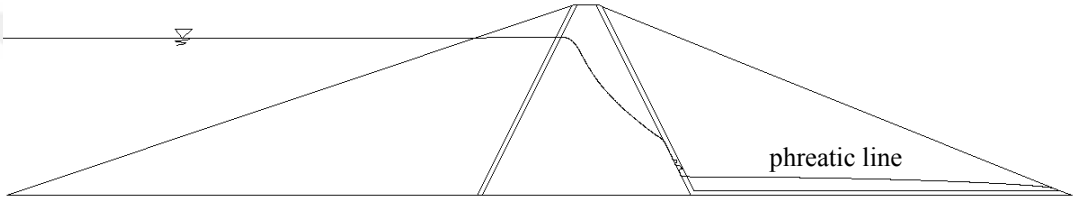

Figure B.7. Phreatic line at day 8 for H=120 m

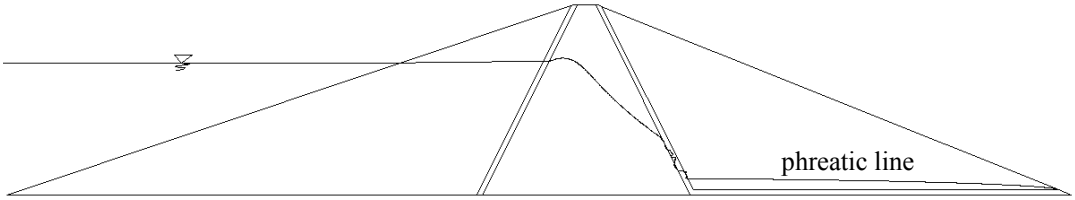

Figure B.8. Phreatic line at day 17 (end of drawdown) for H=120 m

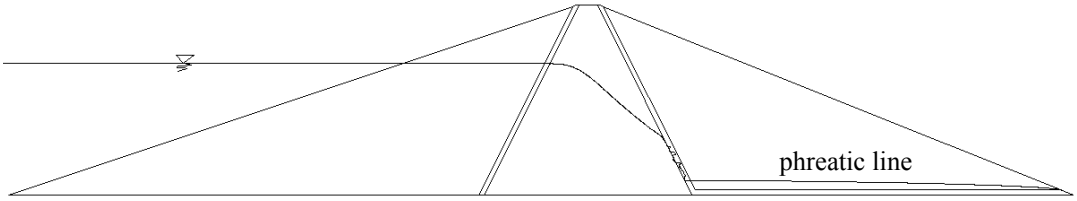

Figure B.9. Phreatic line at day 25 (steady state after drawdown) for H=120 m

C. Time-Dependent Phreatic Lines Under Rapid Fill Condition

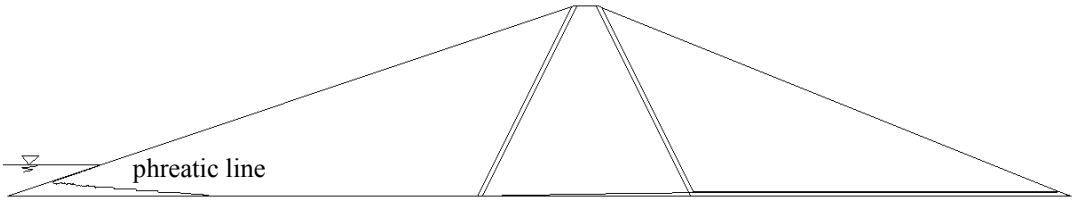

Figure C.10. Phreatic line at day 10 for H=120 m

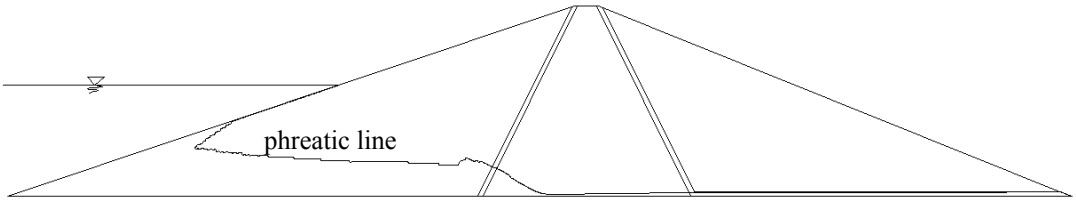

Figure C.11. Phreatic line at day 35 for H=120 m

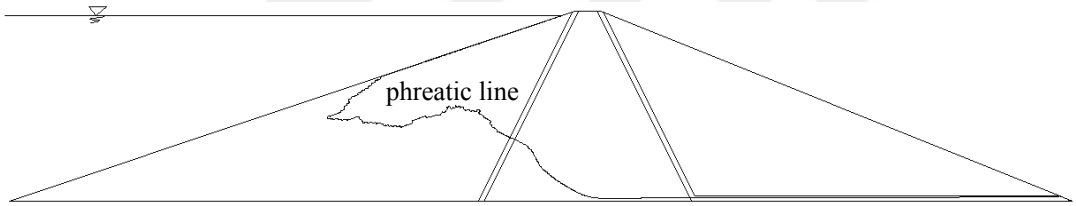

Figure C.12. Phreatic line at day 59 (end of rapid fill) for H=120 m

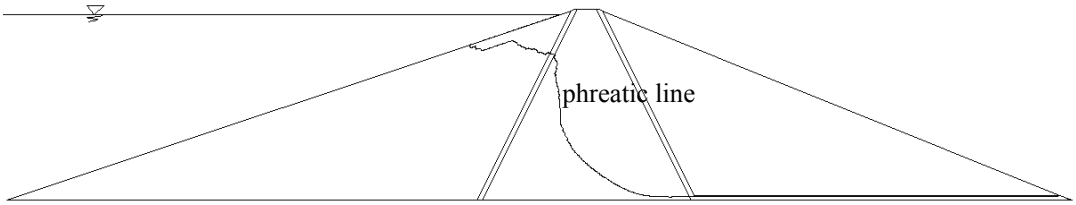

Figure C.13. Phreatic line at day 100 (after rapid fill) for H=120 m